UNIVERSITY OF NAIROBI

GENESIS OF CARBON DIOXIDE AND ASSOCIATED CHARACTERISTICS OF SELECTED MOFETTE SPRINGS IN THE EASTERN MT. KENYA REGION

BY

GEORGE NG'ANG'A MUNGAI

I80/51019/2016

A Thesis Submitted in Fulfillment of the Requirements for Award of the Degree of Doctor of Philosophy in Chemistry of the University of Nairobi

2021

DECLARATION

I declare that this thesis is my original work and has not been submitted elsewhere for examination, award of a degree or publication. Where other people's work or my own work has been used, this has properly been acknowledged and referenced in accordance with the University of Nairobi's requirements.

Signature .... Date .November 20, 2021

George Ng'ang'a Mungai

I80/51019/2016

Department of Chemistry

Faculty of Science and Technology

University of Nairobi

This thesis is submitted for examination with our approval as research supervisors.

Signature   Date

Prof. Hellen N. Njenga   .... 20|11|2021

Department of Chemistry

University of Nairobi

P.O. Box 30197-00100 Nairobi, Kenya

Email: hnnjenga@uonbi.ac.ke

Prof. Eliud M. Mathu   20.11.2021

Department of Geology and Meteorology

South Eastern Kenya University

P.O. Box 170-90200 Kitui, Kenya

Email: emathu@seku.ac.ke

Dr. Vincent O. Madadi   20|11|2021

Department of Chemistry

University of Nairobi

P.O. Box 30197-00100 Nairobi, Kenya

Email: vmadadi@uonbi.ac.ke

DEDICATION

I gladly dedicate this noble work to my dear parents, Mr. and Mrs. Mungai Mwenja.

ACKNOWLEDGEMENT

ABSTRACT

The Eastern Mt. Kenya region has a significant number of mofette or cold CO_2-rich springs which have not been fully investigated previously. They include Gikumene, Kathathantu, Kiambogo, Mbwinjeru, Mulathankari, Nthungu, Rwarera-A, Rwarera-B, Tharu and Ukuu. This study evaluated the origin of CO_2 and geochemistry of these springs in relation to their potential environmental, socio-economic and health impacts. A wide range of instruments were used for the analysis. Non-dispersive infra-red sensor was used for the measurement of ambient CO_2 in the air, cavity ring-down spectroscopy for δ ^{13}C and dissolved inorganic carbon determination, potentiometric titration for alkalinity, ion chromatography and graphite furnace atomic absorption spectrometry for major ions and inductively coupled plasma-optical emission spectrometry for trace elements analysis in water. Host rocks analysis was done by atomic absorption spectrometry, X-ray fluorescence and X-ray diffraction methods. Questionnaires were used to obtain views about the springs from the local community. The springs had average ambient CO_2 levels between 3,417 and 4,804 ppm which were far above the reported global atmospheric CO_2 value of 410.24 ppm in August 2019. The dissolved inorganic carbon δ ^{13}C ranged from -3.597 to +0.283 ‰, Vienna Pee Dee Belemnite. This indicated that the CO_2 was either mantle or deep crust derived probably due to post volcanic degassing with a minor contribution from carbonate minerals. The springs had low temperatures (21.2-29.7 ^{o}C) and slightly acidic pH (5.83-6.81). The results indicated high dissolved inorganic carbon (39,184-89,013 µmol/kg), total alkalinity (14,925-61,810 µmol/L) and electrical conductivity (1,221-5,195 µS/cm). The predominant cation in the waters was Na^+ at 121-1,273 mg/L which was largely counter-balanced by HCO_3^- to form Na-HCO_3 water-type. The levels of As, B, Mn, Ni, Se and F ions in some spring waters exceeded the Kenya Bureau of Standards guideline values. Only As and F ions exceeded the World Health Organization limits. Variations of data between the wet and dry seasons were not statistically significant. Essential trace elements such as Cu, Fe, Mn, Mo, Ni and Zn were present in the rocks. Among the toxic elements, As and Pb dominated in the rocks. From these findings, CO_2 emissions is evident in Mt. Kenya region based on the high dissolved inorganic carbon in the waters and high levels of ambient CO_2 in the air which could influence climate change. There is great socio-economic potential in the region for industrial extraction of CO_2 and processing of the mineral waters. However, there is considerable health risk of long-term consumption of the waters contaminated with As which is a known carcinogen.

TABLE OF CONTENTS

viii

LIST OF TABLES

LIST OF FIGURES

PAGE

ABBREVIATIONS, ACRONYMS AND SYMBOLS

AAS	Atomic Absorption Spectrometry
AD	Alzheimer Disease
APHA	American Public Health Association
ASTM	American Society for Testing and Materials
AWWA	American Water Works Association
CNS	Central Nervous System
CRDS	Cavity Ring-Down Spectroscopy
CRM	Certified Reference Material
CW	Continuous Wave
DIC	Dissolved Inorganic Carbon
DNA	Deoxyribonucleic Acid
DOSHS	Directorate of Occupational Safety and Health Services
EARS	East African Rift System
EC	Electrical Conductivity
EDXRF	Energy Dispersive X-Ray Fluorescence
GDWQ	Guidelines for Drinking-Water Quality
GIS	Geographic Information System
GIT	Gastrointestinal Tract
GPS	Global Positioning System
IAEA	International Atomic Energy Agency
IARC	International Agency for Research on Cancer
IBS	Irritable Bowel Syndrome
IC	Ion Chromatography
ICDD	International Centre for Diffraction Data
ICP-OES	Inductively Coupled Plasma-Optical Emission Spectrometry
IQ	Intelligence Quotient
KEBS	Kenya Bureau of Standards
KNBS	Kenya National Bureau of Statistics
KRV	Kenyan Rift Valley
LOAEL	Lowest Observed Adverse Effect Level
LOI	Loss on Ignition
LOQ	Limit of Quantitation

MORB	Mid-Ocean Ridge Basalt
NACOSTI	National Commission for Science, Technology and Innovation
NDIR	Non-Dispersive Infra-Red
NIST	National Institute of Standards and Technology
NOAA	National Oceanic and Atmospheric Administration
PET	Polyethylene Terephthalate
PDF	Powder Diffraction File
PMT	Photomultiplier Tube
RSD	Relative Standard Deviation
RVP	Rungwe Volcanic Province
SD	Standard Deviation
SDGs	Sustainable Development Goals
SRMs	Standard Reference Materials
Talk	Total Alkalinity
TDI	Tolerable Daily Intake
UN	United Nations
US EPA	United States Environmental Protection Agency
UV/VIS	Ultraviolet-Visible
VPDB	Vienna Pee Dee Belemnite
WEF	Water Environment Federation
WHO	World Health Organization
XRD	X-Ray Diffraction
XRF	X-Ray Fluorescence

SYMBOLS

δ	Delta
λ	Lambda
θ	Theta
r	Correlation coefficient
R^2	Coefficient of determination
$	Dollar
‰	per thousand or per mil

CHAPTER ONE
INTRODUCTION

1.1 Background information

Mofette (in singular mofetta) are cold CO_2-rich springs usually associated with the final phase of volcanic activity. They act as buffer systems saturated with CO_2 which degasses more or less strongly depending on the flow rate of the ascending gas (Koch *et al*., 2008). Carbon dioxide mineral springs worldwide, both hot and cold are often situated along faults or point sources in tectonically active regions. Some carry high concentrations of CO_2 related mostly to passive volcanic degassing (Cartwright *et al*., 2002; Marques *et al*., 2001).

The apparent sources of CO_2 in mofette springs include the mantle (volcanic degassing), sedimentary carbonate rocks, metamorphic processes and breakdown of organic matter (Kämpf *et al*., 2013; Chiodini *et al*., 2008; Mathew *et al*., 2008). Origin of the CO_2 gas can be determined by isotopic ratio analysis of $^{13}C/^{12}C$ (Stefa´nsson, *et al*., 2016). The ratio is expressed by delta notation per mil or parts per thousand Vienna Pee Dee Belemnite ($\delta\ ^{13}C$ ‰ VPDB). For mantle derived CO_2 gas, the ^{13}C value is -6 ±2.5 $\delta\ ^{13}C$ ‰ VPDB (Mason *et al*., 2017). The carbonate rocks gives -5 to +4 $\delta\ ^{13}C$ ‰, degradation of organic matter -22 to -25 $\delta\ ^{13}C$ ‰ and for metamorphic processes $\delta\ ^{13}C$ ‰ is above +2 (Tjaša *et al*., 2014; Jeong *et al*., 2005; Cartwright *et al*., 2002; Céron *et al*., 1998; Harris *et al*., 1997; Hoefs, 1997).

Carbon dioxide is the second most abundant emitted volcanic gas after water vapour and it is followed by SO_2. The juvenile CO_2 has a large presence in the mantle because of the oxidation of carbon-rich sources like carbonates, carbonaceous shales, petroleum, coal and oil shales into CO_2 and H_2O (Dasgupta and Hirschmann, 2010; Symonds *et al.*, 1994). Volcano fractures sometimes tap the shallow-level magma chamber and may form vent openings called fumaroles through which volcanic gases are emitted to Earth's surface. Although it might never reach the surface, the residual magma beneath dormant volcanoes can still emit gases. Volcanic gases may continue to be released from inactive volcanoes for a long period via the fumaroles or through point sources scattered over large areas of permeable ground as diffuse degassing structures. It is estimated that this process could emit almost half the CO_2 released by fully active craters (Kucharič *et al*., 2015; Irwin, 2012; Shinohara, 2008). The flux of CO_2 into the atmosphere has implications on Earth's climate and habitability due to its greenhouse effect (Mason *et al*., 2017; Alan, 2000).

Carbon dioxide mixes with groundwater to form weak carbonic acid (H_2CO_3) as it moves to the Earth's surface. Groundwater enriched with CO_2 increases dissolution of minerals derived from host rocks and some, especially heavy metals could be highly toxic to human beings (Jaishankar *et al.*, 2014; Maxwell, 2014; De Oliveira *et al.*, 2011). Carbonic acid dissolves surrounding carbonate mineral rocks such as dolomite [$CaMg(CO_3)_2$], magnesite ($MgCO_3$), calcite ($CaCO_3$, trigonal), aragonite ($CaCO_3$, orthorhombic) and siderite ($FeCO_3$), causing an increase in the amount of soluble metal bicarbonates. Further dissolution of feldspar silicate minerals such as albite ($NaAlSi_3O_8$) could be a source of $Na–HCO_3$ water-type (Hatmann *et al.*, 2013; Hyeon-Su *et al.*, 2005; Andrews *et al.*, 2004).

Equations (1.1) and (1.2) exemplify these processes.

$$MgCO_{3(s)} + H_2CO_{3(aq)} \rightarrow Mg(HCO_3)_{2(aq)} \tag{1.1}$$
(Magnesite)

$$2NaAlSi_3O_{8(s)} + 2H_2CO_{3(aq)} + 9H_2O_{(l)} \rightarrow 2NaHCO_{3(aq)} + Al_2Si_2O_5(OH)_{4(s)} + 4H_4SiO_{4(aq)} \tag{1.2}$$
(Albite)   (Kaolinite)   (Silicic acid)

Mofette springs have been investigated in some parts of the world. Their occurrences are mostly associated with major faults and volcanoes. They include, but are not limited to the following, Rungwe Volcanic Province springs in South West Tanzanian (Barry *et al.*, 2013), Wudalianchi springs in North East China (Mao *et al.*, 2009), the Jungapeo springs at the state of Michoacán in Mexico (Siebe *et al.*, 2007), South Korea springs (Jeong *et al.*, 2005), Saratoga Springs mineral waters in New York, U.S.A (Siegel *et al.*, 2004), cold CO_2-rich spring mineral waters at Daylesford, Victoria in Australia (Cartwright *et al.*, 2002), Southeastern Spain springs (Céron *et al.*, 1998), Bongwan CO_2 springs in South Africa (Harris *et al.*, 1997) and Lower Engadine region springs at the Swiss Alps in Switzerland (Wexsteen *et al.*, 1988).

Carbon dioxide occurs in the Kenya Rift Valley (KRV) at Mount Margaret Estate in Kedong Valley, Lake Magadi, Esageri and Kireita (Bu bois and Wash, 2007). Occurrence of CO_2 outside the Rift System was first investigated at Rurii spring located in Nyambene range (Mungai *et al.*, 2014). Other similar springs have been reported in Meru County in the Eastern slopes of Mt. Kenya, such as Gikumene, Kathathantu, Kiambogo, Mbwinjeru, Mulathankari, Nthungu, Rwarera-A, Rwarera-B, Tharu and Ukuu. However, they have not been studied before and they were selected for investigation in this work.

Mofette springs have socio-economic, health and environmental implications. The mineral waters are often used for drinking, cooking, therapeutic purpose and in recreation Spas. Industrial applications of CO_2 include soft drinks manufacture, refrigeration and in firefighting. The application of CO_2 has also been extended to research and technical fields such as supercritical fluid chromatography, solvent extraction and lasers (Fantarella and Kotlow, 2014; Skoog *et al*., 2007; Harris *et al*., 1997). The CO_2-rich waters usually contain high levels of trace elements which are leached from the underlying rocks. Some essential trace elements include B, Co, Cr, Cu, Fe, Mn, Mo, Ni, Se, and Zn. While elements such as As, Cd, Hg and Pb are highly toxic to humans. For example, use of groundwater contaminated with As is linked with various types of cancers (IARC, 2019; WHO, 2011). Thus water quality requires to be evaluated in order to weigh the health benefits and risks associated with the intake of such waters (Prashanth *et al*., 2015. Study of the genesis of CO_2 is relevant for climate change monitoring since CO_2 is a major greenhouse gas responsible for global warming (Robertson *et al*., 2016). Moreover, CO_2 emissions provide insight into geochemical processes occuring in the mantle and Earth's crust (Bissig *et al*., 2006; Diliberto *et al*., 2002).

The purpose of this study was to investigate the genesis of CO_2 and associated physicochemical parameters in selected springs found in the Eastern slopes of Mt. Kenya in Meru County. The sought information could be useful in evaluating the potential environmental, socio-economic and health impacts of these types of springs.

1.2 Statement of the problem

Mungai *et al* (2014) investigated CO_2 emission at Rurii spring located near the southern edge of Nyambene volcanic hills in Meru County, East of Mt. Kenya. Their work established existence of similar springs in the region whose origin of CO_2 and its relative abundance was not well understood. It is not yet known whether the issuing of CO_2 is a sign of post volcanic degassing associated with Mt. Kenya and Nyambene volcanoes or from other sources like carbonate metasedimentary rocks.

CO_2 is a major greenhouse gas which absorbs infra-red radiation strongly. Hence, evaluating the extent of CO_2 degassing in this region is vital for addressing the potential challenge it may pose to the environment (Kenneth *et al.*, 1997). Assessment of CO_2 levels is necessary to ascertain whether or not, more detailed technical work including intensive prospecting for the mineral is advisable in the study region.

Although mofette waters are rich in essential trace minerals, their acidic nature could also influence contamination of the groundwater with toxic elements like As, Cd, Cr, Cu, Hg, Pb and F[-] which are leached from the host rocks (Cangemi *et al*., 2019). Therefore, it is important to subject such waters to a thorough chemical investigation before it is considered safe for human consumption.

1.3 Overall objective

The major objective of this study was to investigate the source of CO_2 and associated characteristics of selected mofette springs in the Eastern Mt. Kenya region.

1.4 Specific objectives

The specific objectives of the study were to:

i. Assess the basic awareness and views the local community have about the mofette spring waters in the study area.

ii. Measure the levels of CO_2 in the ambient air near the spring sites.

iii. Determine the genesis of CO_2 by measuring $\delta\ ^{13}C$ ‰ values of dissolved inorganic carbon ($\delta\ ^{13}C_{DIC}$).

iv. Analyse the major physicochemical characteristics of the spring waters.

v. Determine the levels of essential trace elements and inorganic contaminants in the spring waters.

vi. Determine the geochemical composition and structure of host rocks adjacent to the springs in relation to the origin of solutes in the waters.

1.5 Justification

There are a number of prominent mofette springs along the Eastern part of Mt. Kenya region, yet no major study has been done to provide satisfactory scientific data for socio-economic, health and environmental impact assessment of the CO_2 springs in the region. Due to the negative impacts of CO_2 on climate, it is important to quantify the passive CO_2 emissions in this region and possibly include them in the global CO_2 budget estimates. The findings will provide a basis for CO_2 flux quantification around the Mt. Kenya region (Aiuppa *et al*., 2019; Brune *et al*., 2017; Maas and Wicks, 2017). This could help in developing climate change mitigation strategies in accordance with the United Nations (UN) Sustainable Development Goals (SDG: 13) on climate action (UN, 2015; Friedlingstein *et al*., 2014; Matthews *et al*., 2009).

Establishing the $\delta\,^{13}C$ isotope values will reveal whether the release of CO_2 from the springs is due to magmatic degassing or from other sources such as carbonate rocks. The research findings could help to close some information gaps on the spatial distribution of the isotopic signature and provide understanding of the CO_2 degassing behaviour of solid Earth in a volcano setting.

Determination of the genesis of dissolved CO_2 will reveal the geochemistry and geophysics of the region with regard to the underlying rock types or lithology and plate tectonics, respectively. This would give a better understanding of the geochemical processes taking place in the Earth's crust and mantle in the study region (Mason *et al.*, 2017; Bissig *et al.*, 2006; Diliberto *et al.*, 2002; Harris *et al.,* 1997). The geochemical data of the host rocks will show the extent of water-rock interaction in relation to the origin of CO_2 and other solutes in water (Mathew *et al.*, 2008).

Such findings could provide vital information to guide the mining industry on the possibility of commercial utilisation of the abundant mineral waters and CO_2 deposits in Mt. Kenya region. Currently, Kenya has one commercial CO_2 mining site at Kireita forest in Kiambu County which generated KSh 4,238.8 million between the years 2007-2017 (Kenya National Bureau of Statistics, KNBS, 2018). Therefore, discovery and exploitation of additional CO_2 mineral sites would enhance the national revenue for development in tandem with the Kenya Vision 2030 (2008).

Considering that the local community uses the spring waters for drinking, cooking, feeding the livestock and selling, characterisation of the water geochemistry will be of great help in assessing its suitability for consumption and/or commercialisation (KEBS, 2018; WHO, 2017; Abdul *et al.*, 2015; WHO, 2011; Chen *et al.*, 2003). In general, this study will contribute new knowledge in relevant fields such as climate change, Earth sciences, economic geology and environmental health.

LITERATURE REVIEW

2.1 Geological setting of the study region

The geology of Kenya may be divided into five major geological successions namely; Archean (Nyanzian and Kavirondian), Proterozoic (Mozambique Belt and Bukoban), Palaeozoic/Mesozoic sediments, Tertiary/Quaternary volcanics and Tertiary/Quaternary sediments. Quaternary volcanism gave rise to the Rift Valley and the volcanic piles of Mounts Kenya, Kilimanjaro and Elgon. Volcanic rocks occurs in the central parts of Kenya from north to south, covering the floor of the Rift Valley and on the peneplains east and west of the rift system (Akech *et al.*, 2013; Mathu and Davies, 1996). Figure 2.1 shows the geological distribution of volcanic and other rock-types in Kenya.
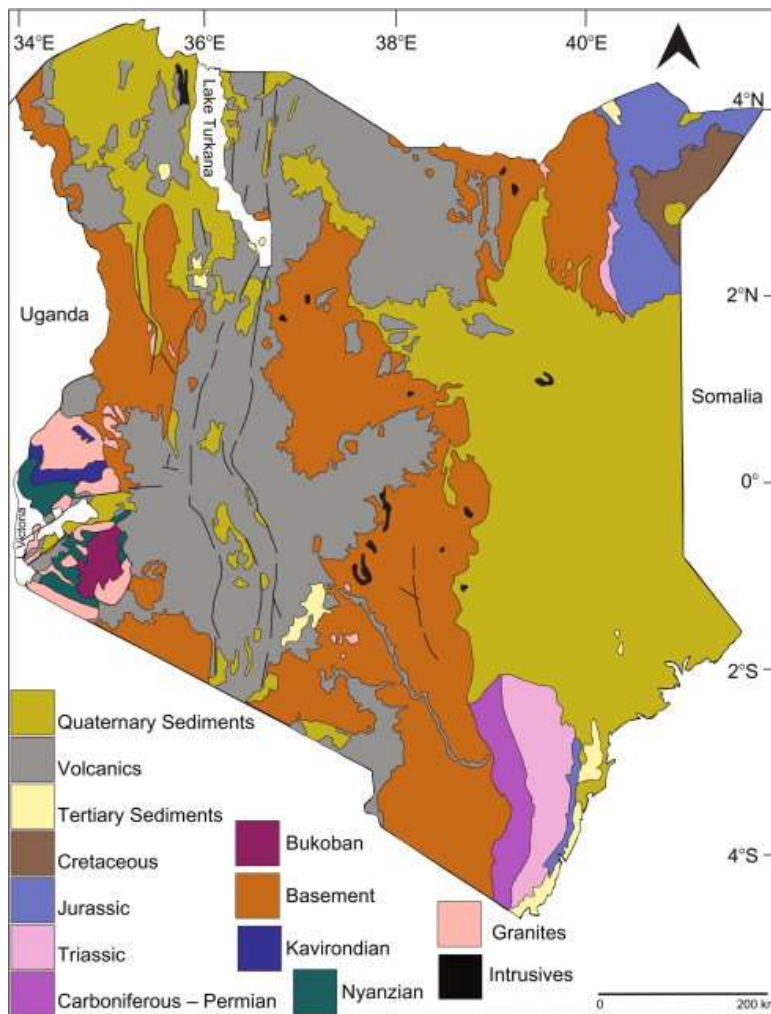
Figure 2.1: Geological map of Kenya.

(Courtesy of Ministry of Petroleum and Mining, Kenya, 2018).

6

Mt. Kenya is an extinct stratovolcano situated in Kenya, whose summit elevation is 5,199 m and lies outside the Kenya Rift Valley (KRV). It is the second tallest mountain in Africa after Mt. Kilimanjaro. The area covered in the study includes the Eastern part of Mt. Kenya, extending from elevation of 1410 m to 1938 m and bounded by latitudes 00º 13.401' N and 00º 05.004' S and longitudes 37º 35.620' E and 37º 40.763' E (Figure 2.2). Additional geological maps for the study area are provided in Appendices C-1, C-2 and B-C.

Figure 2.2: Geology of the Eastern Mt. Kenya showing the location of mofette springs. Modified from geological survey by J. J Shoeman between April and October 1948. (*Courtesy of Department of Geology, University of Nairobi, 2018*).

The volcano flanks have distinct craters and vents that form a number of parasitic cones, younger than the main volcano on the lower foothills of Mt. Kenya (Mason, 2007). The area is dominated by multiple lineaments which are expression of underlying buried faults. The major rock types found in Mt Kenya are basalts, kenytes, trachytes, phonolites and rhomb porphyrites (Baker, 1967; Gregory, 1900).

The Nyambene range extends in a north-east to south-east direction from the foothills of Mt. Kenya and rises to an elevation of 2,134 m. The range consists of an accumulation of basic and intermediate igneous extrusive rocks, with many parasitic cones and vents of later date on the flanks forming distinctive prominent features. A typically radial drainage pattern is observed on the slopes of Mt. Kenya. Rivers from the eastern slopes of Mt. Kenya and the southern flanks of the Nyambene range flow towards the Tana River. There are several springs, water holes and wells in different parts of the region. Most of the CO_2-rich springs occur closely together trending north to south along the eastern slopes of Mt. Kenya. Until now prospecting investors for mineral deposits have paid little attention to this region. The commonest minerals in this area are iron ore (magnetite, Fe_3O_4), mica flakes, low content garnets, rutile (TiO_2) and augite $(Ca,Na)(Mg,Fe,Al,Ti)(Si,Al)_2O_6$. Building stones are extracted in a number of small quarries for local supply (Mason, 2007).

2.2 Volcanic emissions

All volcanoes have a central vent leading to the Earth's surface where volcanic material is released. A stratotype volcano is normally a cone-shaped structure formed mostly through symmetrical accumulation of alternating lava and pyroclastic material around the central vent as shown in Figure 2.3.
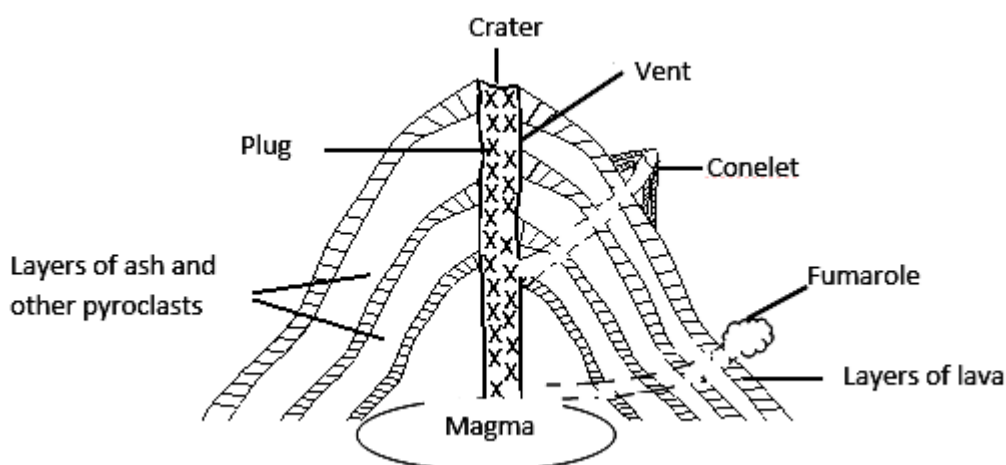
Figure 2.3: General features of a volcano.

The middle vent runs deep into a magma source, which is the storage area for the eruptive material. The main vent may block and force eruptions through other points of weakness on the sides of the cone resulting into formation of parasitic cones or conelets. These fractures sometimes tap the shallow-level magma chamber and may form vent openings called fumarole through which volcanic gases are emitted to the earth's surface (Ulrich, 2003).

Volcanic gases are volatile substances released by active or sometimes by inactive volcanoes. The major constituents of volcanic gases are water vapour, CO_2, SO_2, H_2S, HCl, HF, NH_3, CO, N_2, H_2, CH_4 and Ar. The gases escape through volcano fractures and/or through point sources scattered over large areas of permeable ground as diffuse degassing structures. Some of the gases like CO_2, SO_2, H_2S, HCl, HF and NH_3 dissolve easily and mix with groundwater as they move to Earth's surface. Groundwater contaminated with these gases could be highly noxious (Shinohara, 2008). Mofetta (in plural mofette) is a name applied to a cold discharge accompanied by volcanic degassing consisting chiefly of CO_2 which is a sign of passive volcanic activity. Volcanism is a significant natural cause of climate change on many timescales (Alan, 2000).

In Kenya, carbon dioxide gas was first discovered in the East Africa Rift system issuing from fissures and holes in volcanic rocks on Mt. Margaret Estate, Kedong Valley in 1918, about 50 km northwest of Nairobi. It was tapped and sold on a small scale for aerating bottled drinks such as soda water. In 1922, seepages of the gas were reported from the soil and rocks south of Lake Magadi. The first discovery of major economic importance did not occur until 1946 when a borehole drilled for water at Esageri near Eldama Ravine struck gas at a depth of 137 m and at a pressure of 5.44 atm averaging 98 per cent CO_2. Commercial exploitation began in 1951. In 1957, a borehole was sunk at Kireita, near Uplands in Kiambu County, some 32 km northwest of Nairobi, where a spring was known to give out CO_2. The borehole encountered gas at a pressure of about 2.38 atm with 97.8% CO_2 (Bu bois and Walsh, 2007). The Eastern slopes of Mt. Kenya and the region surrounding the Nyambene range is another important area of focus with numerous CO_2 degassing mofette springs which require to be studied. Mungai *et al.* (2014) reported existence of free CO_2 at Rurii spring within Nyambene range.

2.3 Stable ^{13}C isotope geochemistry and CO_2 genesis

Three known isotopes of carbon exist. These are stable carbon-12 (^{12}C) and carbon-13 (^{13}C), plus carbon-14 (^{14}C) which is radioactive or unstable. The sedimentary carbonates and organic matter have characteristic stable carbon content. This is due to two different types of reactions. One mechanism involves the atmospheric CO_2-dissolved bicarbonate-solid carbonate, equilibrium exchange reactions in the inorganic system which enrich carbonate rocks with ^{13}C isotope as shown in Equations (2.1 and (2.2) (Laughrey and Baldassare, 2003).

$$CO_{2(g)} + H_2O_{(l)} \rightleftharpoons H_2CO_{3(aq)} \tag{2.1}$$

$$H_2CO_{3(aq)} + CaCO_{3(s)} \rightleftharpoons Ca(HCO_3)_{2(aq)} \tag{2.2}$$

The other process is kinetic which occur during photosynthesis leading to concentration of ^{12}C in organic matter since most plants fix ^{12}C more readily than ^{13}C.

$$6CO_2 + 6H_2O \rightarrow C_6H_{12}O_6 + 6O_2 \tag{2.3}$$
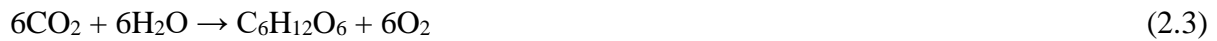
Stable isotope geochemistry is used for establishing the various sources of carbon in CO_2 and dissolved inorganic carbon (DIC) such as thermogenic, inorganic and microbial sources. The ^{13}C/^{12}C ratio is usually expressed using the delta (δ) notation in parts per thousand or per mil as δ ^{13}C ‰ versus Vienna Pee Dee Belemnite (VPDB) standard (Hoefs, 1997).

$$\delta\,^{13}C_{VPDB}\,‰ = 1000\frac{\left(R_{sample} - R_{standard}\right)}{R_{standard}} \tag{2.4}$$

$$\delta\,^{13}C_{VPDB}\,‰ = 1000\left(\frac{R_{sample}}{R_{standard}} - 1\right) \tag{2.5}$$

where R = ^{13}C/^{12}C

The standard is an internationally accepted Pee Dee Belemnite (PDB) reference standard for carbon consisting of calcium carbonate from a Cretaceous marine fossil, Belemnite Americana (from Pee Dee formation in South Carolina, USA). Other standards such as Vienna Pee Dee Belemnite (VPDB) have replaced PDB. The reference VPDB fossil has ^{13}C:^{12}C ratio of 0.0112372 and is available at the International Atomic Energy Agency (IAEA) in Vienna, Austria (Hoefs, 1997). The VPDB standard has been assigned a value of 0 δ ^{13}C ‰. When a sample is enriched with the lighter isotope (^{12}C) as compared with the standard, the δ ^{13}C values are negative. On the other hand, when δ ^{13}C values are positive, it means that the sample is enriched with the heavier isotope (^{13}C) relative to the standard (Chiodini *et al*., 2008; Darling *et al*., 1995). Table 2.1 is a list of variations in δ ^{13}C of CO_2 from different sources.

Table 2.1: Variations of δ ^{13}C from different sources.

Source	δ ^{13}C‰ VPDB
Atmospheric carbon	-8
Volcanic degassing or mantle	-8
Solid carbonates	+4 to -5
Organic matter	-8 to -12
Bacterial oxidation of methane	-20 to -59
CO_2 in coal bed gases	+18.6 to -26

Source: Hoefs (1997).

The various possible combinations of the ^{18}O, ^{17}O, ^{16}O and ^{13}C, ^{12}C isotopes in CO_2 molecules are shown in Table 2.2. Due to their very low abundance, $^{13}C^{17}O^{16}O$ and $^{12}C^{17}O_2$ can be neglected (Laughrey and Baldassare, 2003).

Table 2.2: Different CO_2 isotope combinations.

Mass	Isotopologues	Abundance
44	$^{12}C^{16}O_2$	98.40%
45	$^{13}C^{16}O_2$	1.19%
	$^{12}C^{17}O^{16}O$	0.0748%
46	$^{12}C^{18}O^{16}O$	0.41%
	$^{13}C^{17}O^{16}O$	0.00084%
	$^{12}C^{17}O_2$	0.0000142%

Source: Laughrey and Baldassare (2003).

2.4 Previous studies on genesis of CO_2 and characteristics of mofette springs

A study on the minerals in water and host rocks of Rurii spring at Nyambene Range in Kenya, confirmed that the water was rich in free CO_2 (931-1,015 mg/L) which contributed to the excessive dissolution of minerals from source rocks (Mungai *et al*., 2014). The water had elevated levels of Na^+ (954-1,043 mg/L), K^+ (117-122 mg/L), Ca^{2+} (94-124 mg/L), Mg^{2+} (70-74 mg/L), Cl^- (854-951 mg/L) and SO_4^{2-} (420-492 mg/L). It was characterised by very high total alkalinity and electrical conductivity at 5,528-5,649 mg/L and 5,986-6,014 µS/cm, respectively.

Barry *et al*. (2013) studied the cold 'mazuku' CO_2 vents at Rungwe Volcanic Province in South West Tanzanian which is part of the East African Rift System (EARS). A narrow range of $\delta\ ^{13}C$ from -2.8 to -6.5 ‰ VPDB was observed indicating mantle-derived CO_2 fluxes.

The Bongwan CO_2 springs in KwaZulu-Natal in South Africa were found to have $\delta^{13}C$ values varying from -0.6 to +0.9 ‰ VPDB, an indication that the source of the CO_2 was most likely due to the reaction of acid groundwater with carbonate rocks at depth. The emission of CO_2 was linked to about 80 km long Bongwan gas fault trending north-south (Harris *et al*., 1997). The 97.5% pure CO_2 issuing up to 46 kg/hour has been exploited commercially.

Emission of 240,000 t CO_2 from the upper 100 m of Lake Nyos in Cameroon was reported eight weeks after the eruption on August 21, 1986 (Giggenbach, 1990). The average $\delta\ ^{13}C$ of -3.4 ‰ VPDB and He (R_{air} = 5.5) suggest deep magmatic origins. The cation content (Na^+, K^+, Mg^{2+}, Ca^{2+}, Mn^{2+} and Fe^{2+}) was corresponding to the dissolution of host rock and the waters were close to saturation with respect to siderite. Exsolution of CO_2 gas leads to the precipitation of siderite as iron hydroxide.

Shestakova *et al*. (2018) characterised thermal springs (22 $^\circ$C to 39 $^\circ$C) at Choygan area of southern Siberia in Russia, as HCO_3–Na–Ca type, slightly acidic (pH 6.1–6.9) with total dissolved solids (TDS) ranging from 1,545 mg/L to 2,647 mg/L. The $\delta\ ^{13}C_{DIC}$ isotope values varied from −0.3 to +1‰ which was associated with metamorphism of deep carbonate rocks with a possibility of inputs from other sources. Major ions such as Na^+, K^+, Ca^{2+}, Si^{4+} and Cl^- were consistent with the weathering of silicate phases in the subsurface. The red precipitate on the surface around the springs was a result of the air-oxidation of Fe^{2+} to Fe^{3+}.

In a study of mofette springs of Wudalianchi active volcanoes in North East China, Mao *et al*. (2009), found the springs to be rich in CO_2. HCO_3^- was the predominant anion with TDS above 1,000 mg/L. The $\delta\ ^{13}C_{DIC}$ values ranged from -8.24 to -5.26 ‰ VPDB. This was an indication of upper mantle origin of dissolved CO_2.

Siebe *et al*. (2007) carried out an investigation on CO_2-rich thermal springs of Jungapeo at the state of Michoacán in Mexico. The springs had high HCO_3^-, moderate Ca^{2+}, Mg^{2+}, Na^+, K^+, moderate to low Cl^- and low F^-. The $\delta\ ^{13}C$ values were between -6.7‰ and -7.2‰. Hence, CO_2 mainly originate from the mantle. Gas samples had very low contents of CH_4 and NH_3 and there was no detectable H_2S or H_2.

The CO_2-rich water of Kangwaon, Chungcheong and Kyungpook regions in South Korea could be classified into Ca(Na)-HCO_3, Ca-HCO_3 and Na-HCO_3 water-types (Jeong *et al.*, 2005). The slightly acidic mineral waters (pH 4.8-6.76) contained high CO_2 concentration with a high ion content. From the investigation of host rocks, the genesis of Ca, Mg, Fe and HCO_3^- in the CO_2-rich waters was the carbonate minerals. The C-13 isotope data was -6.6 to +0.9 ‰, showing that the CO_2 was from a deep-seated source or mantle derived, but could be partially mixed with CO_2 derived from carbonate minerals.

In New York (USA), Saratoga Springs mineral waters have historically generated scientific and commercial interests because of their anomalous TDS (above 2000 mg/l) and relatively high CO_2 partial pressures (~5 atm) (Siegel *et al.*, 2004). The δ $^{13}C_{DIC}$ (-5.8 to +0.8 ‰ VPDB) suggested that the source of CO_2 is an inorganic juvenile melt or a deep-seated magmatic source typical of a passive tectonic setting. The likely sources of NaCl component of the spring waters included the crystalline rocks of the Adirondack Mountains or Canadian Shield situated to the north. The mineral waters are sold as a commercial product and are used for drinking and bathing in Spas (Zink, 1993; Swanner, 1988).

A study highlighting isotope and chemical analysis of cold and thermal mineral waters at the Northern part of Portuguese Mainland found high contents of Na^+, K^+, Ca^{2+}, HCO_3^- and free CO_2 (Marques *et al*., 2000). The δ $^{13}C_{DIC}$ values were ranging from -6 to -1 ‰ VPDB which could be attributed to either deep-seated (mantle) origin or mixing of mantle and limestone CO_2. The chemistry of these mineral waters was a manifestation of water-rock interactions favoured by the enriched CO_2 at a low temperature.

In Switzerland, the cold (2–9 ^{o}C) mofette springs in the Swiss Alps Lower Engadine region, contains free CO_2 up to 3,000 mg/L (Wexsteen *et al.*, 1988). The observed water-types included Na-HCO_3-Cl^-, Ca-HCO_3 and Na-Mg-HCO_3-SO_4^{2-} waters. The δ ^{13}C value of about – 4 ‰ VPDB and $^3He/^4He$ (0.1) of the atmospheric value revealed that CO_2 was of crustal origin. The genesis of the CO_2 could be attributed to the dissolution of carbonates rocks and/or decomposition of marine carbonates.

2.5 Characterisation of mofette waters

Mofette waters are associated with anomalous physicochemical features as compared with ordinary surface and groundwaters. They are usually characterised by elevated dissolved inorganic carbon (DIC), total alkalinity, electrical conductivity, total dissolved solids and slightly acidic pH (Shestakova *et al*., 2018; Mungai *et al*., 2014; Mao *et al*., 2009).

2.5.1 Physical parameters (Temperature, pH, EC and TDS)

Temperature governs the solubility of mineral salts in water in addition to controlling most geochemical and biological activities. Gases are generally more soluble at low temperature because they expand when the temperature is increased (Hyeon, *et al*., 2005). The overall pH of most groundwater results from the balance between dissolved CO_2 gas derived from the atmosphere and biological activity in the environment, and dissolved carbonate and bicarbonate derived from the carbonate rock. The CO_2-rich waters have slightly acid pH 4.8 to 6.76. The ability of water to dissolve mineral salts from rocks depends on its pH value (Andrews *et al*., 2004).

Pure water has very low conductivity and can be said to be a non-conductor. Electrical conductivity (EC) of water depends on concentration of dissolved mineral salts and its temperature. Electrical conductivity is usually proportional to total dissolved solids (TDS) present in the water. Total dissolved solids include inorganic salts and small amounts of organic matter that are dissolved in water. The major constituents are cations such as Ca^{2+}, Mg^{2+}, Na^+ and K^+; and anions such as CO_3^{2-}, HCO_3^-, Cl^-, SO_4^{2-}, and NO_3^- (Eaton, 2005). TDS supplies may emanate from natural source, sewage, agricultural runoff and industrial effluent. World Health Organization (WHO) recommends a TDS of not more than 200 mg/L (WHO, 2004). Determination of TDS can be done gravimetrically based on the weight of the residue on evaporation after drying at a temperature of 105-110 ºC or through correlation with electrical conductivity. Multiplying conductivity in µS/cm by 0.64 gives an approximate TDS value in mg/L (Kelvin and Huan, 2016).

2.5.2 Dissolved inorganic carbon

Equation (2.6) shows expression for dissolved inorganic carbon (DIC) in natural waters.

$$DIC = [H_2CO_3] + [HCO_3^-] + [CO_3^{2-}] \tag{2.6}$$

The DIC species are derived via the following equilibrium reactions:

$$H_2CO_{3(aq)} \rightleftharpoons HCO_{3(aq)}^- + H^+_{(aq)} \qquad K_1 = 3.98 \times 10^{-7} \tag{2.7}$$

14

$$\text{HCO}_3^-{}_{(aq)} \rightleftharpoons \text{CO}_3^{2-}{}_{(aq)} + \text{H}^+{}_{(aq)} \qquad K_2 = 5.01 \times 10^{-11} \tag{2.8}$$
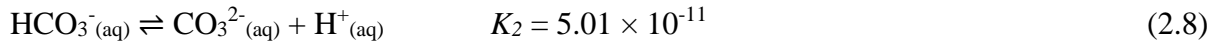
Thus the concentrations of undissociated H_2CO_3 and dissociated HCO_3^- species are equal at about pH = 6.4. Figure 2.4 shows the distribution of DIC species as a function of pH. Undissociated H_2CO_3 are predominantly found below pH 6.4 while CO_3^{2-} is found above pH 10. The HCO_3^- species predominate in the pH range 6.4-10 (Andrews *et al*., 2004).
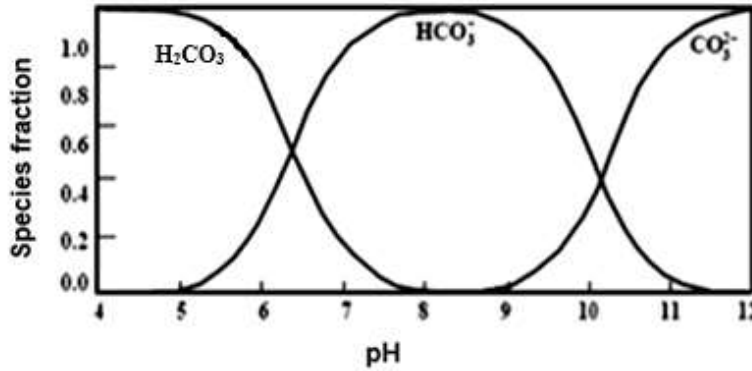
Figure 2.4: Distribution of DIC species against pH.

Cavity ring-down spectroscopy (CRDS) is a convenient method for DIC determination. Standards and samples are treated with 25% H_3PO_4 to release CO_2 gas which is directed into the CRDS system for DIC analysis (Dickinson *et al*., 2017).

2.5.3 Total alkalinity

The carbonates (CO_3^{2-}), bicarbonates (HCO_3^-) and hydroxyl (OH^-) ions represent the major form of alkalinity in groundwater. Groundwater pH is usually in the range of 6.5 to 8.5, hence the contribution of total alkalinity by OH^- and CO_3^{2-} is negligible and alkalinity due to HCO_3^- is the only capacity actually measured. In large quantities, alkalinity imparts a bitter taste to the water. Total alkalinity is established by titration of the sample with 0.01 N H_2SO_4 or 0.02 N HCl to pH 4.5. It is expressed in mol H^+/L (eq/L) or mg/L $CaCO_3$ (Eaton, 2005).

2.5.4 Cations

The huge presence of various major, minor and trace cations in the CO_2-rich water arises from the action of acidic waters on parent rocks. Therefore, the chemical signature of the discharge could have a direct relation to the geochemical composition of the source rocks which may cause contamination of water. For example, siderite mineral ($FeCO_3$) dissolves into carbonic acid to form aqueous iron (II) bicarbonate $Fe(HCO_3)_2$ as shown in Equation (2.9) (Mao *et al*., 2009; Jeong *et al*., 2005; Andrews *et al*., 2004; Koh *et al*., 2002).

$$\text{FeCO}_3{}_{(s)} + 2\text{H}^+{}_{(aq)} + \text{CO}_3^{2-}{}_{(aq)} \rightarrow 2\text{HCO}_3^-{}_{(aq)} + \text{Fe}^{2+}{}_{(aq)} \tag{2.9}$$
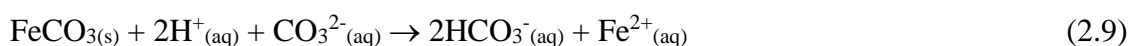
The most commonly used instrumental methods for cations determination in water include atomic absorption spectrometry (AAS), inductively coupled plasma-optical emission spectrometry (ICP-OES), inductively coupled plasma-mass spectrometry (ICP-MS) and ion chromatography (Eaton, 2005; US EPA, 2001; Gros and Gorenc, 1997; US EPA, 1997).

2.5.5 Sulphate

Sulphate mixes with groundwater as a result of water-rock interaction. A high level (1,000-1,200 mg/L) of sulphate in water has laxative effect; it causes noticeable taste and corrodes the water distribution systems. Sulphate ions in water can be determined by ion chromatography (US EPA, 1997) or turbidimetric method whereby $BaCl_2$ crystals are added to the sample under controlled conditions to form insoluble $BaSO_4$. The turbidity due to $BaSO_4$ is measured by ultraviolet-visible (UV/VIS) spectrometer at 420 nm or by a turbidity meter (Eaton, 2005).

2.5.6 Chloride

Chloride ions are abundant in the sea water and sediments of Earth's crust. They occur largely in NaCl, KCl and $CaCl_2$ minerals. The chlorides get dissolved into the groundwater from various rocks or may come from volcanic gases containing HCl (Shinohara, 2008). The Mohr method can be used to determine chloride in water. The sample is titrated with standard 0.0141 N $AgNO_3$ solution using K_2CrO_4 or Na_2CrO_4 indicator. Brick-red Ag_2CrO_4 precipitate forms at the end-point (Christian, 2004). Alternatively, ion chromatography can be used (US EPA, 1997).

2.5.7 Fluoride

Fluorides get into water by dissolving fluoride minerals like cryolite (Na_3AlF_6), fluorite (CaF_2) and apatite $Ca_5(Cl,F,OH)(PO_4)_3$ (Rutley, 1988). Another likely source of fluoride in water is volcanic gases which contain HF (Shinohara, 2008). The fluoride content in water can be determined by ion chromatography (Gros and Gorenc, 1997; US EPA, 1997) or by using fluoride ion-selective electrode (ISE) which has a reference electrode built in. Determination by the fluoride selective electrode involves adding total ionic-strength adjustment buffer (TISAB) to the samples and standards to attain same ionic strength and pH 5.3-5.5. Therefore, measurement of concentration rather than activity can be done directly. The instrument is calibrated with five or six NaF standard solutions of different concentrations over a narrow range to bracket the unknown.

A plot of potential (E value) versus the logarithm of fluoride ions concentration [F⁻] in the standard solutions yields a straight line graph, which is then used to determine F⁻ ions concentration in the sample (Sunitha and Reddy, 2014).

2.6 Classification of water-types

The cations and anions composition of water is used to classify the water-types according to the dominant ions. The concentrations of ions are expressed in milli-equivalents per litre (meq/L), where meq/L = mmol/L × absolute ionic charge value. The major cations found in water are usually Na^+, K^+, Ca^{2+} and Mg^{2+} while the most abundant anions are HCO_3^-, CO_3^{2-}, Cl^- and SO_4^{2-} (Sadashivaiah *et al.*, 2008; Koh *et al.*, 2002; Freeze and Cherry, 1979). The chemical composition or hydrochemical facies of the water samples can be represented by a Piper diagram (Piper, 1944) which is computed using software programs such as GW_Chart (Figure 2.5).
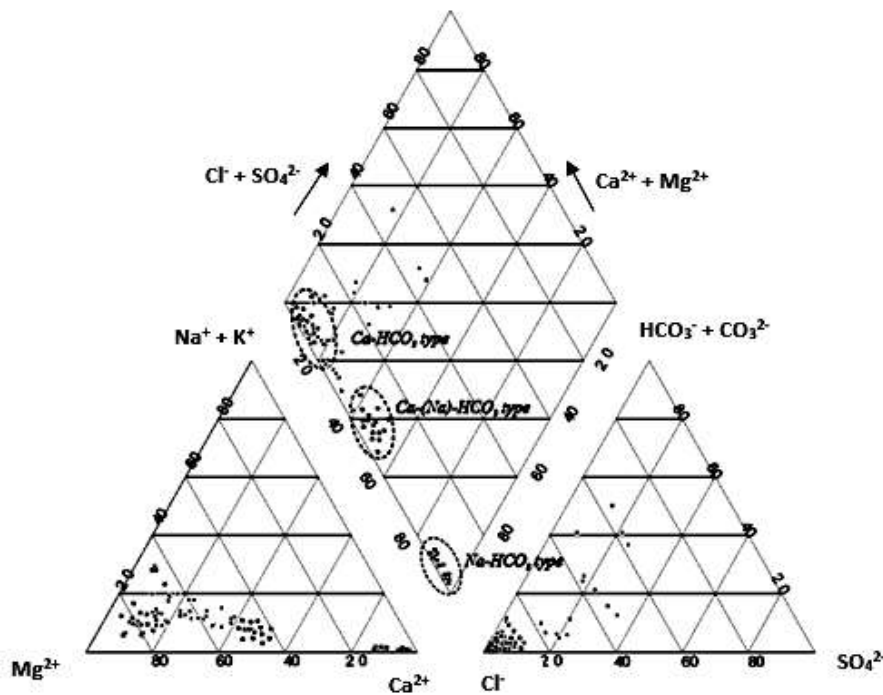
Figure 2.5: Piper diagram of CO₂-rich waters classification in Korea (Koh *et al.*, 2002).

The cations and anions are presented separately on ternary plots. A ternary plot shows the ratios of three variables as positions fitted on an equilateral triangle. The three variables sum to a constant usually, 1.0 or 100%. At the three apexes of cation plot are $Na^+ + K^+$, Ca^{2+} and Mg^{2+}. Anion plot has $HCO_3^- + CO_3^{2-}$, Cl^- and SO_4^{2-} at the apexes. The two ternary plots are combined to form a diamond.

17

The dominant ion must be greater than 50% of the total. Thus, water classified as Na-HCO$_3$ water-type has more than 50% of total cation and more than 50% of total anion as Na$^+$ and HCO$_3^-$, respectively. Hydrochemical facies are essential in understanding the complex hydrogeochemical processes due to water-rock interaction in the subsurface (Kuma, 2013; Homma and Tsukahara, 2008).

2.7 Quality and health effects of CO$_2$-rich waters

Intake of carbonated water enhances digestive solubility of food and improves intestinal physiology by stimulating secretion and motility of the digestive tract. Such waters are suitable remedy for conditions such as indigestion also known as dyspepsia, constipation and irritable bowel syndrome (IBS). Studies on humans have shown that bicarbonated mineral waters minimises cardiovascular risks through breakdown of cholesterol into bile salts and their subsequent removal from the body (Batayney *et al*., 2012; Albertini *et al*., 2007; Gasbarrini *et al*., 2006; Schoppen *et al*., 2004; Grassi *et al*., 2002).

Trace elements occur in various environmental matrices at concentrations ranging from 1 ppb to 100 ppm (Skoog *et al*., 2004). These elements may be easily leached into the CO$_2$-rich waters from rocks. The essential trace elements are B, Co, Cr, Cu, Fe, Mn, Mo, Ni, Se and Zn. They are termed as essential trace or micro elements because their requirement in the body is less than 100 mg/day and deficiency leads to serious disorders. These elements regulate crucial biological pathways by acting as cofactors for various enzymes and forming centers for stabilisation of enzymes and proteins (Prashanth *et al*., 2015; Wada, 2004).

On the other hand, some trace elements like As, Cd, Cr, Cu, Pb and Hg produce high degree of toxicity in the human body and are of great public health concern. These metals interfere with functioning of body cells by binding to enzymes, structural proteins and nucleic acids. They are known to affect the nervous and circulatory systems, cause multiple organ damage and some especially As have carcinogenic effects (Zhang *et al*., 2019; Golekar *et al*., 2013; He *et al*., 2005; Davidson *et al*., 2004; WHO *et al*., 1996).

2.7.1 Essential trace elements

Boron (B) is an essential trace nonmetal in the human body. It occurs naturally in groundwater as it leaches from rocks and soils containing borates and borosilicates. Boron helps in bone formation and functioning of the central nervous system (CNS), promotes hormonal action, has anti-inflammatory effects which reduce arthritic symptoms and

minimise risk for some types of cancer. Its health benefits diminish with intake of less than 1000 µg/day (Nielsen, 2014). Boron is associated with toxicity of the male reproductive system. Testicular lesions form in rats, mice and dogs when given boric acid or borax in drinking water or food (Bakirdere *et al*., 2010). Cobalt (Co) is naturally occurring and an essential trace metal in humans. It is a vital component of vitamin B_{12} which is involved in healthy functioning of blood cells, nerve cells, amino acid metabolism and DNA synthesis (Czarnek *et al*., 2015).

Chromium (Cr) is widely distributed in the Earth's crust in minerals such as chromite, $FeCr_2O_4$. The most common oxidation states are +2, +3 and +6. Chromium (III) is an essential trace nutrient in humans. It enhances sensitivity of insulin to glucose metabolism. Chromium deficiency leads to impairment of glucose tolerance while toxicity causes dermatitis, renal failure and pulmonary cancer. According to the International Agency for Research on Cancer (IARC), Cr^{6+} and Cr^{3+} are classified in Group 1 (human carcinogen) and Group 3 (not classifiable as to its carcinogenicity to humans), respectively. The ratio of Cr^{3+} to Cr^{6+} in natural waters varies widely and significant high concentrations of Cr^{6+} may occur. Chromium (VI) is reduced to the less toxic chromium (III) in the gastrointestinal tract (WHO, 2011; Cefalu and Hu, 2004). Copper (Cu) is an essential trace mineral and a drinking-water contaminant as well. Copper helps in the synthesis of blood haemoglobin, bone development and connective tissue metabolism. In high doses, it can cause kidney dysfunction, stomach and gastrointestinal bleeding (Uauy *et al*., 2008).

Iron (Fe) is the second most abundant metal in the Earth's crust after Al. The range of Fe in natural fresh waters is 500-50,000 µg/L. It is an important trace nutrient in the body whose functions include oxygen transport, electron transport, enzymes cofactor and DNA synthesis. Its deficiency in the body leads to iron deficiency anaemia. However, excess Fe has ability to form damaging free radicals and its levels in the body tissues require strict regulation (Abbaspour *et al*., 2014; Pham-Huy *et al*., 2008). Manganese (Mn) is abundant in the Earth's crust usually present together with iron. It is an essential trace element in humans. The springs could be relied on for Mn intake. Manganese acts as a cofactor for various enzymes involved in digestion, reproduction, antioxidant defense, immune response, respiration and neuronal activities. Some epidemiological studies have associated high levels of Mn in drinking water with neurotoxicity such as tremors (Chen *et al*., 2018).

Molybdenum (Mo) occurs naturally in soil. It occurs at very low concentrations in drinking water (usually less than 0.01 mg/L) which are not of health concern. Molybdenum is an essential trace element with an estimated daily requirement of 0.1–0.3 mg for adults. It is present in enzymes such as sulphite oxidase, aldehyde oxidase and xanthine oxidase/dehydrogenase. Sulphite oxidase catalyses conversion of sulphite formed during metabolism of sulphur-containing amino acids into the less toxic sulphate which is safely removed from the body (Wada, 2004).

Nickel (Ni) occurs naturally in various mineral forms. It is vital trace nutrient in humans. The tolerable daily intake (TDI) of 12 µg/kg body weight is established as the lowest observed adverse effect level (LOAEL) (WHO, 2011). Nickel is involved in hormonal activity and lipid metabolism in the human body. The most common adverse effect of Ni is allergic contact dermatitis. There is no sufficient evidence of carcinogenic effect as a result of oral exposure to Ni. However, IARC has classified inhaled nickel compounds in Group 1 (carcinogenic to humans) and metallic nickel in Group 2B (possibly carcinogenic) (Zdrojewicz et al., 2016; Cempel and Nikel, 2006).

Selenium (Se) is a metalloid that occurs in the Earth's crust mostly in association with sulphur minerals. It is an essential trace mineral in humans. In most cases, the concentration of Se in drinking water is lower than 10 µg/L but higher in some seleniferous regions. Selenium constitutes selenoproteins whose functions include providing antioxidant and anti-inflammatory effects in the body. Deficiency of selenium is associated with severe cardiomyopathy (Keshan disease). Selenium toxicity (selenosis) effects include gastrointestinal disturbances and dermatological effects (skin discolouration, hair and nail loss). Other effects are decayed teeth, degeneration of motor neurons and prevalence of cancers (Rayman, 2012; Vincent et al., 2001).

Silicon (Si) is the second most abundant element on the Earth's crust after oxygen. It is present in various forms of silicate minerals and occur in drinking water as silicic acid (H_4SiO_4) which is usually not ionised. Rondeau et al. (2009) findings showed that risk of Alzheimer's disease (AD) or dementia reduced in a cohort which had 10 mg/day increase in Si intake compared to others. Similar studies suggested that Si protects against the occurrence of aluminium (Al) induced dementia by enhancing Al excretion and reducing its absorption in the body (Guyonnet et al., 2017).

Zinc (Zn) is an essential trace mineral in humans. Oral intake of Zn is relatively nontoxic. Zinc requirement for adult males is 15–20 mg/day. It enhances normal growth and development during pregnancy, childhood and adolescence. Reproductive (spermatogenesis), nervous, immune, dermatological and gastrointestinal systems are the most affected by Zn deficiency. Excess absorption of Zn interferes with Cu and Fe uptake (Roohani *et al*., 2013; Wada, 2004).

2.7.2 Toxic trace elements

Silver (Ag) occurs naturally in form of oxides, sulphides and some salts and it has no clear biological role in the human body. Chronic exposure to soluble Ag causes heavy blue-gray discolouration of the skin and hair (argyria), and eyes (argyrosis) due to deposition of silver metal or silver sulphide. It may affect other parts of the body like the liver, kidneys, digestive system and blood cells. Levels below 5 µg/L Ag can be tolerated without risk to health (Lansdown 2006; Pamela *et al*., 2005). Aluminium (Al) is abundant in silicate rocks and constitutes 8 % of the earth's crust. However, it is not among essential elements for life. There has been observed a positive correlation between Al levels in the body and various adverse conditions like Alzheimer disease (AD), dialysis encephalopathy, Parkinsonism dementia and amyotrophic lateral sclerosis. Individuals with impaired kidney function, infants under the age of one year and the elderly are at higher risk of Al toxicity. Aluminium influences neuronal gene expressions on binding to the phosphate groups of DNA and RNA. Al has some similar characteristics to Fe^{3+} and binds to transferrin (an iron-binding protein) thus affecting iron homeostasis. Hence, considering its long half-life in the body, there is need to control unnecessary Al exposure to human population (Exley, 2016; Kawahara *et al*., 2007).

Arsenic (As) in natural waters is of great health concern because it is considered to be carcinogenic. It is a metalloid that occurs widely in the Earth's crust and exhibits oxidation states -3, 0, +3 and +5. Oxidation state +5 is the most common in water as arsenate (AsO_4^{3-}). Natural waters usually contain 1–2 µg/L As. In groundwaters where there are sulfide and sedimentary mineral deposits derived from volcanic rocks, As levels are usually elevated (Herath *et al*., 2016). Arsenic is not classified as essential in humans. Long term exposure to high levels of As leads to arsenicosis which is a manifestation of different medical complications such as dermal lesions. It affects various organ systems in the human body such as integumentary (skin, hairs and nails), nervous, cardiovascular, hematopoietic (bone

21

marrow, erythrocytes and spleen), immune, endocrine, renal and reproductive systems. It induces changes in DNA which have been linked with many body disorders and cancer development on the skin, prostate, lungs, liver, bladder and kidney. It is classified in Group 1 (carcinogenic to humans) by the International Agency for Research on Cancer (IARC, 2019; Abdul *et al*., 2015; WHO, 2011; Chen *et al*., 2003).

Barium (Ba) is usually present in igneous and sedimentary rocks. Barium is associated with nephropathy in laboratory animals and has potential to cause hypertension in humans (Kravchenko *et al*., 2014). Beryllium (Be) is mostly found naturally as beryllium aluminium silicate (beryl), $Be_3Al_2Si_6O_{18}$. It occurs in natural water at low levels since most soluble beryllium salts are hydrolysed and precipitated as insoluble $Be(OH)_2$ close to neutral pH range (Cooper and Harrison, 2009). However, concentrations can be elevated at pH below 5 or above 8 with the formation of water-soluble complexes. Absorption of Be in the gastrointestinal tract is limited due to the formation of insoluble precipitates with subsequent excretion. There is no reliable information on the oral toxicity to humans associated with beryllium in drinking water (WHO, 2011).

Cadmium (Cd) in water is derived from natural sources such as volcanic activity and weathering of parent rocks. Cadmium is not an essential trace element and is highly toxic to humans (Liu *et al*., 2015). It mainly accumulates in the human kidneys causing damage. Cadmium is presumably carcinogenic and International Agency for Research on Cancer has classified it under Group 2A (probably carcinogenic to humans) (IARC, 2019; WHO, 2011; Barbie *et al*., 2005). Mercury (Hg) is a nonessential element to humans, highly toxic and bioaccumulative. Toxic effects of Hg include neurological disorders, kidney damage, benign tumours and genotoxicity (Jaishankar *et al*., 2014).

Lead (Pb) is found naturally in the Earth's crust. It is not essential in the body and is a highly toxic heavy metal. Levels of Pb in drinking water are usually <5 µg/L. Lead accumulates over time in the brain, kidney, liver and bones. It causes low intelligence quotient (IQ) in children due to impaired neurodevelopment, behavioural disorders (aggression, irritability), kidney damage, impaired fertility, adverse pregnancy outcomes (miscarriages and low birth weights) and hypertension (Wani *et al*., 2015).

2.8 Guideline values for drinking-water quality

Since 1958, the World Health Organization (WHO) has published several editions of International Standards for Drinking-Water and subsequently Guidelines for Drinking-Water Quality (GDWQ). The fourth edition of the GDWQ was published in 2011 and was incorporated with the first addendum in 2017. The publications are concerned primarily with the protection of consumers against adverse health effects from water supplies. The guideline values for inorganic contaminants of health significance in drinking water according to WHO and Kenya Bureau of Standards are summarised in Table 2.3 (KEBS, 2018; WHO, 2011).

Table 2.3: Guidelines values for inorganic contaminants in drinking water.

Parameter	WHO guideline value (mg/L)	KEBS guideline value (mg/L)
Aluminium	-	-
Arsenic	0.01 (A, T)	0.01
Barium	0.7	0.7
Beryllium	-	-
Boron as boric acid	2.4	0.3
Cadmium	0.003	0.003
Chromium	0.05 (P)	0.05
Copper	2	1
Iron	-	-
Fluoride	1.5	1.5
Lead	0.01 (A, T)	0.01
Manganese	-	0.5
Mercury	0.006	0.001
Nickel	0.07	0.02
Nitrate (as NO_3^-)	50	50
Nitrite (as NO_2^-)	3	0.003
Phosphates	-	2.2
Selenium	0.04 (P)	0.01
Silver	-	-
Zinc	-	-

(A) Provisional guideline value since the calculated guideline value is below the achievable quantification level.

(P) Provisional guideline value because of uncertainties in the health database.

(T) Provisional guideline value because the calculated guideline value is below the level that can be achieved through practical treatment methods and source protection.

- Occurs in drinking-water at concentrations below those of health concern.

2.9 CO_2 flux and climate change

Solid Earth degassing exerts major variations in atmospheric CO_2 levels resulting into greenhouse effect with time (Robertson *et al*., 2016). Brune *et al*. (2017) concluded that the long-term climate change and continental fragmentation could possibly be linked via massive CO_2 flux in rift systems. Other reports indicate that super-continent breakup and widespread continental rifting could lead to long-term, massive CO_2 emissions and produce prolonged greenhouse phenomena like that of the Cretaceous (Lee *et al*., 2016).

Deep CO_2 escapes to the surface by volcanism at mid-oceanic ridges, subduction zones and hotspots or through metamorphism of carbonate rocks at the plate convergence zones (Dasgupta and Hirschmann, 2010). However, much higher CO_2 emissions arise from degassing along normal faults and circulation of hydrothermal fluids without volcanic eruptions (Jolie *et al*., 2016; Hutchison *et al*., 2015). From recent studies, the estimated CO_2 emission from the central and northern Main Ethiopian Rift (MER) is 0.52-4.36 Mt yr^{-1} (Hunt *et al*., 2017). Lee *et al*. (2016) reported flux of mantle-derived CO_2 (approximately 4 $Mtyr^{-1}$) through fault systems away from active volcanoes in the Magadi-Natron basin (near the Kenya-Tanzania border) within the East African Rift System (EARS). Aiuppa *et al*. (2019) established that global CO_2 flux from subaerial volcanoes is not adequately quantified which limits the understanding of the deep carbon cycle in the earth.

2.10 Applications and mining of carbon dioxide in Kenya

Carbon dioxide has wide application in life. It is used in fire extinguishers because it neither burns nor does it support combustion and it is denser than air. It is used in the manufacture of carbonated drinks due to its pleasant taste and preservative property. Dry ice (solid CO_2) is used for refrigeration. Supercritical fluid CO_2 is applied as a mobile phase in chromatography and as a solvent to perform extractions (Skoog *et al*., 2007). Carbon dioxide gas is used in development of lasers such as fractional CO_2 skin resurfacing laser (Fritz, 2014).

The economic impact of CO_2 mining in Kenya is quite significant. The mineral is extracted at Kireita spring by Carbacid (CO_2) Limited which is a subsidiary of Carbacid Investment Plc. The mineral production and sales value of CO_2 from year 2007 to 2017 is shown in Table 2.4. This amounts to an annual average of KSh 385.345 million and a total of KSh 4, 238.8 million for the eleven-year period (KNBS, 2018). Therefore, discovery and exploitation of additional CO_2 mineral sites in other parts of Kenya would boost the national income.

Table 2.4: Quantity and value of CO$_2$ mineral production in Kenya from 2007-2017.

Year	Quantity (Tonnes)	Value (KSh million)
2007	11,028	78.6
2008	22,030	117.9
2009	15,711	84.0
2010	16,345	98.0
2011	15,197	411.0
2012	19,919	503.0
2013	18,436	495.6
2014	19,450	503.9
2015	19,750	525.6
2016	15,493	831.8
2017	11,855	589.4
Total	84,984	4,238.8

(Source: KNBS, 2018).

2.11 Theory of instrumentation

The main instrumental methods employed in this study were non-dispersive infrared (NDIR) CO$_2$ sensor, cavity ring-down spectroscopy (CRDS), ion chromatography (IC), inductively coupled plasma-optical emission spectrometry (ICP-OES), flame atomic absorption spectrometry (AAS), graphite furnace atomic absorption spectrometry (GFAAS), X-ray fluorescence (XRF) and X-ray diffraction (XRD).

2.11.1 Non-dispersive infrared (NDIR) CO$_2$ sensor

Gases like CO$_2$ absorb infrared (IR) light, causing the molecules to vibrate (stretch or bend). An IR spectrum of a particular molecule is unique and can act as a fingerprint or signature to identify the molecule of interest. CO$_2$ has absorbance bands in the IR region of the electromagnetic spectrum at wavelengths of 2.7 μm (combination), 4.26 μm (stretch) and 15 μm (bend) as shown in Figure 2.6. The strong absorbance with minimal interference at 4.26 μm (~2350 cm^{-1}) caused by asymmetrical stretching vibrations is generally used in NDIR sensors (Park *et al*., 2010).
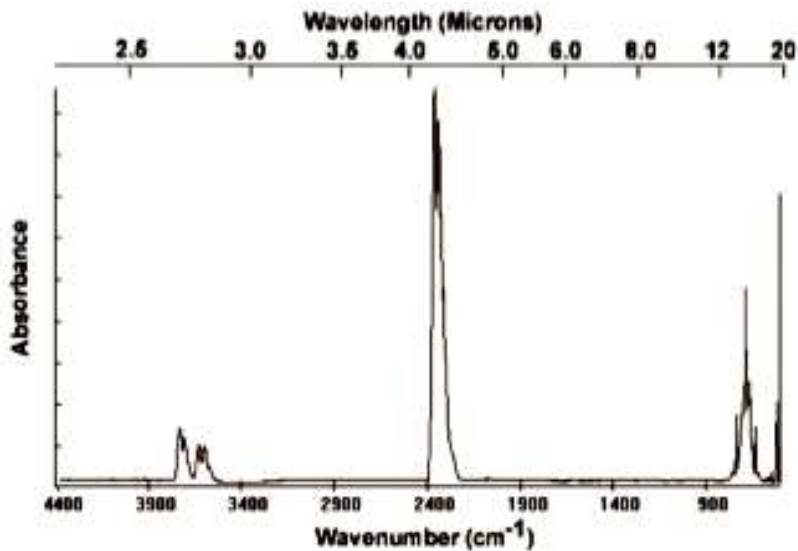
Figure 2.6: Typical IR spectrum of CO₂.

The term non-dispersive means that all the light passes through the gas sample and then gets filtered before reaching the detector. Polychromatic light coming from the incandescent bulb is passed through the gas sample which absorb the light in proportion to the amount of CO_2 present (Figure 2.7). The internal wall reflections of light increases its path length hence increasing sensitivity of the device. The remaining light fall on an optical filter which absorbs all other wavelengths of light except that at 4.26 μm absorbed by CO_2 (Kaur *et al*., 2015; Wang *et al*., 2005). The absorbance of the CO_2 is directly proportional to its concentration over a limited concentration range, in accordance with the Beer- Lambert's law.

A = ε c l   Beer-Lambert's law   (2.10)

where A is the measured absorbance, c is the concentration of the absorbing species, l is the path length (sensor cavity depth) and ε is a proportionality constant known as molar absorptivity or molar extinction coefficient (Christian, 2004).
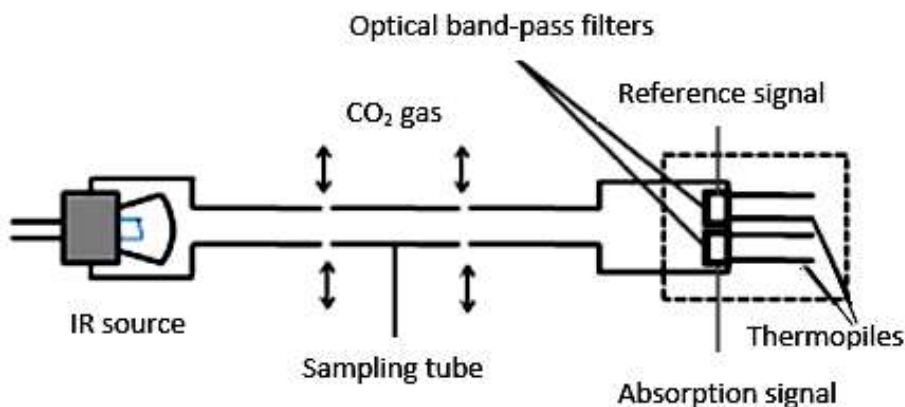
Figure 2.7: A schematic diagram of a NDIR gas sensor.

2.11.2 Cavity ring-down spectroscopy (CRDS)

Cavity ring-down spectroscopy (CRDS) uses a high sensitivity path length of up to several kilometers which enables gases to be monitored in seconds or less at parts per million (ppm) to parts per billion (ppb) levels (Wahl *et al.*, 2006). In CRDS, the near infrared light from a tunable laser diode enters an empty cavity containing two or more high reflectivity mirrors (Figure 2.8).
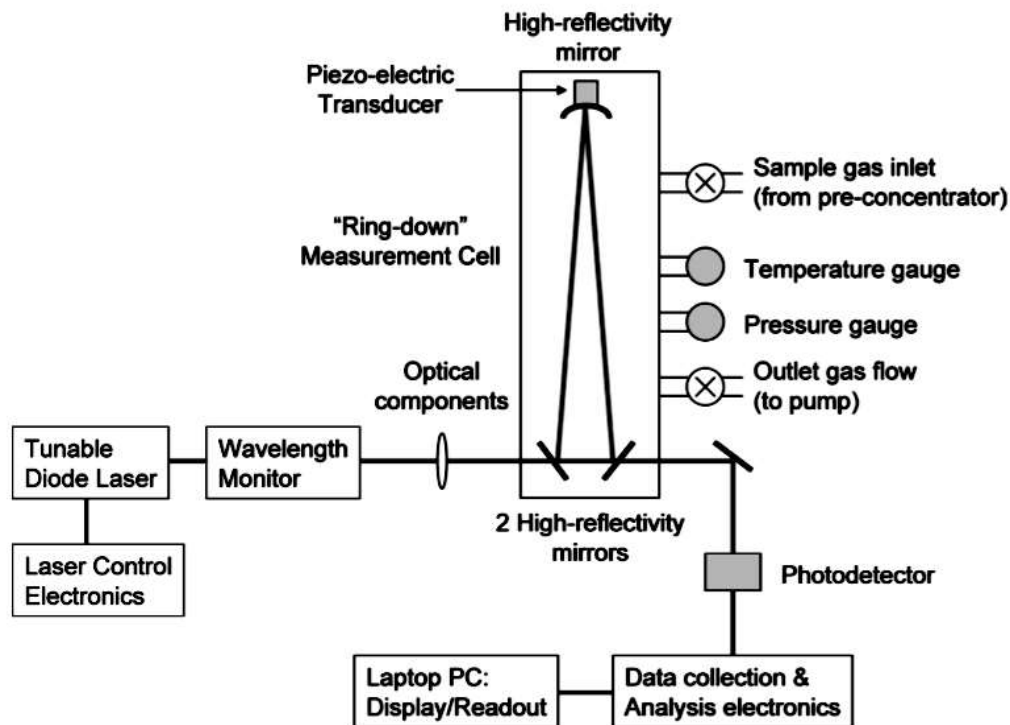
Figure 2.8: Schematic diagram of Picarro CRDS instrument.

The cavity is quickly filled with circulating laser light which bounces continuously between the mirrors (about 100,000 times). As a result, the effective path length can be over 20 km for a cavity of just 25 cm in length. A small amount of light leaking through one of the mirrors is sensed by the photodetector and produce a signal that is directly proportional to the light intensity in the cavity. The photodetector signal reaches a threshold level in a few microseconds and the continuous wave (CW) laser is immediately turned off. The light intensity inside the cavity steadily leaks out and decays exponentially over time to zero because the mirrors reflectivity is slightly less than 100% (99.999%). This decay or "ring-down", is measured in real-time by the photodetector giving the amount of time taken for the ring-down to happen (Dickinson *et al.*, 2017).

27

The transmitted light, I (t, λ), from the CRDS is given by Equation 2.11.

$$I(t, \lambda) = I_0 e^{-t/\tau(\lambda)} \tag{2.11}$$

where I_0 is the transmitted light at the time the light source is shut off, $\tau(\lambda)$ is the ring-down time constant, and $1/\tau(\lambda)$ is the decay rate.

When a targeted light absorbing gas such as CO_2 is introduced into the cavity, a second loss mechanism (absorption) within the cavity takes place. This accelerates the ring-down time compared to that of an empty cavity. The quantitative measurements of the analyte is derived from the difference between these rings-down times and is therefore independent of laser intensity fluctuations or absolute laser power. The optical loss or absorption by the gas is rendered into a time measurement (Figure 2.9). When a sample is inserted, the instrument takes multiple absorption spectra (6261.5 to 6262.4 cm^{-1}) and computes the average value of $^{13}C/^{12}C$ isotopic ratio in CO_2 (Wahl *et al.*, 2006).
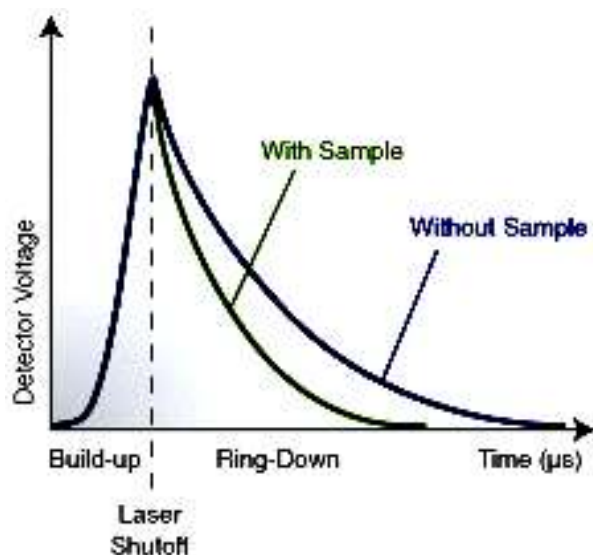
Figure 2.9: Light signal intensity as a function of time in a CRDS system.

The C-13 content of a sample is calculated by comparison with a reference CO_2 gas calibrated against VPDB standard and expressed using the delta (δ) notation in parts per thousand or per mil (δ ^{13}C ‰). Calibration of the instrument is done with Certified Reference Materials (CRMs) NBS 18 and NBS 19 traceable from the National Institute of Science and Technology (NIST) which have certified $\delta^{13}C$-VPDB values of -5.014 ‰ and +1.95 ‰, respectively. Other internal standard materials with measured $\delta^{13}C$-VPDB values such as $NaHCO_3$ (-2.753 ‰) or $CaCO_3$ (-9,650 ‰) may also be used (Mahar *et al.*, 2014).

2.11.3 Ion chromatography (IC)

Chromatography is an analytical technique of separating mixtures of substances based on their distribution between mobile and stationary phases. The mobile phase travels in a given direction. Ion-exchange processes are based on exchange equilibria between ions carried by the mobile phase and ions of like charge on the surface of insoluble stationary phase (resin). The ions of the mobile phase compete with the analyte ions for the active sites on the ion-exchange packing. Separation of different ions depends on their relative affinity to the ion-exchange sites on the resin as guided by the mass-action law (Skoog *et al*., 2007; Michalski, 2006).

The most commonly used stationary phase cation-exchangers are the strong acid sulphonic group, $R\!-\!SO_3^-H^+$, and the weak acid carboxylic group, $R\!-\!COO^-H^+$. Anion exchangers include the strong base quaternary amine group, $R\!-\!N(CH_3)_3^+OH^-$, and weak base primary amine, $R\!-\!NH_3^+OH^-$. Equation (2.12) shows an anion-exchange resin interaction with analyte anions, $A^{n-}_{(aq)}$.

$$nR\!-\!N(CH_3)_3^+OH^-_{(s)} + A^{n-}_{(aq)} \rightleftharpoons [R\!-\!N(CH_3)_3^+]_n A^{n-}_{(s)} + nOH^-_{(aq)} \qquad (2.12)$$
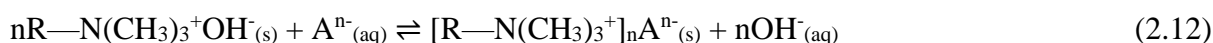
Elution of the analyte with a dilute solution of a base (mobile phase) shifts the equilibrium in Equation 2.9 to the left, causing part of A^{n-} anions in the stationary phase to be transferred to the mobile phase. The analyte ions continue moving down the column in a series of transfers between the stationary and mobile phases until they arrive at the detector. In ion chromatography (IC), the detector usually measures electrolytic conductivity of the eluate. A chromatogram of results is recorded as a plot of conductivity versus retention time (Figure 2.10).
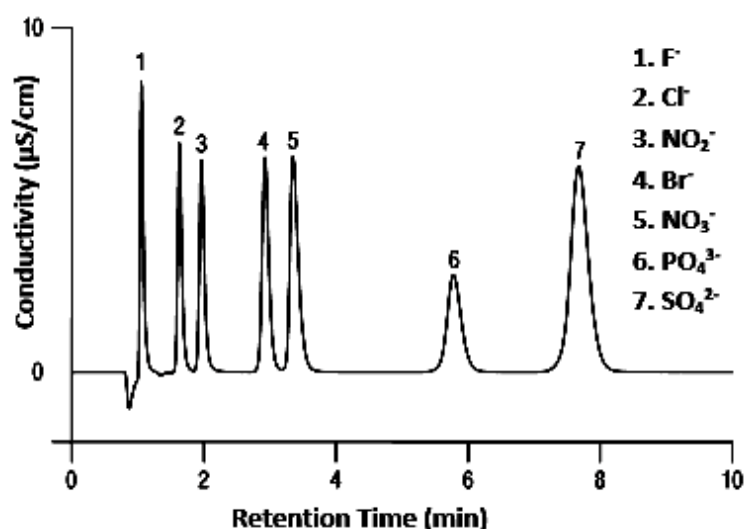
Figure 2.10: Typical anion chromatogram profile.

Qualitative determination is achieved by matching the retention time of analyte against standard signal. Quantitative information is obtained by comparing peak area or peak height of the analyte to the calibration curve of respective standards. IC is particularly important for the determination of inorganic anion and cation mixtures because it is fast, convenient and has greater precision compared to wet-chemical methods (Gros and Gorenc, 1997; US EPA, 1993).

Conductivity interference of the eluting solution is overcome by placing an eluent suppressor column between the ion-exchange (analytical) column and the detector (Figure 2.11). The chemical suppressor column contains a second ion-exchange resin that converts the ions of the eluting solution to molecular species of limited ionisation without affecting the conductivity due to analyte ions (Rouessac and Rouessac, 2007).
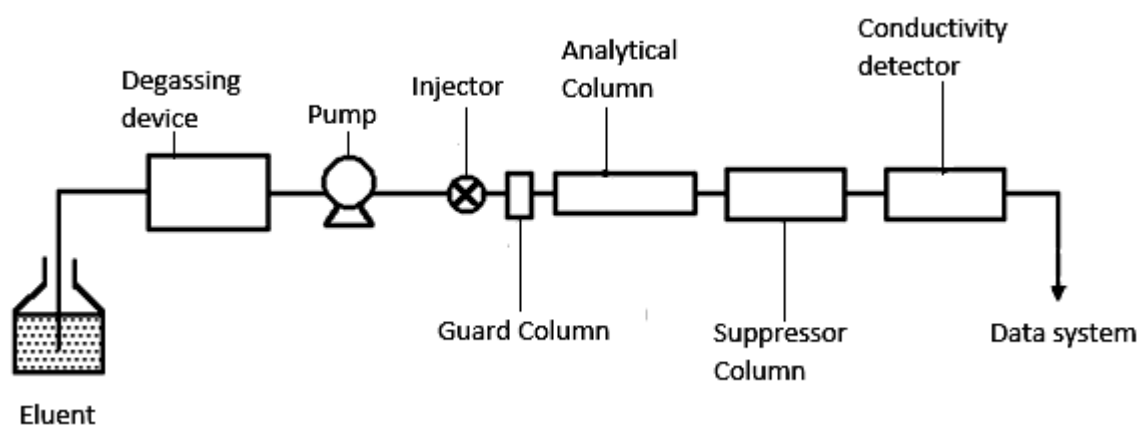
Figure 2.11: Features of ion chromatography system.

For anion separations, the suppressor packing is the acid form (H^+) of a cation-exchange resin and $NaHCO_3$, Na_2CO_3 or $NaOH$ is the eluting agent which exhibits high conductivity. Equation (2.13) shows the process taking place as $NaHCO_{3(aq)}$ passes through the acid form suppressor column. The $H_2CO_{3(aq)}$ formed is largely undissociated and does not contribute significantly to the conductivity.

$$NaHCO_{3(aq)} + resin^-H^+(s) \rightleftharpoons resin^-Na^+_{(s)} + H_2CO_{3(aq)} \tag{2.13}$$

Equation (2.14) shows the interaction between the analyte anions emerging from the ion-exchange column, $Na_nA_{(aq)}$, and the suppressor column.

$$Na_nA_{(aq)} + resin^-H^+_{(s)} \rightleftharpoons nresin^-Na^+_{(s)} + H_nA_{(aq)} \tag{2.14}$$
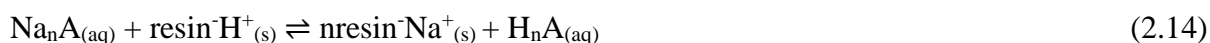
The suppressor column does not retain the analyte anions but converts them into acid form, $H_nA_{(aq)}$. Thus, suppressor column enhances anions conductivity detection while suppressing the background conductivity.

When cations are being analysed, the suppressor column is an anion-exchange resin in the OH^- form and HCl is the eluent. The product of the reaction is H_2O molecules which have limited conductivity (ASTM, 1999).

$$HCl_{(aq)} + resin^+OH^-_{(s)} \rightleftharpoons resin^+Cl^-_{(s)} + H_2O_{(l)} \tag{2.15}$$

Micromembrane suppressors that operate continuously are used in which the suppressor and eluent solutions flow in opposite directions on either side of the permeable ion-exchange membrane to regenerate the packing back to the acid or base form. In modern IC instruments, regeneration of suppressor solutions containing H^+ or OH^- ions is achieved automatically by electrolysis so that interruptions in the use of the instrument for regeneration is avoided (Rouessac and Rouessac, 2007; Skoog *et al*., 2007; Haddad, 2004).

2.11.4 Inductively coupled plasma-optical emission spectrometry (ICP-OES)

Plasma is an electrically conducting gaseous mixture containing cations and electrons. ICP-OES is based on the emission of light upon the relaxation of electrons from excited states under plasma conditions. An ICP torch is used for the atomisation and excitation of analyte. The ICP source consists of a flowing stream of argon gas ionised by an applied radio frequency (RF) field typically oscillating at 27 to 40 MHz. The field is inductively coupled to the ionised gas by a water-cooled copper coil surrounding a quartz torch that supports and confines the plasma. The ''seed'' electrons and ions are generated in the argon gas inside the induction region using a spark from a Tesla coil. These ions and electrons are accelerated by the magnetic field and collide with other argon atoms, causing further ionisation in a chain reaction manner. The ICP sustains a temperature of approximately 10 000 K mainly at its core due to the RF-induced collisions (Higson, 2006; Hou and Jones, 2000; Botto, 1984).

The solution to be analysed is conducted by a peristaltic pump through a nebulizer into a spray chamber. Sample aerosol generated is carried into the plasma torch which subjects the constituent atoms to temperatures of about 6000 to 8000 K. Energy transfer from the plasma to the sample stream causes desolvation, atomisation and ionisation of the target elements. The high temperature of the plasma excites atomic emission efficiently and allows determination of many elements. Ionisation of a high percentage of atoms produces ionic emission spectra which are quantitatively detected by the spectrometer (Figure 2.12).
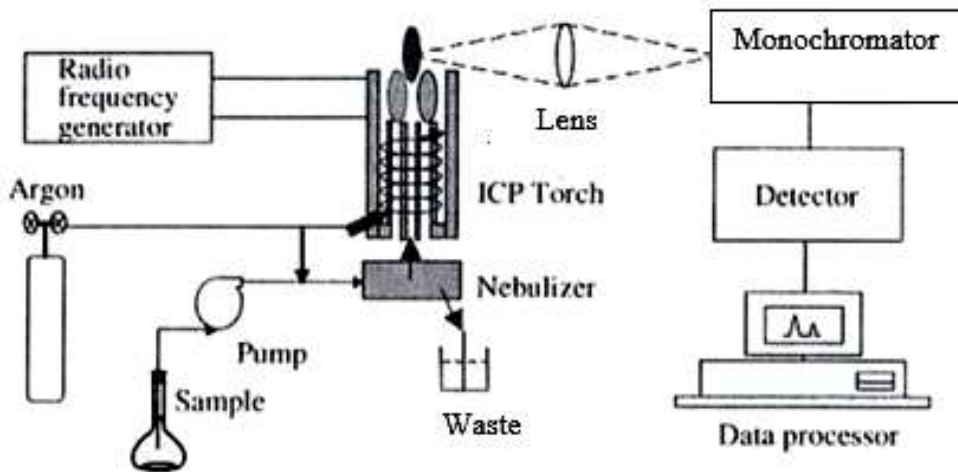
Figure 2.12: ICP-OES instrument main features.

The light emitted from the ICP is focused onto the entrance slit of either a sequential monochromator or a simultaneous multi-channel polychromator that effects dispersion into respective wavelengths. A precisely aligned exit slit isolates a portion of the emission spectrum for intensity measurement using a photomultiplier tube (PMT) which is connected to a computer-controlled readout system (Garbarino *et al.*, 1985). The total number of photons or intensity emitted is directly proportional to the concentration of the element in the sample based on the Beer-Lambert's law. Standard solutions containing the element of interest are used to produce a calibration curve that is relied on to obtain the unknown concentration in the samples by interpolation (Figure 2.13).
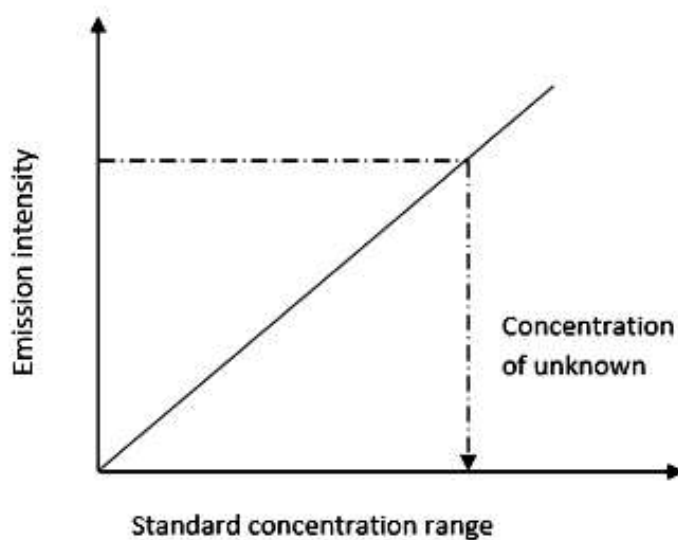
Figure 2.13: A typical external-standard calibration curve.

The efficient excitation provided by the ICP gives low detection limits for many elements. The extended linear dynamic range of four to six orders of magnitude displayed by the ICP-OES permits the analysis of elements over a wide concentration range, without the need to dilute the samples frequently. These factors, combined with high degree of selectivity, good precision and accuracy permits effective multi-element determination of trace metals in parts per million (ppm) to parts per billion (ppb) range (Fassel, 1986).

2.11.5 Atomic absorption spectrometry (AAS)

The working principle of AAS involves the tendency of atomised element to absorb energy coming from a light beam of a specified wavelength. This causes transition of the atoms from ground to excited states and the decrease of light intensity after absorption is measured (Skoog *et al*., 2004). In flame AAS, the sample is aspirated via a nebulizer into the flame (Figure 2.14). The analyte species is atomised by the hot flame consisting of either acetylene-air or acetylene-nitrous oxide mixture with temperatures round 2200 and 3000 °C, respectively. A hollow cathode lamp (HCL) or an electrodeless discharge lamp (EDL) produces a light beam at a wavelength specific to the analyte species which is passed through the flame where absorption takes place. The light then passes through the monochromator which selects a narrow band of wavelength that enters into the photomultiplier detector and the resulting signal is displayed on the read-out.
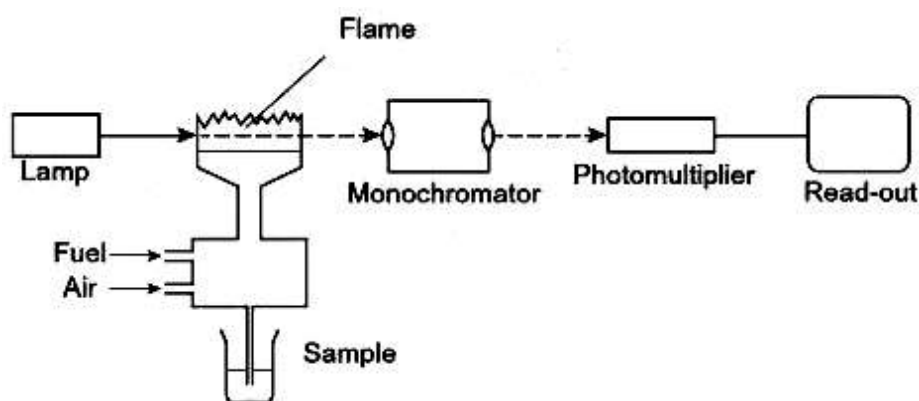
Figure 2.14: Flame atomic absorption spectrometer.

The amount of energy absorbed is proportional to the concentration of the analyte in the sample as per Beer-Lambert's law. Quantitative analysis is based on calibration curves with respective standards (Christian, 2004). Figure 2.15 shows the linear calibration plot for the method of standard-addition. The concentration of the unknown sample is calculated from the slope and y-intercept of the plot or determined by extrapolation.
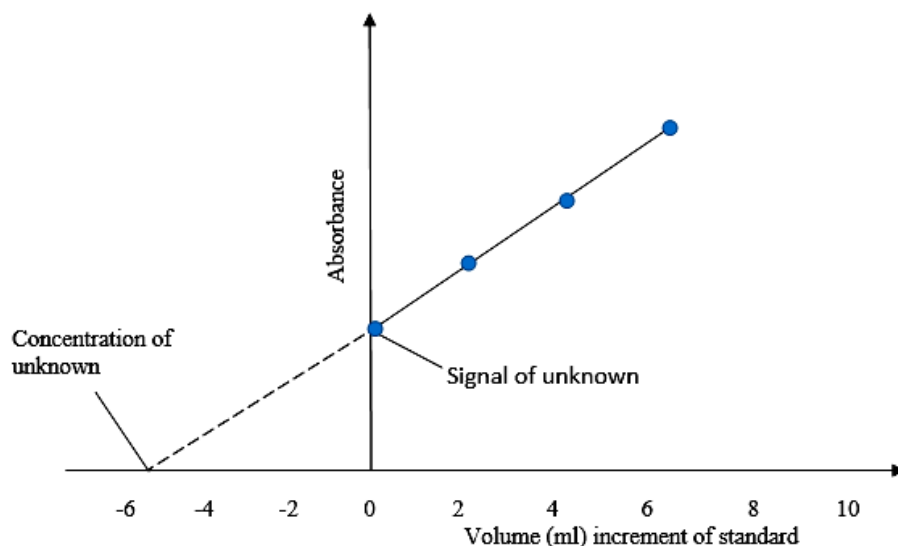
Figure 2.15: Standard-addition calibration plot.

AAS has proved to be reliable and flexible technique for the analysis of many metals in parts per million (ppm) range and is limited only by the availability of a suitable hollow cathode discharge lamp for the element in question. Most atomic absorption instruments are also equipped for operation in an emission mode, which may provide better linearity for strongly emitting elements such as sodium and potassium.

Graphite furnace AAS uses electrical heating element to atomise the sample instead of the fuel/oxidant flame (Figure 2.16). Compared to Flame AAS, graphite furnace AAS has greater sensitivity thus lower detection limits up to parts per billion (ppb) or lower. It can analyse little volumes of samples (10 μL or less) and hence suitable for micro-analysis applications. Graphite furnace AAS allows the determination of different forms of samples ranging from solids, solutions and gaseous vapours (Higson, 2006).
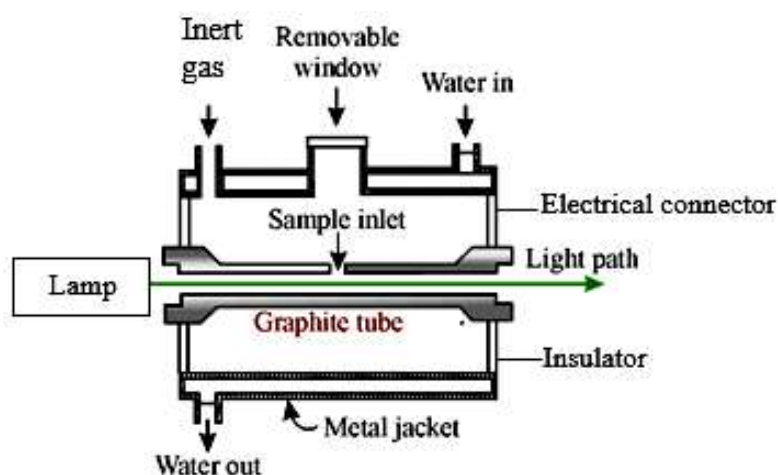
Figure 2.16: Graphite furnace tube.

2.11.6 X-ray fluorescence (XRF)

XRF is a non-destructive (ND) technique used for elemental analysis of materials upon collision with X-ray radiation. It is fast and sample preparation is easy. X-rays are short-wavelength (about 10^{-3} Å to 100 Å) electromagnetic radiation produced by the deceleration of high-energy electrons or by electronic transitions of electrons in the inner orbitals of the atoms. XRF technique is largely confined to the region of about 0.1 Å to 25 Å (Skoog *et al.*, 2007).

Continuum primary X-ray radiation can be generated by bombardment of a metal target such as tungsten, molybdenum or chromium with a beam of high-energy electrons. Electrons are produced at a heated cathode filament in an X-ray tube and accelerated towards a metal anode (target) using a potential difference as great as 100 keV. The irradiation of a sample by these primary photons having sufficient energy to eject electrons from the inner K and L shells of the constituent atoms. This produces characteristic spectra (secondary fluorescence X-rays) of these atoms as other outer orbital electrons move to fill the vacated positions. An element can only emit X-ray when the energy of the incident X-ray is greater than the binding energy of the element's inner-core electrons. The wavelengths of the secondary fluorescence X-rays are independent of the primary radiation, depending only upon the nature of the excited atoms (Higson, 2006). Figure 2.17 illustrates a simplified diagram of energy-dispersive spectrometer (EDXRF).
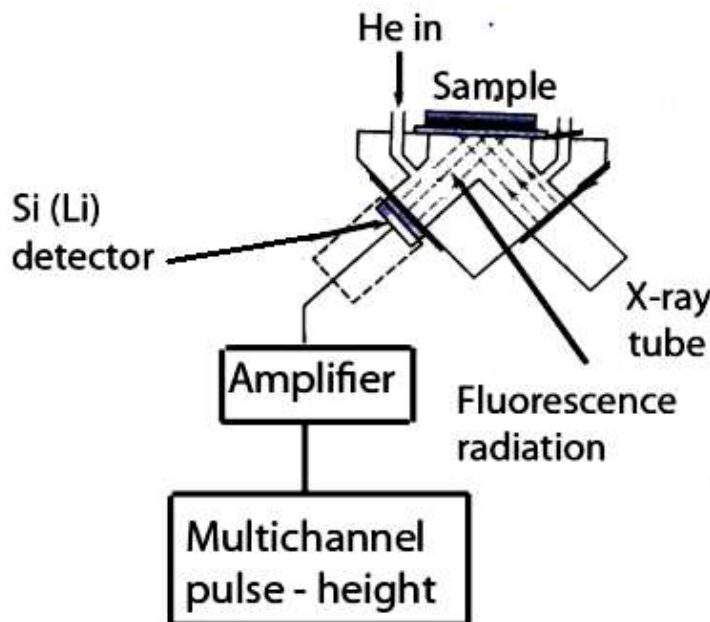
Figure 2.17: Schematic design of EDXRF.

Energy-dispersive spectrometers (EDXRF) have a detector that can measure the different energies of the characteristic emitted spectra to yield a graph of intensity (Y-axis) versus energy (X-axis). The unique line spectra produced by each element could be used to identify the element. Relative intensities of the elemental lines in different samples would also give an estimate of concentrations (Tsuji *et al*., 2012; Skoog *et al*., 2004).

The minimum acceleration voltage required for the excitation of the lines of each element increases with atomic number. Fluorescence appears in the broad energy range from 40 eV to more than 100 keV. XRF is usually associated with the excitation and relaxation of electrons with larger energetic transitions that correspond to the absorption and emission of X-ray radiation (which may apply to elements with atomic weight greater than 20). XRF spectrometry is mostly used for identifying and quantifying heavy metals within compounds or in their elemental form, particularly the major oxides of Si, Al, Ca, Fe, K, Mg, Mn, Na, and Ti in rocks (Ryan *et al*., 2017; Lemiere *et al*., 2014; Rouessac and Rouessac, 2007). Technological advances in electronics miniaturisation have enabled the manufacture of portable EDXRF spectrometers.

2.11.7 X-ray diffraction (XRD)

X-ray diffraction is a nondestructive method for determining the arrangement of atoms and mineral phase composition in a crystalline sample. X-ray diffraction is a form of elastic scattering of radiation by electrons (scatterers). X-rays are used to produce the diffraction pattern because their wavelength λ is typically the same order of magnitude as the spacing *d* (1–100 Å)*,* between planes in the crystal (Bunaciu *et al*., 2015; Garman and Schneider, 1997).

When a monochromatic beam of X-rays passes through a crystalline sample, constructive interference takes place and the rays are diffracted under Bragg's Law conditions (Stanjek and Häusler, 2004).

$$n \lambda = 2\,d \sin \theta \qquad \text{Bragg's Law} \qquad (2.16)$$

Where *n* is any integer, and λ is the wavelength of the X-ray beam, *d* is the spacing between diffracting planes in the crystal and θ is the incident angle. The law relates the diffraction angle and the lattice spacing in the crystalline sample to the wavelength of X-ray (Figure 2.18).
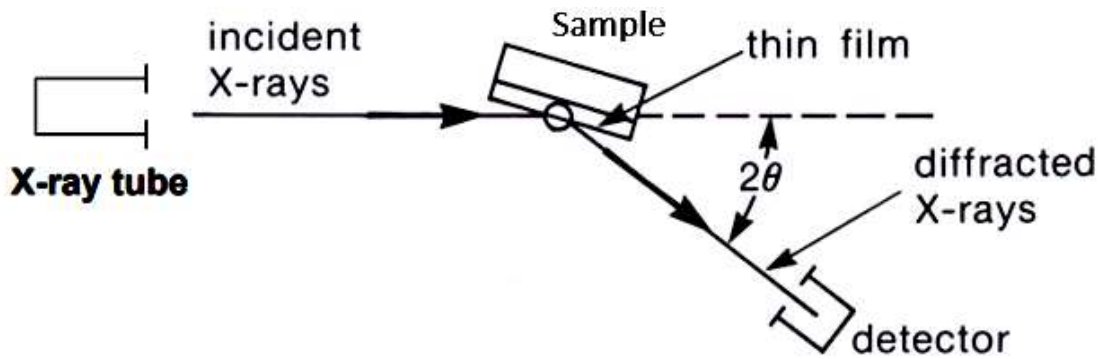
Figure 2.18: Basic features of XRD diffractometer.

A unique fingerprint X-ray diffraction pattern called diffractogram is produced which is characteristic of the sample crystalline structure or mineral phase. Diffractogram plot represents the intensity of diffraction pattern as a function of the diffraction angles (Figure 2.19). Identification of a crystalline phase is based on comparison between the diffraction angles of a reference material and the sample under investigation. The International Centre for Diffraction Data (ICDD) produces databases such as the Powder Diffraction File (PDF) which contains over 300,000 diffraction patterns for reference purposes (Faber and Fawcett, 2002).
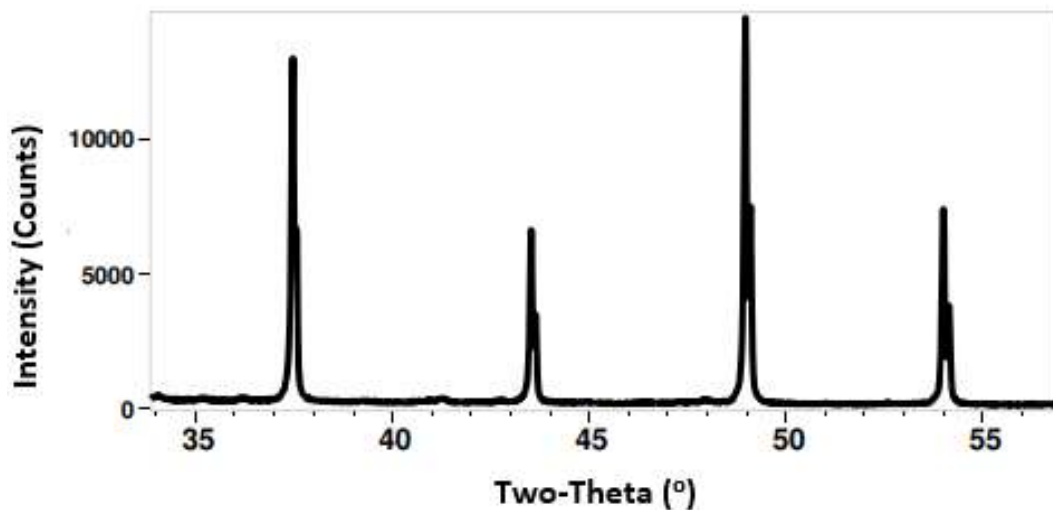
Figure 2.19: A typical XRD pattern.

2.12 Evaluation of analytical data

Evaluation of accuracy level of analytical data is vital because data of unknown reliability could be useless. Various statistical tools are applied in assessment of analytical data such as standard deviation (SD), relative standard deviation (RSD), correlation coefficient, coefficient of determination and *t*-test. Data analysis can be computed using Microsoft Excel Software or other types of statistical packages like Statistical Package for the Social Sciences (SPSS) and RStudio Open Source (Skoog *et al*., 2007).

2.12.1 Standard deviation

Standard deviation (SD) shows the spread of data around the mean for a set of replicate measurements. It is a measure of the variation of replicate measurements which is attributed to random errors. Sample standard deviation (s) is calculated for data sets with 10 or less data values as expressed in Equation (2.17) (Huck, 2004).

$$s = \sqrt{\frac{1}{N-1}\sum_{i=1}^{N}(x_i - \bar{x})^2}$$

(2.17)

where N refers to the number of degrees of freedom, x_i is the measured value and $\bar{x}$ is the mean value.

Relative standard deviation (RSD) or coefficient of variation is the standard deviation when expressed in percentage form. RSD < ±5% is considered acceptable for research purpose.

$$RSD = (s/\bar{x}) \times 100$$

(2.18)

2.12.2 Correlation coefficient

Correlation is a statistical measure of how a pair of data sets fluctuates together. Pearson correlation coefficient (r) is commonly used to measure the strength and direction of linear relationship between two variables. Correlation is positive when both variables increases and negative when one variable increases while the other decreases (Figure 2.20). The value of correlation coefficient varies between +1 and -1 such that $-1 \leq r \leq +1$. A value of +1 shows a perfect positive correlation and -1 indicates perfect negative correlation while 0 indicates no correlation at all. A correlation r > 0.8 is normally described as strong and weak for a correlation r < 0.5 (Zaid, 2015).
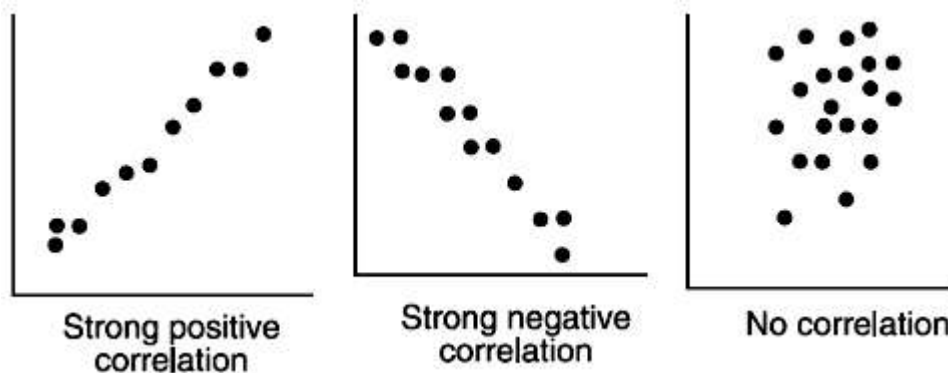
Figure 2.20: Correlation patterns.

2.12.3 Coefficient of determination

Coefficient of determination (r^2 or R^2) shows the proportion of variance or fluctuation of one variable that can be predicted from the other variable. It denotes the strength of a linear relationship between two variables and represents the percent of the data that is closest to the regression line (line of best fit) or how well the regression line represents the data (Skoog *et al*., 2007).

The coefficient of determination is such that $0 \leq r^2 \leq 1$. In a case where r = 0.9, r^2 = 0.81 which means that 81% of the variation can be explained by the linear relationship between two variables. Hence, the unknown values of a given variable may be derived from the linear regression equation. High regression values ($r^2 > 0.99$) are considered appropriate for the application of scientific data (Figure 2.21).
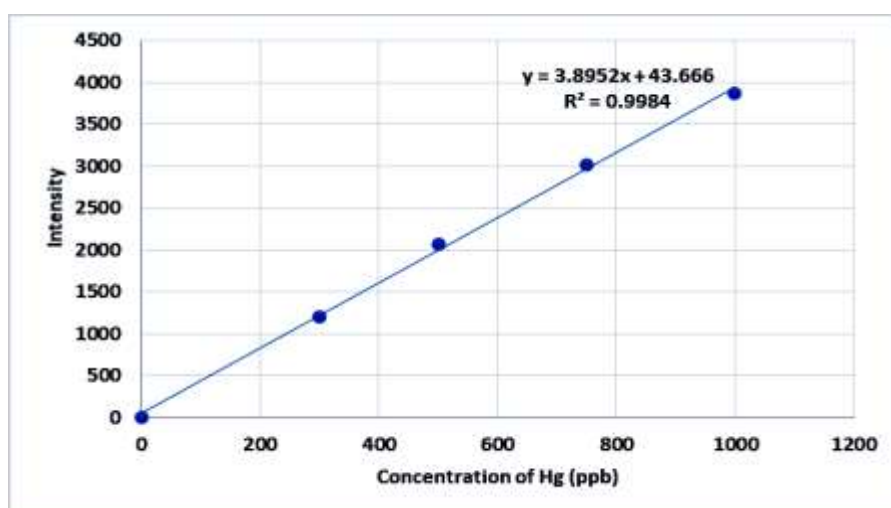
Figure 2.21: Coefficient of determination.

2.12.4 Student's t-test

A *t*-test also referred to as Student's *t*-test is a form of inferential statistic which helps to establish if there is a significant difference between the means of two related data sets such as data representing wet and dry seasons. It is normally used to compare the means of two data sets and show whether they came from the same population. It is a tool for testing hypothesis or an assumption applicable to a population (Roussas, 1997). The *t*-test uses the Student's *t*-distribution values or critical values as indicated in Table 2.5 to determine the statistical significance.

Table 2.5: Student's *t*-distribution values.

Degrees of Freedom *N*-1	Confidence level (%)					
	90	95	97.5	99	99.5	99.9
1	3.078	6.314	12.706	31.821	63.657	318.313
2	1.886	2.920	4.303	6.965	9.925	22.327
3	1.638	2.353	3.182	4.541	5.841	10.215
4	1.533	2.132	2.776	3.747	4.604	7.173
5	1.476	2.015	2.571	3.365	4.032	5.893
6	1.440	1.943	2.447	3.143	3.707	5.208
7	1.415	1.895	2.365	2.998	3.499	4.782
8	1.397	1.860	2.306	2.896	3.355	4.499
9	1.383	1.833	2.262	2.821	3.250	4.296
10	1.372	1.812	2.228	2.764	3.169	4.143

The most commonly used significance level is $\alpha = 0.05$. For a two-tailed test, the level of significance is split into half, $\alpha/2$ or $0.05/2$ and the confidence level is computed as follows: $100(1 - \alpha/2)$, or $100(1 - 0.05/2) = 97.5\%$. For testing hypothesis, the number of degrees of freedom is one less than the population size (*N*-1). For a two-tailed test, with sample size and significance level of 10 and $\alpha = 0.05$, respectively, the critical value ($t_{1-\alpha/2, N-1}$) is found at the intersection of the row representing 9 degrees of freedom and the column for 97.5% confidence level. The critical value is ± 2.262. If the absolute value of the test statistic is less than the critical value (2.262), then there is no significant statistical difference between the means of the two data sets and vice versa. That is, if the absolute value of test statistic is less than the critical value, alternative hypothesis is accepted instead of the null hypothesis (Rees, 2001; Roussas, 1997).

CHAPTER THREE
MATERIALS AND METHODS

3.1 Geographical setting of the study area

The study area is located in Meru County on the Eastern slopes of Mt. Kenya which is about 250 km North-East of Nairobi, Kenya (Figure 3.1).

Figure 3.1: Physical map of Meru County and location of mofette springs.

(Source: Department of Geography and Environmental Studies, University of Nairobi, 2018).

The sites were selected on the basis that volcanic CO_2 degassing seemed to occur through diffuse degassing structures in form of small mofette springs scattered throughout the foothills of the mountain. This suggested that, there could be Earth fractures which act as conduits for the escaping gas from shallow-level magma chamber. The springs in the study area are spread within a distance of about 30 km. Table 3.1 shows the Global Positioning System (GPS) coordinates of the sampling sites and elevation above the sea level.

Table 3.1: Sampling sites GPS location coordinates and elevation.

Spring	Coordinates	Elevation (m)
Gikumene (GIK)	N 00° 01.154' E 037° 38.983'	1566
Kathathantu (KAT)	S 00° 04.799' E 037° 39.639'	1491
Kiambogo (KIA)	S 00° 05.004' E 037° 40.763'	1410
Mbwinjeru (MBW)	S 00° 01.545' E 037° 37.905'	1647
Mulathankari (MUL)	N 00° 02.449' E 037° 40.584'	1425
Nthungu (NTH)	N 00° 00.668' E 037° 38.629'	1601
Rwarera-A (RWA)	N 00° 13.333' E 037° 37.534'	1413
Rwarera-B (RWB)	N 00° 13.401' E 037° 36.759'	1414
Tharu (THA)	S 00° 04.467' E 037° 35.620'	1938
Ukuu (UKU)	S 00° 02.616' E 037° 38.322'	1614

3.2 Sampling criteria

According to the data from the Kenya Meteorological Department (2019), the study area received high rainfall during the months of March-May and November-December in 2018. Table 3.2 shows the rainfall distribution in the study region from March 2018 to February 2019. The researcher considered possibility of seasonal variations in the collected data as a result of increase in volume of water during the wet season. Hence, Water sampling was conducted in May 2018 (wet season) and then repeated in February 2019 (dry season).

Table 3.2: Rainfall data for Meru County from March 2018 to February 2019.

Month	Mar	Apr	May	Jun	Jul	Aug	Sep	Oct	Nov	Dec	Jan	Feb
Amount (mm)	250	473	267	38	18	5	36	76	250	168	80	1

Source: Kenya Meteorological Department, Meru Station, No. 8937065 (2019).

The sampling was conducted at Gikumene, Kathathantu, Kiambogo, Mbwinjeru, Mulathankari, Nthungu, Rwarera-A, Rwarera-B, Tharu and Ukuu springs. Three water samples were collected from each spring per season. For the host rocks, the sampling was undertaken once in May 2018 because their chemical composition was not expected to vary with season. Three grab samples of surface rocks were collected from each spring.

3.3 Instrumentation and chemicals

The main instruments and chemicals (analytical grade) used during the analysis are given in sections 3.3.1 and 3.3.2, respectively. Instrumental analysis was done in collaboration with laboratories at the Kenya Bureau of Standards (KEBS), Directorate of Occupational Safety and Health Services (DOSHS) and Ministry of Petroleum and Mining, in Kenya. Some of the analysis was supported by the University of Hamburg in Germany.

3.3.1 Instruments

Portable conductivity/TDS/pH/Temp meter Tester (HANNA instruments: HI 98129).

NDIR CO_2 Sensor (AZ INSTRUMENT CORP: Testo 435).

CRDS (Picarro Inc. G2101-i Isotopic CO_2).

Potentiometric titrator (Metrohm: 888 Titrando, pH probe: LL Aquatrode + PT 1000).

IC System (Metrohm: 881 Compact IC pro – Anion, Compact IC pro – Cation).

Graphite furnace AAS (Jena Analytik: ContrAA HR-CS- AAS 800 G).

Microwave digester (Anton Paar: Multiwave 5000 PRO).

ICP-OES (Agilent Technologies: 5110 ICP-OES).

AAS (GERMINI BV: VARIAN SPECTRAA-10).

Portable XRF spectrometer (BRUKER: S1 TITAN 800).

Benchtop XRD system (BRUKER: D2 PHASER 2nd Gen.).

3.3.2 Chemicals

Buffers pH 4.01 (HANNA instruments H170004) and 7.01 (HANNA instruments H170007).

Analytical grade HNO_3 (69%), HCl (37%), HF (48%), NaOH (98%), Na_2CO_3 (≥99.5%), $NaHCO_3$, $C_7H_5NO_4$ (99%) and $HgCl_2$ (98%), from Sigma-Aldrich.

TraceCERT® 1000 mL mixed cations and anions IC standard from Sigma-Aldrich.

TraceCERT® 100 mg/L multi-element ICP-OES standard solution from Sigma-Aldrich.

IC check standards (IC-CAT-1 6 component multi-cation standard and IC-1 7 component multi-anion standard) traceable to the National Institute of Standards and Technology (NIST).

ICP-OES check standard (Standard Reference Material, SRM 1643d traceable to NIST).

Rock standards SY-4 and MRG-1 from Canadian Certified Reference Materials Project (CCRMP).

δ ^{13}C NIST traceable CRMs, NBS 18 (-5.014‰), NBS 19 (+1.95‰) and analytical grade CaCO$_3$ (-9.650‰).

3.4 Collection of preliminary views about mofette spring waters from the local community

A questionnaire tool was designed for the purpose of gathering individual experiences about the springs from members of the local community. The structure and full details of the questionnaire are contained in appendix B. Six respondents drawn from the nearby villages were engaged in the exercise per spring giving a total of sixty participants. The inclusion criteria for selecting the respondents was primarily based on the age (18 years and above was acceptable) and whether they were residents within the study area (only those who resided in the study area were eligible). The exclusion criteria that disqualified some of the prospective respondents included lack of cooperation or interest towards the research activity.

The questionnaire mainly contained closed-ended questions to guide the participants to give direct responses. For example, *Does the water have any smell*? In this case the expected response was either *Yes or No*. Likert scale was applied where necessary (Alvin and Ronald, 2008). For example, *How often do you use this water?* Here, the respondents were supposed to choose one answer rated as follows; *most regularly, regularly, not regularly, rarely or not at all*. It also had a few open-ended questions to allow the respondents to state freely some of their views, such as; *Which are the main negative effects of the waters to the users including animals, if any?* The questionnaires were administered either through writing or interview forms depending on the literacy level of the respondent.

3.5 Assessment of CO_2 in the ambient air around the spring sites

Carbon dioxide concentration in the ambient air about 10 cm above the surface of the springs was measured directly using NDIR CO_2 sensor (Testo 435) during the sampling as shown in Figure 3.2 (Park *et al.*, 2010, Frodl and Tille, 2006).

Figure 3.2: Measurement of ambient CO_2 at Mbwinjeru spring using NDIR CO_2 Sensor (Testo 435).

(*Courtesy of Directorate of Occupational Safety and Health Services, DOSHS, Kenya*)

3.6 Determination of the genesis of CO_2 by measuring δ ^{13}C ‰ values of dissolved inorganic carbon (δ ^{13}C$_{DIC}$).

The origin of CO_2 gas dissolved in the water samples was determined by measuring the ^{13}C/^{12}C isotopic ratio in the dissolved inorganic carbon (DIC) which is expressed as ^{13}C ‰ VPDB (Srivastava and Vekouteren, 2018; Laughrey and Baldassare, 2003).

3.6.1 Water sampling for the $\delta^{13}C$ isotope and DIC measurement

Three water samples for DIC and ^{13}C$_{DIC}$ isotope analysis were collected from each spring using 13 mL glass vials. One drop of saturated $HgCl_2$ solution prepared by dissolving excess $HgCl_2$ salt in water was added to each vial to preserve the sample. Caution was taken to ensure that no headspace was left by filling the vials completely with water in order to minimise interference from atmospheric CO_2. Figure 3.3 shows a photograph taken in the field during the sampling.
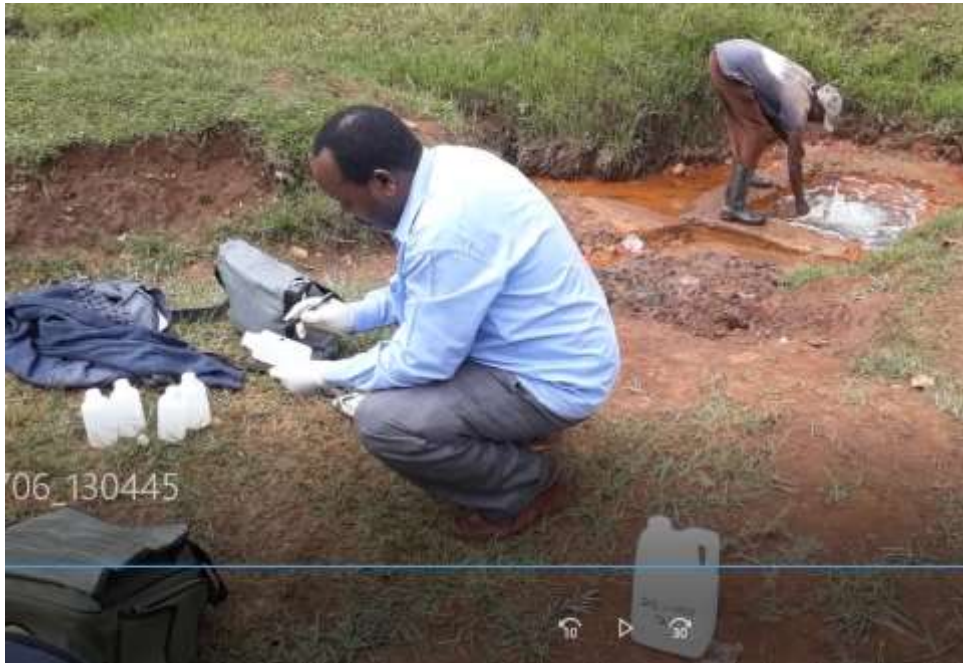
Figure 3.3: Sample collection at Nthungu spring and a villager drawing the water for drinking.

3.6.2 $\delta^{13}C$ *isotope and DIC measurement*

Cavity Ring-Down Spectroscopy (CRDS) method was used for both $\delta^{13}C$ and DIC determination after acid extraction of CO_2 from the water samples (Dickinson *et al*., 2017; Mahar *et al*., 2014; Becker *et al*., 2012; Wahl *et al*., 2006). The instrument (Picarro CRDS G2101-i Isotopic CO_2 Analyzer (Figure 3.4), was calibrated using Certified Reference Materials, NBS 18 (-5.014 ‰), NBS 19 (+1.95 ‰) and analytical grade $CaCO_3$ (-9.650 ‰).

Figure 3.4: Picarro cavity ring-down spectrometer (G2101-i Isotopic CO₂).

(*Courtesy of Institute for Geology, University of Hamburg, Germany*)

Six NBS 18, NBS 19 and $CaCO_3$ standards (0.3, 0.7, 1.0, 1.3, 1.6 and 2.0 mg, for each standard) were weighed into 13 mL vials. The vials were tightly closed and evacuated for five seconds with a vacuum pump (Membrane pump KNF N035.1.2AN.18), set to approximately 850 mbar. Nitrile gloves and safety glasses were put on to avoid contact with the poisonous $HgCl_2$ which had been added during sampling to preserve the water samples. A volume of 2 mL of each sample was drawn with a syringe and transferred into a previously weighed and evacuated vial. The vial was reweighed. Similarly, a method blank was prepared by transferring 2 mL of reagent water into a pre-weighed and evacuated vial.

To measure the δ ^{13}C isotope and DIC of a standard, a sample and blank, 2 mL of 25% (v/v) H_3PO_4 was added to it for the purpose of releasing CO_2 gas. The released CO_2 gas was directed into the Picarro CRDS system. The emerged gas was transported by a constant nitrogen gas flow (75 mL/min for 4 min) and stored in flushed gas bags in the Liaison (A0301) compartment of the Picarro CRDS system. The CO_2 was pumped from the gas bags successfully into the measuring cell. The δ ^{13}C and DIC results of a sample were obtained by comparison with a reference CO_2 gas released from the calibration standards.

3.7 Analysing of major physicochemical characteristics of the spring waters

The physical parameters investigated included temperature (T), pH and electrical conductivity (EC) which were measured in the field during sampling. Total alkalinity (Talk) was determined potentiometrically in the laboratory. The cation species (Li^+, Na^+, NH_4^+, K^+, Ca^{2+} and Mg^{2+}) and anions (Br^-, Cl^-, F^- NO_2^-, NO_3^-, PO_4^{3-}, and SO_4^{2-}) were analysed by ion chromatography (IC). Strontium (Sr^{2+}) was determined by graphite furnace AAS because it was lacking in the mixed multi-ion standard employed for the IC analysis of cations, which was done in Germany.

3.7.1 Water sampling, pre-treatment and in situ measurements

Three water samples were collected and filtered through 0.45 μm filters into clean 300 mL polyethylene terephthalate (PET) bottles without being treated with acid for the ion chromatography and total alkalinity determination. Another set of three 50 mL samples per spring were collected for Sr analysis. They were filtered through 0.45 μm filters, acidified with 500 μL of 69% HNO_3 and preserved at 4 °C in the refrigerator.

Temperature, pH and electrical conductivity of the waters were measured in situ during the sampling using a portable meter (HANNA Instruments HI 98129). The meter was calibrated using 4.01 and 7.01 pH buffers. About 50 ml of each water sample was placed in a clean beaker that had been rinsed with the sample. The electrode was inserted into the water and after the reading became stable, the pH value was recorded.

To measure EC, the meter was calibrated using a standard 0.01 N KCI solution whose conductivity is 1413 µS/cm at 25 °C. The electrode was cleaned with distilled water before measuring the conductivity of each sample (Rusydi, 2018; Van der Aa, 2003). Temperature was recorded by the meter simultaneously during pH and EC measurement.

3.7.2 Total alkalinity (HCO_3^- and CO_3^{2-})

Total alkalinity (Talk) was determined by an automatic potentiometric titration system (Metrohm: 888 Titrando) shown in Figure 3.5. Three replicate samples measuring 30 mL each were titrated with standard 0.02 N HCl to pH 4.5 endpoint. Dickson Standard, Batch 108, was used as check standard.
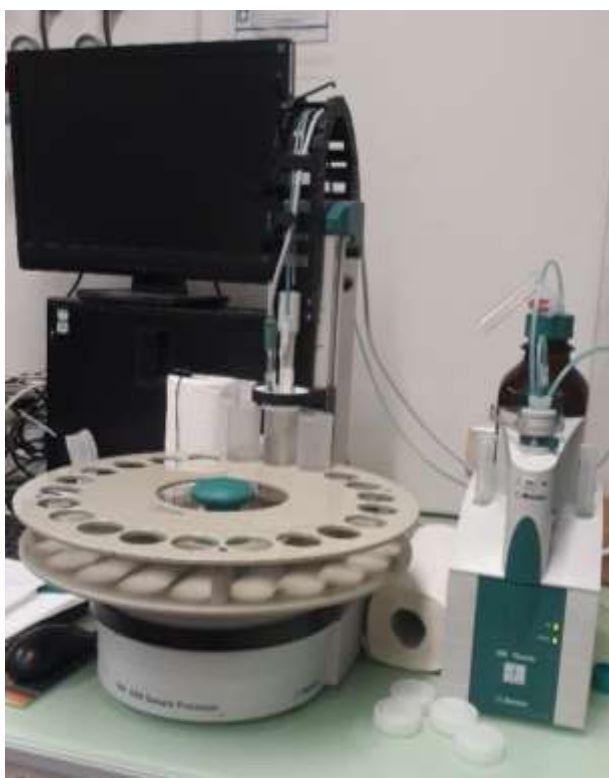
Figure 3.5: Automatic potentiometric titrator (Metrohm: Software Tiamo 2.3, 814 USB sample processor, 888 Titrando, pH probe: LL Aquatrode + PT 1000).

(*Courtesy of Institute for Geology, University of Hamburg, Germany*)

3.7.3 Major ions analysis by IC

As explained in Section 3.7.1, water samples were collected from each spring and filtered into clean PET bottles for the analysis of major ions in the laboratory. Ion chromatography instrument (Metrohm system: 881) equipped with chemical suppressor columns was used to measure the concentration of major ions (Figure 3.6).

Figure 3.6: Ion chromatography instrument (Metrohm system: 881 Compact IC pro – Anion, Cation).

(*Courtesy of Institute for Geology, University of Hamburg, Germany*)

Calibration solutions were made from TraceCERT®, 1000 mL multi-ion standard. A series of calibration standards were prepared with Milli-Q water from the stock solution by applying dilution factors of 20, 25, 30, 35, 40, 50, 60, 70, 80 and 100 as shown in Table 3.3. For the cations analysis, 6.1010.430 Metrosep C 4-150 column was used while anions were analysed with 6.1010.430 Metrosep Asupp 5-150 column. The eluents were composed of 339.2 mg/L Na_2CO_3 and 106 mg/L $NaHCO_3$ for anions while 107.1 mg/L HNO_3 and 116.9 mg/L $C_7H_5NO_4$ (dipicolinic acid, DPA) were used for the cations.

A volume of 20 µL of standards and samples aliquots were injected into the IC system for analysis after filtration through 0.45 µm filters (Michalski, 2006; Gros and Gorenc, 1997; US EPA Method 300.1, 1997). Ten replicates of Milli-Q calibration blanks were analysed for each element and the obtained standard deviations were multiplied by ten to establish their limits of quantitation (LOQ) (Mermet, 2008).

Table 3.3: Concentrations (mg/L) of IC calibration standards.

DILUTION	0	20	25	30	35	40	50	60	70	80	100
F^-	17.088	0.854	0.863	0.570	25.7	0.488	0.342	0.285	0.244	0.214	0.171
Cl^-	60.701	3.035	2.428	2.024	1.734	1.518	1.214	1.012	0.867	0.759	0.607
NO_2^-	19.893	0.995	0.796	0.663	0.569	0.497	0.398	0.332	0.284	0.249	0.199
Br^-	18.485	0.924	0.739	0.616	0.528	0.462	0.37	0.308	0.264	0.231	0.185
NO_3^-	48.121	2.406	1.925	1.604	1.375	1.203	0.962	0.803	0.688	0.601	0.481
PO_4^{3-}	47.13	2.356	1.885	1.571	1.346	1.178	0.942	0.786	0.674	0.589	0.471
SO_4^{2-}	207.798	10.39	8.312	6.926	5.937	5.195	4.156	3.464	2.968	2.598	2.078
Li^+	43.438	2.172	1.738	1.448	1.241	1.086	0.869	0.724	0.621	0.543	0.434
Na^+	84.86	4.243	3.394	2.829	2.425	2.122	1.697	1.414	1.212	1.061	0.849
NH_4^+	60.26	3.013	2.41	2.009	1.722	1.507	1.205	1.004	0.861	0.753	0.603
K^+	84.355	4.218	3.374	2.812	2.410	2.109	1.687	1.406	1.205	1.055	0.844
Ca^{2+}	164.554	8.228	6.582	5.485	4.702	4.114	3.291	2.742	2.351	2.057	1.646
Mg^{2+}	171.379	8.569	6.855	5.713	4.896	4.284	3.428	2.856	2.448	2.142	1.714

3.7.4 Strontium analysis by graphite furnace AAS

Graphite furnace atomic absorption spectrometry (GFAAS) method was used for Sr^{2+} analysis at 460 nm wavelength (Figure 3.7).

Figure 3.7: Contra AAS graphite furnace (HR-CS- AAS 800 G; Jena Analytik).

(*Courtesy of Institute for Geology, University of Hamburg, Germany*)

Method of standard-addition calibration was applied. Strontium nitrate, $Sr(NO_3)_2$, 1000 mg/L standard stock solution in 2% HNO_3 was used to prepare the standards. Two 20 mL sample aliquots were spiked with 1 μg/L and 2 μg/L of freshly prepared Sr standard and then diluted to 50 mL. Strontium measurements were done on 5 μL of the original sample that had not been spiked and the other two spiked samples to obtain a three-point calibration curve. Concentration of the unknown sample was calculated from the slope and y-intercept on the linear calibration plot or by extrapolation (Skoog *et al*., 2007; L'vov, 1988).

3.8 Determination of the levels of essential trace elements and inorganic contaminants in the spring waters.

Nineteen trace elements were analysed by ICP-OES method. They included Ag, Al, As, B, Ba, Be, Cd, Co, Cr, Cu, Fe, Hg, Mn, Mo, Ni, Pb, Se, Si, and Zn.

3.8.1 Water sampling and pre-treatment for ICP-OES analysis

Three water samples were collected straight from each spring in thoroughly cleaned and sterilized 300 mL PET bottles. The water samples were filtered through 0.45 μm millipore filters and the pH reduced to less than 2 by adding 1 mL of concentrated HNO_3 to each sample bottle. The purpose was to minimise the precipitation and adsorption of cations on the walls of the container. The samples were preserved at approximately 4 °C in a refrigerator to prevent change in volume due to evaporation (Eaton, 2005).

3.8.2 Digestion of water samples for ICP-OES analysis

Each water sample was digested with concentrated analytical grade HNO_3 in order to free the metals associated with particulates and dissolve all the analytes of interest. Digestion also reduced interference by organic matter (Eaton, 2005). A volume of 5 mL water sample was placed into a 50 mL digestion vessel, 5 mL of concentrated HNO_3 was added and then the vessel was capped tightly. The mixture was shaken and allowed to stand for 5 minutes. The vessel was loaded into a rotor then transferred into a microwave digester (Anton Paar-Multiwave 5000 PRO) for 15 minutes at 120 °C. After digestion, the sample was allowed to cool to room temperature. The sample vessels was taken to the fume hood and opened carefully. It was kept in the fume hood for 10 minutes to allow venting of gases. The contents were finally transferred into a 50 mL volumetric flask which was topped up with de-ionised water. De-ionised water sample was digested using the same procedure to prepare calibration blank.

3.8.3 Trace element analysis

Trace elements were analysed by ICP-OES instrument (Agilent Technologies: 5110) shown in Figure 3.8, as per US EPA Method 200.7 Revision 5.0 (Cauduro and Ryan, 2017; Kapadnis *et al*., 2016; US EPA, 2001). External calibration standards (100, 250, 500, 750 and 1000 ppb) were prepared from a 100 mg/L multi-element NIST traceable standard stock solution. The instrument was calibrated using the freshly prepared respective standards and calibration curves established (with linear regression coefficient, $R^2 \geq 0.995$). The digested samples were run after calibrating the instrument and concentrations of the different parameters were determined from their respective calibration curves by interpolation. The limit of quantitation (LOQ) for each element was established by analysing ten replicates of calibration blank and multiplying the obtained standard deviation by ten.

Figure 3.8: ICP-OES instrument (Agilent Technologies 5110).

(*Courtesy of Kenya Bureau of Standards, KEBS, Kenya*)

3.9 Determination of geochemical composition and structure of host rocks adjacent to the springs in relation to the origin of solutes in the waters.

Geochemical analysis of the rock samples was performed using AAS, XRF and XRD techniques. Loss on ignition (LOI) values were determined and added together with their respective AAS results. Three replicate samples from each spring were analysed.

3.9.1 Sampling of rocks

Three grab samples were taken from the host rocks around each spring for analysis. The samples were collected from the surface rocks within an area of approximately 10 m^2 around the springs. Weathered surface was scrapped off and the rocks were then placed in canvas bags.

3.9.2 Digestion of rock samples and standards for AAS analysis

The samples were dried in an oven at 110 ^{o}C for 24 hours. They were ground into fine powder and filtered through a 100 μm mesh. For each sample, 0.1000 g was weighed into a Teflon beaker. A volume of 1 mL aqua-regia (concentrated HCl and HNO_3 in the ratio of 3:1), was added followed by 3 mL of concentrated HF. The samples were left to stand for 12 hours. Then 50 mL of saturated boric acid was added to the sample and the mixture left to stand for 1 hour after which 46 mL of distilled water was added. From this digested sample, 5 mL was taken and diluted to 50 mL with 50% (v/v) boric acid (Eaton, 2005; Christian, 2004). Rock standards were prepared by weighing 0.1000 g of SY-4 and MRG-1 standards traceable from the Canadian Certified Reference Materials Project (CCRMP). The rock standards were digested following the same procedure used for the samples.

3.9.3 AAS analysis of rocks

Different concentrations of calibration standards for major oxides were freshly prepared from the digested SY-4 and MRG-1 rock standards as listed in Table 3.4.

Table 3.4: AAS calibration standards.

Oxide	Standard	Concentration (%)		
Al_2O_3	SY-4	2.07	10.35	20.69
CaO	SY-4	0.81	4.03	8.05
Fe_2O_3	SY-4	0.62	3.11	6.21
K_2O	SY-4	0.17	0.83	1.66
MgO	SY-4	0.05	0.27	0.54
MnO	SY-4	0.01	0.06	0.11
Na_2O	SY-4	0.71	3.55	7.1
SiO_2	SY-4	4.99	24.95	49.9
TiO_2	MRG-1	0.75	3.69	7.38

The AAS instrument (VARIAN SPECTRA A-10) shown in Figure 3.9 was then calibrated for each oxide using the prepared standards. Determination of percentage oxides of the major rock forming elements was done in triplicates for every spring. The AAS operating conditions were as shown in Table 3.5.

Figure 3.9: AAS instrument (VARIAN SPECTRA A-10).

(*Courtesy of Geochemistry Laboratory at the Ministry of Petroleum and Mining, Kenya*)

Table 3.5: AAS operating parameters.

Oxide	Wavelength (nm)	Current (mA)	Slit width (nm)	Flame gases*	Flow rate (L/min)
Al_2O_3	309.3	10	0.5	N_2O-C_2H_2	4.5
CaO	422.7	3	0.5	N_2O- C_2H_2	4.5
Fe_2O_3	248.3	5	0.2	Air- C_2H_2	1.5
K_2O	766.5	5	1.0	Air- C_2H_2	1.5
MgO	285.2	3	0.5	N_2O- C_2H_2	1.5
MnO	279.5	5	0.2	Air- C_2H_2	1.5
Na_2O	589.0	5	0.5	Air- C_2H_2	1.5
SiO_2	251.6	15	0.2	N_2O- C_2H_2	4.5
TiO_2	364.3	20	0.5	N_2O- C_2H_2	4.5

  * C_2H_2 = Acetylene, N_2O = Nitrous oxide.

3.9.4 Determination of LOI in rocks

Approximately 1 g of sample was placed in a clean weighed crucible in triplicates. The weight of the sample and crucible was recorded. The sample in the crucible was put in the oven and heated to 1000 ºC. The sample was then removed from the oven, cooled in a desiccator and reweighed. The percent LOI was calculated using the following expression.

$$\% \text{ LOI} = \frac{(\text{wt. of sample + crucible after heating}) - \text{wt. of crucible}}{(\text{wt. of sample + crucible before heating}) - \text{wt. of crucible}} \times 100$$

$$(3.1)$$

3.9.5 XRF analysis of rocks

About 2 g of each ground rock sample (~100 microns) was transferred into the sample holder and scanned with a portable EDXRF (BRUKER S1 TITAN) to a maximum potential of 50 keV (Figure 3.10). Percentage compositions covering Mg-U elemental range were obtained by analysing three replicate samples per spring.

Figure 3.10: Portable XRF Analyzer (BRUKER S1 TITAN 800).

(*Courtesy of Geochemistry Laboratory at the Ministry of Petroleum and Mining, Kenya*)

3.9.6 XRD analysis of rocks

About 2 g of each ground rock sample (~100 microns) was put in a sample holder and scanned up to 70° ($2\theta^{o}$) in the X-ray diffractometer (BRUKER D2 PHASER 2nd Gen.) shown in Figure 3.11. Mineralogical compositions were obtained by XRD search and match analysis of peaks using the computer programmed powder diffraction file (PDF) database.

Figure 3.11: The researcher working with XRD instrument (BRUKER D2 PHASER 2nd Gen.).

(*Courtesy of Geochemistry Laboratory at the Ministry of Petroleum and Mining, Kenya*)

3.10 Quality control

Different approaches for analytical methods validation were adopted. Instruments were calibrated with specific standards before use and high regression values (R^2 >0.99) were ascertained. Calibration verification of the instruments was done by analysing a calibration blank between sample and standard readings to verify the baseline stability. A mid-point calibration standard was analysed after each batch of 3 samples and consequently re-calibrated the instrument when necessary (Eaton, 2005).

Water and rocks CRMs traceable to NIST were analysed as quality control samples to validate the accuracy of analytical methods and laboratory standards. Recoveries within ±5% of the check standard certified value was considered applicable. The check standards were analysed in triplicates to verify the reproducibility of the methods and precision of <±5% RSD was acceptable (US EPA, 2001).

The samples were also spiked with known amount of respective standards to verify the level of matrix interference and good recoveries ranging from 95.65 to 101.44% were achieved. The accepted percent recoveries usually range from 85-115% (Eaton, 2005). Limits of quantitation (LOQ) were established by analysing ten replicates of calibration blanks and multiplying the obtained standard deviation by ten. This ensured that the measured values in the samples were reliably detected and quantified (Kapadnis *et al*., 2016). The quality control data is given in Appendices A-1 to A-5.

3.11 Data analysis and interpretation

The results were computed using Microsoft Excel 2016 to obtain the mean, relative standard deviation (RSD), Pearson correlation coefficient (r), coefficient of determination (r^2) and *t*-test. GW_Chart v.1.30.0 software was used to draw Piper diagrams for the modelling of the springs' water-types (Koh *et al*., 2002). The analysed results were presented in tables, graphs and charts. The acquired data was discussed and compared with results from other similar studies done in different parts of the World. The relevant conclusions and recommendations from the study were reported based on inductive and deductive interpretation of the data (Huck, 2004; Rees, 2001).

CHAPTER FOUR

RESULTS AND DISCUSSION

4.1 Introduction

Two of the specific objectives of this study were to quantify CO_2 emitted from selected springs found in the eastern slopes of Mt Kenya in Meru County and also to establish the genesis of this gas. The springs' names and their codes are Gikumene (GIK), Kathathantu (KAT), Kiambogo (KIA), Mbwinjeru (MBW), Mulathankari (MUL), Nthungu (NTH), Rwarera-A (RWA), Rwarera-B (RWB), Tharu (THA) and Ukuu (UKU).

Noting that the spring waters were used by local residents for domestic and livestock purposes, a questionnaire survey was administered to nearby residents for the purpose of gathering local knowledge regarding the general characteristics, uses and effects of the spring waters. This was followed by characterisation of the spring waters and surrounding rocks. Composition of water was anticipated to show seasonal variations, therefore water sampling was done during the wet and dry seasons, specifically in May 2018 and February 2019, respectively. For the rocks, one sampling programme was carried out as no seasonal variation was expected. In situ measurements of temperature, pH, EC and ambient CO_2 were done during these sampling periods. Laboratory investigations were carried out on 6 samples of water (each season 3 samples) and 3 rock samples from each of the 10 mofette springs. This chapter presents the results, correlations and discussions obtained in this study.

4.2 Photographs of some of the springs sites

Figures 4.1 to 4.6 are photographs taken by the author on 16th and 17th September 2016, during a reconnaissance trip to the study area.

Figure 4.1: Rwarera-A spring site in Ruiri covered with sedimentary carbonate rocks.

Figure 4.2: Mulathankari spring near Meru town.

Figure 4.3: Mbwinjeru spring near Kariene market.

Figure 4.4: Tharu spring and surrounding host rocks, about 8 km from Nkubu town.

Figure 4.5: Kiambogo spring located in a quarry near Nkubu town.

Figure 4.6: The researcher standing on host rocks at Rwarera-B spring in Ruiri.

As observed in the photographs (Figures 4.3, 4.4 and 4.5), brown precipitate which is $Fe(OH)_3$ occurs at Mbwinjeru, Tharu and Kiambogo springs. The $Fe(OH)_3$ forms when aqueous Fe^{2+} is oxidised to the less soluble Fe^{3+} after the water is discharged at the surface according to equation (4.1) (Andrews *et al*., 2004).

$$4Fe^{2+}_{(aq)} + O_{2\,(g)} + 10H_2O_{(l)} \rightarrow 4Fe(OH)_{3\,(s)} + 8H^+_{(aq)} \tag{4.1}$$
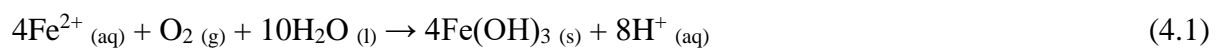
4.3 Local community views about the mofette spring waters.

Preliminary information relating to the uses, general characteristics and effects of the 10 selected mofette springs was obtained from the residents in the study area using questionnaires. The total administered questionnaires were 60 (6 respondents per spring) with a 100% return rate. The data was analysed using Microsoft Excel 2016 and the percentage findings are summarised in Table 4.1.

All the sampled respondents were adult male (58.3%) and female (41.7%) residents of Meru County who were well familiar with the study area. They confirmed the widespread occurrence of CO_2-rich springs in the region which are locally called *Muonyo*. A total of 19 springs were reported including the 10 representative springs covered during the study. These are Ukuu, Kang'ara, Kitheru, Keeru, Nthungu, Gacingiri (Gikumene), Konyokanyi, Kiambogo, Mwiteria, Kieni kia Mwiriga (Kanje/Mulathankari), Ciothirai, Ginturuie, Tharu, Kathathantu, Konyo ka Mburi (Rwarera-A), Konyo Kanyi (Rwarera-B), Kirugagu, Nkiriri and Mbwinjeru. According to the local residents, slightly more than a half (57.9%) of the spring waters emerged quietly or bubbled slowly. The springs emerging or bubbling vigorously were likely to contain more CO_2 dissolved at high pressure. The most vigorous discharge was encountered at Nthungu.

Majority of the respondents (63.3%) used the water most regularly while the rest used it regularly. The area residents liked drinking the carbonated mineral waters especially due to its characteristic soda and mineral taste. They also used the spring waters for cooking maize meal (*ugali*) and porridge because it gives salty flavour and a brown colouring to the food. The bicarbonate was noted to make easier the cooking of tough vegetables. The waters were frequently fed to livestock as supplement for mineral salts. Local commercialisation of the mineral waters was acknowledged by 65% of the respondents. The water was usually packed by some vendors and sold locally at KSh 10 for a 500 ml bottle.

All the respondents (100%) acknowledged that the waters had a peculiar taste. Most respondents representing 63.3 % experienced a sour taste. The sour taste could be attributed to the dissociation of weak H_2CO_3 as indicated earlier by Equation (2.4) to yield H^+ (acidic medium). Some respondents (25%) indicated bitter taste which could be due to the large quantities of alkalinity in the waters. The rest gave other types of tastes such as salty, soda and lemon tastes. The salty taste could be imparted by NaCl in the waters.

Table 4.1: Preliminary results of the questionnaires.

Item	Response (%)
Gender of respondent	Male (58.3); Female (41.7)
Age of respondent	18-35 Years (65); Over 35 Years (35)
Respondent's County of residence	Meru (100); Other (0)
Are there mofette springs (*Muonyo*) in your area? If yes, give their name(s)	Yes (100); No (0) 19 springs were reported
How does the water seem to emerge from the source of the springs named above?	Emerge vigorously (42.1); Emerge quietly (57.9)
How often do you use this water?	Most regularly (63.3); Regularly (36.7); Not regularly (0); Rarely (0); Not at all (0)
For what purpose is the water mainly used?	Drinking-Yes (100); No (0) Livestock- Yes (85); No (15) Cooking- Yes (80); No (20) Selling- Yes (65); No (35)
Does the spring water have a special taste? If yes, describe the taste.	Yes (100); No (0) Sour (63.3); Bitter (25); Others (specify)- salty, soda and lemon tastes (11.7)
After fetching the water, does the special taste remain the same with time? If no, for how long does the taste last?	Yes (0); No (100) Less than a day (50); 1-2 days (50); 3-4 days (0); Over 4 days (0)
When you observe the water, is it colourless? If no, describe the colour.	Yes (100); No (0)
Does the water have any smell? If yes, describe the smell.	Yes (0); No (100)
Does any precipitate or solid form in the fetched water after sometime? If yes, describe the colour of precipitate.	Yes (75); No (25) Brown precipitates
Does the water show any reaction with common substances? E.g. when preparing food. If yes, what is the nature of the reaction?	Yes (50); No (50) Maize meal (*ugali*)/porridge turn yellow and develops an appealing taste
Which are the main positive effects of the water to the users including animals, if any?	Reduce hyperacidity, indigestion and constipation Yes (100) No (0) Enhance feeding rate in livestock Yes (100) No (0)
Which are the main negative effects of the water to the users including animals, if any?	None
Do the springs affect the nearby environment (soil, air, plants, animals or buildings)?	No
Provide any other relevant information about these kind of springs.	None

It was pointed out that the sharp taste in the spring waters lasts for a short period (< 3 days). The high underground pressure maintains the excess CO_2 into solution. But the pressure decreases when the water emerge at the Earth's surface and the gas escape into the atmosphere to attain equilibrium. Consequently, the strength of the taste decreased with time. The waters were described to be completely colourless indicating the absence of colouring matter. They were also odourless. Carbon dioxide itself is odourless and is not expected to impart any smell. Lack of smell ruled out to a larger extent the degassing of other volcanic gases with characteristic odours such SO_2, H_2S, HCl and NH_3 (Shinohara, 2008).

Respondents (75%) indicated that brown precipitates formed within a day when the water was left to stand. The brown precipitates were also observed on the ground surface in most springs as illustrated in the photographs (Figures 4.3, 4.4 and 4.5). This was attributed to precipitation of Fe^{3+} as $Fe(OH)_3$ formed by air-oxidation of Fe^{2+} in water as described earlier in Equation 4.1 (Shestakova *et al*., 2018; Giggenbach, 1990). During cooking of maize meal (*ugali*) and porridge, the food turned brown, according to 50% of the respondents. Again, this was attributed to the rapid oxidation of Fe^{2+} to Fe^{3+} at elevated temperature.

Respondents (100%) indicated that the spring waters reduced hyperacidity in the stomach. This could be based on the neutralisation reaction between the HCO_3^- and CO_3^{2-} (alkalinity ions) in water with the H^+ from HCl in the stomach to form weakly dissociated H_2CO_3. The waters were also credited with relieving indigestion or dyspepsia effects in the gastrointestinal tract (GIT). This could be possible due enhancement of digestion of food in the stomach by H_2CO_3. The dissolved solutes especially sulphate induces laxative effect which alleviates constipation (Albertini *et al*., 2007). The enhanced digestion and constipation relieve in livestock increases the feeding rate which consequently result in good health and body vigour.

Beside the reported therapeutic benefits associated with the dissolved CO_2, the waters could be expected to replenish the body with vital major and trace elements as described ahead in sections 4.6.2 and 4.7, respectively (Prashanth *et al*., 2015; Wada, 2004). There were no negative effects reported as a result of using the spring waters by humans and livestock. However, long term ingestion of the CO_2-rich mineral waters could raise serious health concern due to probability of significant levels of toxic solutes in the waters. Toxic elements like As, Cd, Cr, Hg, and Pb may be leached from the subsurface rocks as discussed ahead in

sections 4.8.3 and 4.8.5. Hence, there is need for thorough scientific (biochemical and epidemiological) data to guide the intake of such naturally existing mineral-rich waters (Zhang *et al*., 2019; Thomas *et al*., 2016; Abdul *et al*., 2015; Wani *et al*., 2015; Jaishankar *et al*., 2014; WHO, 2011; Barbie *et al*., 2005; Cefalu and Hu, 2004). The respondents did not associate the springs to any adverse effects on the local natural environment. However, continuous CO_2 degassing coupled with deforestation could be anticipated to contribute to global warming (Kucharič *et al*., 2015). Accumulation of CO_2 in the valleys could also cause asphyxiation of organisms (Barry *et al*., 2013).

4.4 Ambient CO_2 at the spring sites

The concentrations of ambient CO_2 near the springs were measured using non-dispersive infrared (NDIR) CO_2 sensor (Testo 435). The mean CO_2 concentrations of three samples drawn from each spring are shown in Table 4.2.

Table 4.2: Ambient CO_2 (ppm) in air above the springs.

Ambient CO_2		GIK	KAT	KIA	MBW	MUL	NTH	RWA	RWB	THA	UKU	Average
Wet season	Mean (n = 3)	518	5,803	5,253	8,175	1,225	4,598	2,844	536	4,727	490	3,417
	RSD (±)	2.1	3.8	3.3	2.7	3.2	3.9	4.6	3.3	2.5	3.4	
Dry season	Mean (n = 3)	752	10,967	12,138	9,105	2,485	4,188	2,885	569	4,187	759	4,804
	RSD (±)	3.3	4.7	4.2	3.8	2.6	3.4	4.1	3.7	3.1	4.2	

The August 2019 global weekly average for atmospheric CO_2 was 410.24 ppm as reported by the National Oceanic and Atmospheric Addministration (NOAA) at Mauna Loa (NOAA, 2019). The CO_2 mean for all the springs were 3,417 and 4,804 ppm during wet and dry seasons, respectively, showing that the springs had higher average ambient CO_2 levels than the global average value. This implied that the waters underlying the springs were carbonated and under pressure. When the water emerges at the surface, pressure is reduced and the excess CO_2 is released into the air.

For eight springs, the average CO_2 values were higher during the dry season than the wet season. This could be attributed to higher temperature during the dry season which decrease solubility of CO_2 in water. As temperature increases the gas gain more kinetic energy and escapes into the air. Kathathantu, Kiambogo and Mbwinjeru springs which are located in

enclosed valleys had the highest CO_2 quantities. This may be attributed to the fact that CO_2 is heavier than air and hence accumulates in the valleys. Where the springs are located in open places, the CO_2 is quickly dispersed by wind, hence the low values. The large accumulation of CO_2 in the valleys can cause asphyxiation, killing small organisms and birds (Barry *et al*., 2013).

The CO_2 flux at continental rifts is a major environmental concern because of the greenhouse and climate change effects associated with it (Brune *et al*., 2017). Emission of CO_2 from mineral springs in Slovak republic is estimated at 4 Mt yr^{-1}. This may contribute remarkably to aggregated emissions from countries with related geological and hydrogeological structures (Kucharič *et al*., 2015). Similarly, CO_2 venting in Mt. Kenya region may require to be fully accounted for and be included in the estimates for global CO_2 budget.

On the other hand, the data shows that Mt. Kenya region has potential for commercial exploitation of CO_2 gas and mineral waters which may require further feasibility studies. Kenya has a single commercial CO_2 mining plant at Kireita forest in Kiambu County which is under Carbacid Investment Plc through its subsidiary Carbacid (CO_2) Limited (KNBS, 2018). A similar CO_2 extraction plant can be established in Mt. Kenya region subject to economic viability.

4.5 $\delta^{13}C$ data and genesis of CO_2

Table 4.3 summarises the results for the dissolved inorganic carbon $\delta^{13}C_{DIC}$ values measured using Picarro CRDS (cavity ring-down spectroscopy).

Table 4.3: $\delta^{13}C_{DIC}$ values (‰ VPDB) in the spring waters.

$\delta^{13}C_{DIC}$		GIK	KAT	KIA	MBW	MUL	NTH	RWA	RWB	THA	UKU
Wet season	Mean (n = 3)	-2.515	-3.386	-3.597	-2.236	-2.19	-0.191	-0.507	-0.584	-1.443	-1.978
	RSD (±)	0.8	0.6	0.3	0.7	1.3	0.9	0.5	1.4	0.8	1.1
Dry season	Mean (n = 3)	-2.168	-3.394	-3.341	-1.73	-2.369	+0.283	-0.065	+0.178	-1.273	-1.838
	RSD (±)	0.6	0.4	0.7	0.5	0.9	0.7	1.4	0.5	0.8	1.1

The obtained $\delta^{13}C$ values ranged from -3.597 to -0.191 and -3.394 to +0.283 ‰ VPDB, during the wet and dry seasons, respectively. The dry season seemed to have higher $\delta^{13}C$ values than the wet season. The main reason could be lower rate of discharge during the dry season which increases the time for water-rock interaction hence more dissolution of carbonate rocks as compared to the wet season. This increases the level of ^{13}C isotope derived from the rocks which results in higher $^{13}C/^{12}C$ ratio, hence higher $\delta^{13}C$ values in water.

The reported $\delta^{13}C$ values in this study (-3.597 to +0.283 ‰) were above or close to upper levels of the mantle range which is at -6 ± 2.5 ‰ (Mason *et al*., 2017). Therefore, the ultimate source of CO_2 in the study region is likely to be mantle but variably enriched with ^{13}C from deep carbonate rocks especially the calcite precipitated in basalt as shown in Equation 4.2 (Stefansson *et al*. 2016; Thomas *et al*., 2016).

$$CaAl_2Si_2O_8 + CO_{2(g)} + 2H_2O_{(l)} \rightarrow Al_2Si_2O_5(OH)_{4(s)} + CaCO_{3(s)} \tag{4.2}$$
  (Anorthite)   (Kaolinite)   (Calcite)

The ^{13}C isotope mean content of global volcanic gases lies between -3.8 and -4.6 ‰ while the mean-oceanic ridge basalt (MORB) value is -6 ‰ VPDB hence not all volcanic gases have the same source for carbon (Mason *et al*., 2017). A study of groundwater in Iceland showed $\delta^{13}C_{DIC}$ range of -27.4 to +2.0 ‰ VPDB. This points to mixed sources such as atmosphere, carbonates, upper mantle and lower crust (Stefansson *et al*., 2016). The apparent source of CO_2 (whether crust, limestone, organic or mantle) may be altered by carbon isotope fractionation in the process of degassing through assimilation of organic carbon near the surface and calcite precipitation in the subsurface geothermal or hydrothermal systems beneath volcanoes (Mason *et al*., 2017).

The $\delta^{13}C$ data (-3. 597 to +0.283 ‰) from the study of mofette springs in the Eastern Mt. Kenya region which is located outside the Kenya Rift Valley (KRV) is slightly different from those reported elsewhere in the world. This suggests that in addition to the mantle derived CO_2, carbonates in deep crust could be the other source of $^{13}C_{DIC}$. The findings from this study are presented together with those of other workers in Table 4.4. The summarised information shows that dissolved $^{13}C_{DIC}$ mantle range is about -3 to -8 ‰ VPDB while the carbonate derived is above -3 ‰.

Table 4.4: Comparison of δ ^{13}C$_{DIC}$ values from this study with those of other workers.

Study	Location	δ ^{13}C$_{DIC}$ range (‰ VPDB)	Inferred dissolved CO_2 source
This study	*Eastern Mt. Kenya, Meru County, Kenya*	*-3.597 to +0.283*	*Mantle and carbonates in deep crust*
Shestokova *et al.* (2018)	Choygan, Siberia, Russia	−0.3 to +1	Metamorphism of carbonate rocks at depth
Barry *et al.* (2013)	Rungwe Volcanic Province, Tanzania	-2.8 to -6.5	Mantle-derived
Mao *et al.* (2009)	Wudalianchi, North East China	-8.24 to -5.26	Upper mantle
Siebe *et al.* (2007)	Jungepeo, Michoacan, Mexico	-6.7 to -7.2	Mantle with some organic sources
Jeong *et al.* (2005)	Kangwaon, Chungcheong, South Korea	-6.6 to +0.9	Mantle and carbonate minerals
Marques *et al.* (2000)	Northern part of Portuguese mainland	-6 to -1	Mantle and limestone
Harris *et al.* (1997)	Bongwan springs, KwaZulu-Natal, South Africa	-0.6 to +0.9	Carbonate rocks at depth
Giggenbach (1990)	Lake Nyos, Cameron	Average of -3.4	Magmatic origin
Pierre *et al.* (1988)	Swiss Alps Lower Engadine region, Switzerland	about -4	Carbonate rocks and/or marine carbonates

4.6 Major physicochemical characteristics of the springs

The physical characteristics analysed included; temperature (T), pH, electrical conductivity (EC), dissolved inorganic carbon (DIC), total alkalinity (Talk) and difference DIC-Talk. Also investigated were the major cations and anions in water namely; Li^+, Na^+, NH_4^+, K^+, Ca^{2+}, Mg^{2+}, Sr^{2+}, Br^-, Cl^-, F^-, NO_2^-, NO_3^-, PO_4^{3-} and SO_4^{2-}. The correlation between the parameters and *t*-tests have been discussed. Classification of the water-types is also included in this section.

4.6.1 Physical characteristics of the spring waters

A portable meter was used for measuring Temperature (T), pH and electrical conductivity (EC) during water sampling. Dissolved inorganic carbon (DIC) was analysed using Picarro cavity ring-down spectrometer (Picarro CRDS) while total alkalinity (Talk) due to HCO_3^- and CO_3^{2-} was obtained by potentiometric titration. Three samples were analysed (n = 3) per spring during the wet season and a similar number was analysed again in the dry season.

The main physical parameters of the springs analysed during the wet and dry seasons are summarised in Tables 4.5 and 4.6, respectively.

Table 4.5: DIC values and other physical parameters in waters for the wet season.

Spring		T °C	pH	EC (µS/cm)	DIC (µmol/kg)	Talk (µmol/L)	DIC-Talk (µmol/L)
GIK	Mean	21.2	6.01	1,221	43,003	14,939	28,064
	RSD (±)	0.5	0.9	1.5	1.2	1.0	1.4
KAT	Mean	22.4	6.23	2,450	59,149	27,375	31,774
	RSD (±)	0.2	0.4	1.2	0.8	2.5	2.9
KIA	Mean	23.1	6.22	2,410	55,811	23,987	31,824
	RSD (±)	0.4	0.7	2.4	1.4	2.1	1.7
MBW	Mean	23.2	6.47	3,780	88,414	48,335	40,079
	RSD (±)	0.3	0.4	2.2	2.5	1.5	2.4
MUL	Mean	21.2	6.41	3,140	66,777	42,103	24,674
	RSD (±)	0.4	0.3	1.8	1.7	2.2	3.6
NTH	Mean	24.4	6.43	3,610	72,464	45,272	27,192
	RSD (±)	0.6	0.8	2.1	2.9	2.4	2.8
RWA	Mean	23.8	6.52	4,930	87,434	57,708	29,726
	RSD (±)	0.3	0.5	1.6	2.5	1.6	2.5
RWB	Mean	25.2	6.45	4,520	77,739	50,431	27,308
	RSD (±)	0.5	0.4	2.3	1.8	3.1	2.5
THA	Mean	29.5	6.81	5,120	81,075	61,627	29,448
	RSD (±)	0.2	0.7	1.4	0.9	1.8	2.3
UKU	Mean	23.3	6.42	3,790	75,313	44,633	30,680
	RSD (±)	0.6	0.5	1.5	2.3	2.3	1.7

Table 4.6: DIC values and other physical parameters in waters for the dry season.

Spring		T ^{o}C	pH	EC (μS/cm)	DIC (μmol/kg)	Talk (μmol/L)	DIC-Talk (μmol/L)
GIK	Mean	21.9	5.83	1,375	39,184	14,925	24,259
	RSD (±)	0.2	0.5	1.8	2.7	3.6	2.6
KAT	Mean	23.2	6.03	2,753	54,008	23,926	30,082
	RSD (±)	0.2	0.3	1.2	3.1	3.9	3.2
KIA	Mean	23.4	6.02	2,590	47,569	24,433	23,136
	RSD (±)	0.5	0.6	2.7	3.6	1.4	1.8
MBW	Mean	23.5	6.34	3,858	81,268	48,421	32,847
	RSD (±)	0.3	0.4	1.6	2.9	3.2	2.0
MUL	Mean	21.8	6.34	3,505	66,799	41,531	25,268
	RSD (±)	0.2	0.6	3.2	3.5	1.7	2.4
NTH	Mean	24.8	6.34	3,715	70,240	45,247	24,993
	RSD (±)	0.7	0.3	2.8	1.5	3.4	2.2
RWA	Mean	24.3	6.37	4,980	89,013	57,385	31,628
	RSD (±)	0.4	0.8	2.5	3.2	2.5	3.1
RWB	Mean	25.6	6.47	4,625	72,403	50,247	22,156
	RSD (±)	0.5	0.6	3.4	2.6	2.8	2.5
THA	Mean	29.7	6.57	5,195	87,286	61,810	25,476
	RSD (±)	0.2	0.5	2.9	2.8	4.4	3.8
UKU	Mean	23.8	6.33	3,990	72,653	44,562	28,091
	RSD (±)	0.3	0.2	2.6	3.5	3.2	2.4

The springs were characterised by relatively low discharge temperatures (wet season 21.2-29.5 ^{o}C and dry season 21.8-29.7 ^{o}C) and were generally cold. Low temperature allows large volume of CO_2 to remain dissolved in the waters (Marques *et al*., 2000). According to Thomas *et al*. (2000), a low subsurface temperature increases the aqueous solubility of CO_2. The dissolved CO_2 is in form of weak carbonic acid (H_2CO_3). The resultant CO_2-rich water gives slightly acidic pH which leads to increased dissolution of carbonate and silicate minerals. This can be explained by the acid hydrolysis reactions taking place as in Equations (4.3) and (4.4) (Andrews *et al*., 2004).

$$CaCO_{3(s)} + H_2CO_{3(aq)} \rightarrow Ca(HCO_3)_{2(aq)} \tag{4.3}$$

(Calcite)

$$Mg_2SiO_{4(s)} + 4H_2CO_{3(aq)} \rightarrow 2Mg(HCO_3)_{2(aq)} + H_4SiO_{4(aq)} \qquad (4.4)$$

(Forsterite)   (Silicic acid)
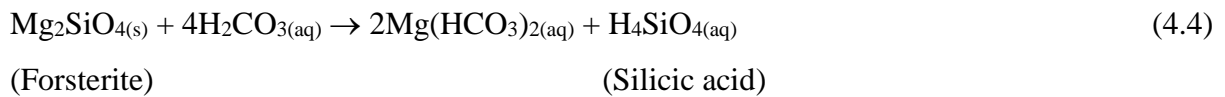
Reported values of EC (wet 1,221-5,120; dry 1,375-5,195 µS/cm), DIC (wet 43,003-91,075; dry 39,184-8,9013 µmol/kg) and Talk (wet 14,939-61,627; dry 14,925-61,810 µmol/L) were high because of CO_2-enhanced dissolution of various carbonate and silicate minerals from the parent rocks (Crundwell, 2014; Assayang *et al*., 2009). Since the rate of dissolution increases with temperature, THA spring which had relatively higher temperatures (29.5-29.7 ºC) than the other springs had relatively higher EC values (5,120-5,195 µS/cm). Given that the pH range of the springs in both seasons was 5.83-6.81, the alkalinity of the waters was dominated by HCO_3^- compared to CO_3^{2-} (Andrews *et al*., 2004).

Figure 4.7 shows the comparison of the EC values between the wet and dry seasons. The values were slightly higher during the dry season than wet season probably because the volume of water is low and takes longer period of time to circulate in the subsurface rocks which in turn increase its mineralization. In addition dilution during the wet season could lower the concentration of minerals in water.
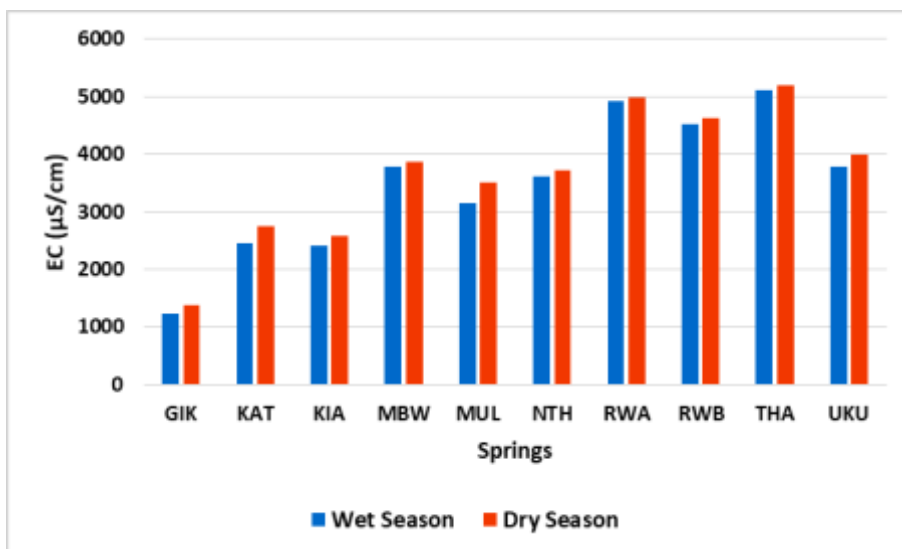
Figure 4.7: Comparison of EC between the wet and dry seasons.

The levels of DIC were slightly higher during the wet season compared to the dry season in most springs as shown in Figure 4.8. This could be due to the lower discharge temperatures during the wet season which resulted to higher solubility of CO_2 in the spring waters (Marques *et al*., 2000).
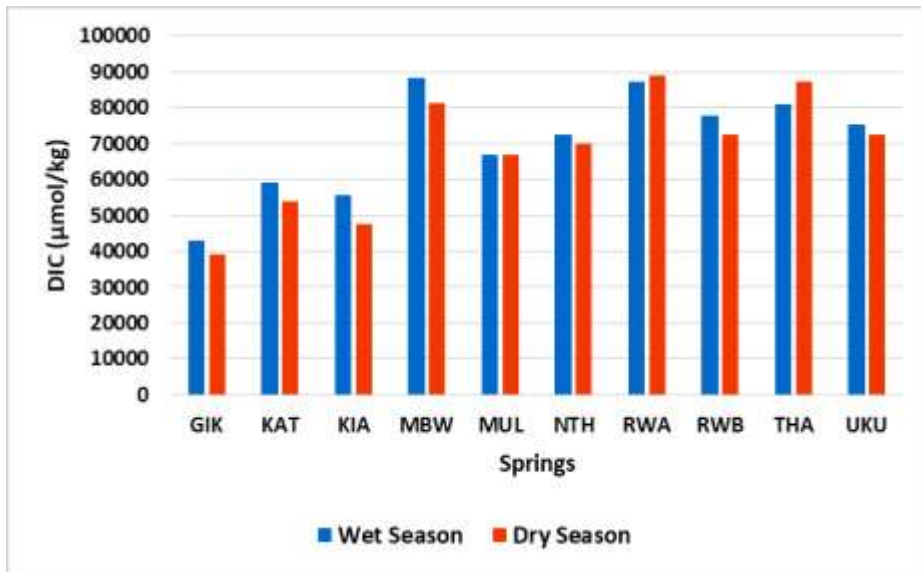
Figure 4.8: Comparison of DIC between the wet and dry seasons.

The differences in Talk levels between the wet and dry seasons were apparently small as shown in Figure 4.9. Thus implying little seasonal variation in CO_2 degassing. DIC-Talk values (wet 28,064-40,079; dry 24,259-32,847 µmol/L) represents the free CO_2 and/or undissociated H_2CO_3 at equilibrium with HCO_3^- and CO_3^{2-} in the system. In general, the results depicted high concentration of DIC species or rather large content of dissolved CO_2, with RWA and THA springs having the highest. This could be a sign of passive CO_2 degassing through buried faults in the region and the springs could therefore be harnessed for commercial extraction of CO_2 and production of mineral waters (Harris *et al*., 1997; Swanner, 1988; Zink, 1993).
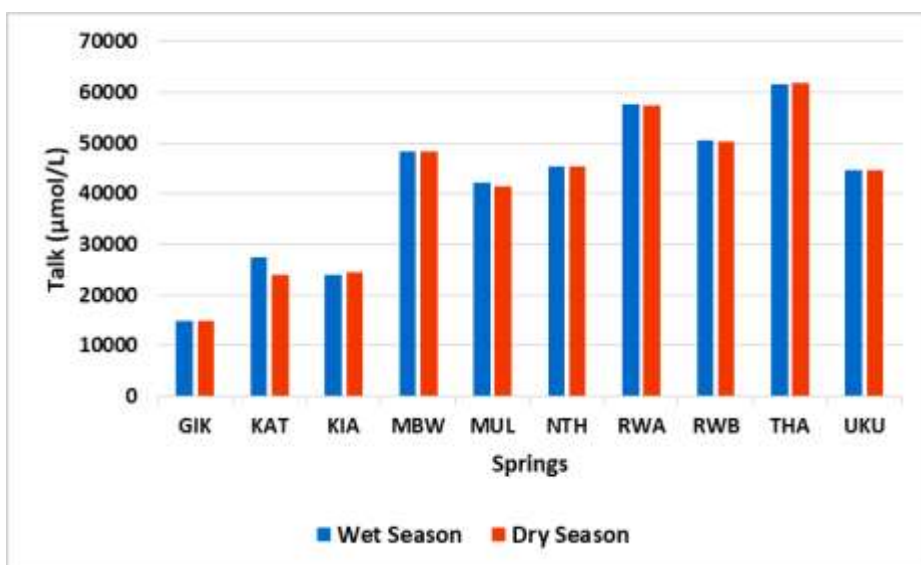
Figure 4.9: Comparison of Talk between the wet and dry seasons.

4.6.2 Chemical composition of major cations and anions in the waters

Chemically suppressed ion chromatography technique was used for the determination of ions except for Sr^{2+} which was done by graphite furnace AAS. Three samples (n = 3) were analysed in each spring per season. Table 4.7 and 4.8 shows the concentration of major ions and anions in the spring waters during the wet and dry weather, respectively.

Table 4.7: Major ions in the spring waters (mg/L) for wet season.

Ion		GIK	KAT	KIA	MBW	MUL	NTH	RWA	RWB	THA	UKU
Li^+	Mean	0.10	0.41	51	0.36	<0.1	50	0.35	0.72	1.08	0.66
	RSD	2.01	1.11	1.52	1.71	-	1.8	1.34	2.07	1.38	1.31
Na^+	Mean	127.1	515.1	457.6	799.9	382.1	464.6	831.8	735	1,259	807.2
	RSD	1.70	1.58	1.26	1.47	0.82	1.41	1.44	0.75	1.45	1.52
K^+	Mean	18.33	44.93	41.3	67.9	35.45	40.23	71.64	65.48	90.99	71.25
	RSD	1.88	1.34	1.05	1.40	1.43	1.53	1.66	1.53	1.34	1.26
NH_4^+	Mean	<0.35	<0.35	<0.35	<0.35	<0.35	<0.35	<0.35	<0.35	<0.35	<0.35
	RSD	-	-	-	-	-	-	-	-	-	-
Ca^{2+}	Mean	4.6	80.68	68.36	12.36	108.2	16.32	23.04	7.32	37.76	9.84
	RSD	2.98	4.34	1.33	4.76	2.78	0.26	3.63	3.11	0.58	4.0
Mg^{2+}	Mean	60.82	44.62	37.73	60.77	172.1	39.41	171.9	164.6	46.73	37.9
	RSD	1.5	1.68	1.44	1.05	0.99	1.51	0.83	1.63	1.47	1.66
Sr^{2+}	Mean	0.39	0.44	0.38	0.98	1.36	0.56	0.29	0.3	1.32	1.28
	RSD	2.31	0.37	2.22	3.25	1.73	3.40	3.12	3.14	3.23	1.26
Br^-	Mean	<0.004	0.72	<0.004	<0.004	<0.004	<0.004	<0.004	<0.004	0.8	0.8
	RSD	-	2.5	-	-	-	-	-	-	4.06	2.91
Cl^-	Mean	16.26	141.9	128.2	90.03	53.96	53.61	265.8	286.3	224.5	173.6
	RSD	1.16	0.12	0.25	0.15	0.4	0.2	0.18	0.33	0.44	0.02
F^-	Mean	<0.17	**1.63***	**1.52***	0.4	<0.17	<0.17	<0.17	<0.17	**1.96***	0.32
	RSD	-	3.2	2.9	2.5	-	-	-	-	3.4	3.6
NO_2^-	Mean	<0.13	0.18	0.32	<0.13	<0.13	<0.13	<0.13	<0.13	<0.13	0.4
	RSD	-	3.5	3.8	-	-	-	-	-	-	2.7
NO_3^-	Mean	<0.06	<0.06	<0.06	<0.06	<0.06	<0.06	<0.06	3.472	<0.06	<0.06
	RSD	-	-	-	-	-	-	-	3.5	-	-
PO_4^{3-}	Mean	<3.17	<3.17	<3.17	<3.17	<3.17	<3.17	<3.17	<3.17	<3.17	<3.17
	RSD	-	-	-	-	-	-	-	-	-	-
SO_4^{2-}	Mean	<0.33	9.7	7.68	<0.33	8.74	<0.33	84.19	77.28	<0.33	<0.33
	RSD	-	1.26	1.44	-	0.27	-	0.26	0.41	-	-

* Above 1.5 mg/L, KEBS and WHO guideline for drinking-water quality.

< Below the limit of quantitation (LOQ).

72

Table 4.8: Major ions in the spring waters (mg/L) for dry season.

Ion		GIK	KAT	KIA	MBW	MUL	NTH	RWA	RWB	THA	UKU
Li^+	Mean	<0.10	0.35	0.34	0.69	<0.10	0.62	0.7	0.67	1.1	0.68
	RSD	-	1.09	3.80	1.10	-	1.42	1.92	2.12	1.75	1.94
Na^+	Mean	121	498.7	460.7	803.8	381	810.5	797.4	728.3	1,273	832.3
	RSD	1.44	1.39	1.39	1.42	1.04	3.68	1.41	1.40	1.54	1.75
K^+	Mean	17.86	44.15	42.12	68.44	34.4	72.89	70.24	65.6	92.39	72.34
	RSD	1.42	1.72	1.64	1.22	1.99	1.6	1.57	1.16	1.79	1.58
NH_4^+	Mean	<0.35	<0.35	<0.35	<0.35	<0.35	<0.35	<0.35	<0.35	<0.35	<0.35
	RSD	-	-	-	-	-	-	-	-	-	-
Ca^{2+}	Mean	78.8	76.8	65.68	130.9	183	103.9	103.8	104.1	71.1	78.68
	RSD	1.88	4.32	2.73	2.79	1.85	4.13	3.04	3.8	3.47	4.3
Mg^{2+}	Mean	64.66	42.48	37.92	62.64	171.9	69.53	165	169.6	48.89	39.89
	RSD	1.69	1.80	1.05	1.81	1.25	1.20	1.69	1.55	2.65	1.33
Sr^{2+}	Mean	0.44	0.48	0.40	1.08	1.99	1.0	2.15	1.66	1.52	1.6
	RSD	2.13	2.18	1.31	2.55	1.62	3.01	4.13	2.52	1.72	1.25
Br^-	Mean	<0.004	<0.004	<0.004	<0.004	<0.004	<0.004	0.96	0.96	0.8	0.64
	RSD	-	-	-	-	-	-	1.7	1.2	1.8	1.3
Cl^-	Mean	16.29	166.4	153.3	83.39	53.64	94.5	199.2	204.4	235.5	177.7
	RSD	0.65	0.10	0.15	0.14	0.35	0.17	0.31	0.23	1.84	0.45
F^-	Mean	<0.17	1.25	1.35	0.87	<0.17	<0.17	<0.17	<0.17	**2.18***	0.7
	RSD	-	0.3	0.8	0.5	-	-	-	-	0.9	0.5
NO_2^-	Mean	<0.13	<0.13	<0.13	<0.13	<0.13	<0.13	<0.13	0.55	<0.13	0.51
	RSD	-	-	-	-	-	-	-	0.3	-	0.7
NO_3^-	Mean	<0.06	<0.06	<0.06	<0.06	<0.06	0.19	0.12	<0.06	<0.06	<0.06
	RSD	-	-	-	-	-	0.5	0.4	-	-	-
PO_4^{3-}	Mean	<3.17	<3.17	<3.17	<3.17	<3.17	<3.17	<3.17	<3.17	<3.17	<3.17
	RSD	-	-	-	-	-	-	-	-	-	-
SO_4^{2-}	Mean	1.54	9.02	7.58	<0.33	8.6	4.99	89.38	87.55	<0.33	<0.33
	RSD	3.43	1.39	1.3	-	1.07	1.44	0.31	0.43	-	-

*Above 1.5 mg/L, KEBS and WHO guideline for drinking-water quality.

< Below the limit of quantitation (LOQ).

The predominant cation was Na^+ ranging from 127.1 to 1,259 mg/L and 121 to 1,273 mg/L in wet and dry seasons, respectively. It was followed by Mg^{2+}, Ca^{2+} and K^+, in that order. The amounts of Li^+ and Sr^{2+} were relatively low while NH_4^+ ion was below the LOQ (< 0.35 mg/L). This implied occurrence of feldspar, mafic and limestone-based rocks in the region (Mason, 2007; Baker, 1967; Gregory, 1900). Abundance of Na^+ in the cations indicates that silicates are the dominant source of weathering products. The dissolution of Na-feldspar mineral, albite is shown in Equation (4.5) (Andrews *et al*., 2004).

$$2NaAlSi_3O_{8(s)} + 2H_2CO_{3(aq)} + 9H_2O_{(l)} \rightarrow 2NaHCO_{3(aq)} + 4H_4SiO_{4(aq)} + Al_2Si_2O_5(OH)_{4(s)} \quad (4.5)$$

(Albite)   (Silicic acid) (Kaolinite)

Chloride was the second most significant anion after the alkalinity ions (HCO_3^-). The high NaCl levels produced the slight salty taste in the water. Sulphate ion was generally low in most springs but relatively high at RWA (84.19-89.38 mg/L) and RWB (77.28-87.55 mg/L). In some cases, parameters such as Li^+, NH_4^+, Br^-, F^-, NO_2^-, NO_3^-, PO_4^{3-} and SO_4^{2-}, were below their limits of quantitation (LOQ).

In a similar study, abundance of Na^+ ranging from 954 to 1,043 mg/L was observed at Rurii spring at Nyambene Range in Kenya (Mungai *et al.*, 2014). According to Marques *et al.* (2000), cold and thermal mineral waters in the Northern part of Portuguese Mainland had elevated levels of Na^+ (365-1,246 mg/L), K^+ (28-105 mg/L), Ca^{2+} (22-203 mg/L), HCO_3^- (1,724-4,716 mg/L) and free CO_2 (350-4,670 mg/L). At Lake Nyos in Cameroon, Na^+, K^+, Mg^{2+}, Ca^{2+}, Mn^{2+} and Fe^{2+} content in the CO_2-rich waters was associated with the dissolution of host rock (Giggenbach, 1990). Investigation of springs at Choygan area of southern Siberia in Russia showed that major ions in the waters were consistent with silicate weathering (Shestakova *et al.*, 2018).

It is important to note that the F^- levels at THA (both seasons), KAT (wet season) and KIA (wet season) were above the WHO and KEBS permissible maximum limit in drinking-water which is 1.5 mg/L (KEBS, 2018; WHO, 2011). Water runoff may add F^- from nearby sources raising its levels in the wet season at KAT and KIA springs which are situated in enclosed valleys. This indicated possible occurrence of fluoride containing rocks in these sites. Ingestion of excess F^- can lead to chronic dental fluorosis and osteosclerosis especially in children below the age of seven years (Allibone *et al.*, 2012; Kalia *et al.*, 2010; Hansell and Oppenheimer, 2004). Several methods can be used to remove F^- in water such as adsorption, coagulation-precipitation, ion exchange, membrane separation process and electrochemical techniques (Waghmare and Arfin, 2015; Onyango and Matsuda, 2006).

The concentrations of most ions in the waters were higher during the dry season than in the wet season as exemplified by Ca^{2+} which is illustrated in Figure 4.10. This could be due to the reduction in groundwater volume during the dry season which consequently leads to increase in concentration of the solutes. Low discharge rate also allows longer circulation time for water-rock interaction hence more dissolution of mineral ions.
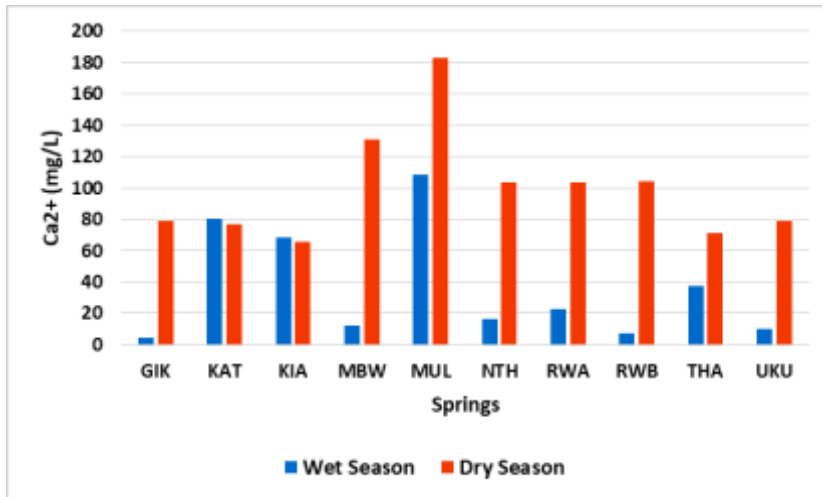
Figure 4.10: Comparison of Ca^{2+} between the wet and dry seasons.

The levels of the dominant cation Na^+ remained relatively constant in both seasons as shown in Figure 4.11. This implied insignificant seasonal variations of the cation and the possibility of the water being saturated with respect to Na^+ ion, except for NTH. Sodium compounds are highly water soluble. Excess dilution may have contributed to the low levels of Na^+ at NTH.
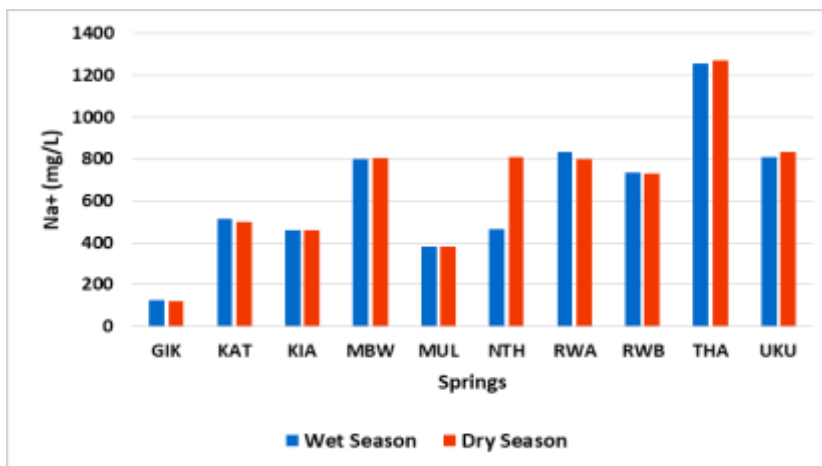
Figure 4.11: Comparison of Na^+ between the wet and dry seasons.

4.6.3 Seasonal correlations of various parameters in the waters

Figures 4.12 to 4.19 are Pearson correlation charts which gives the relationship between seasonal variations of some parameters measured in the spring waters. Apparently, all the parameters showed high degree of positive correlations ranging from +0.662 to +0.998.

The results in Figure 4.12 indicate a strong positive correlation coefficient (r > +0.9) for δ ^{13}C between the wet and dry seasons. This suggests that some springs had consistently low δ ^{13}C values during the wet and dry seasons while others had consistently high values in both seasons. Seasonal correlation of DIC was very high as shown in Figure 4.13 and hence consistent among the springs between the two seasons.
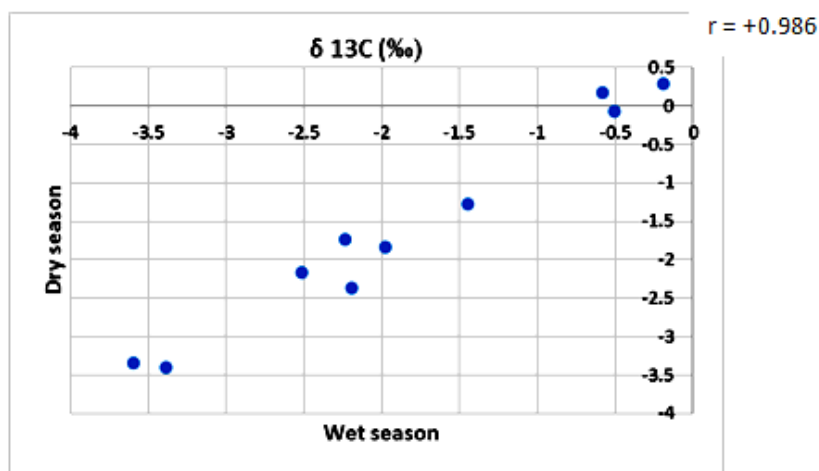
Figure 4.12: Pearson correlation of δ ^{13}C between wet and dry seasons.
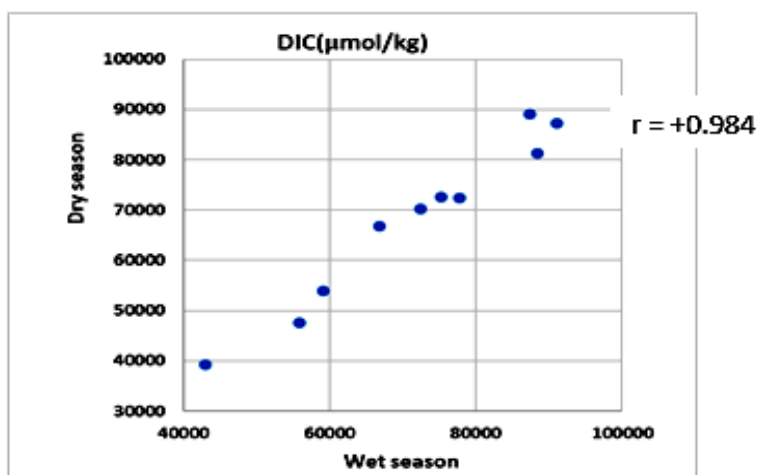
Figure 4.13: Pearson correlation of DIC between wet and dry seasons.

A very strong linear relationship for Talk was established between the wet and dry seasons as indicated in Figure 4.14. This reflects large consistency in seasonal variation of Talk from one spring to the other. Figure 4.15 illustrates EC seasonal variation among the springs. The results showed very high positive correlation which suggests a good linear relationship between the low and high EC measurements during the wet and dry seasons.
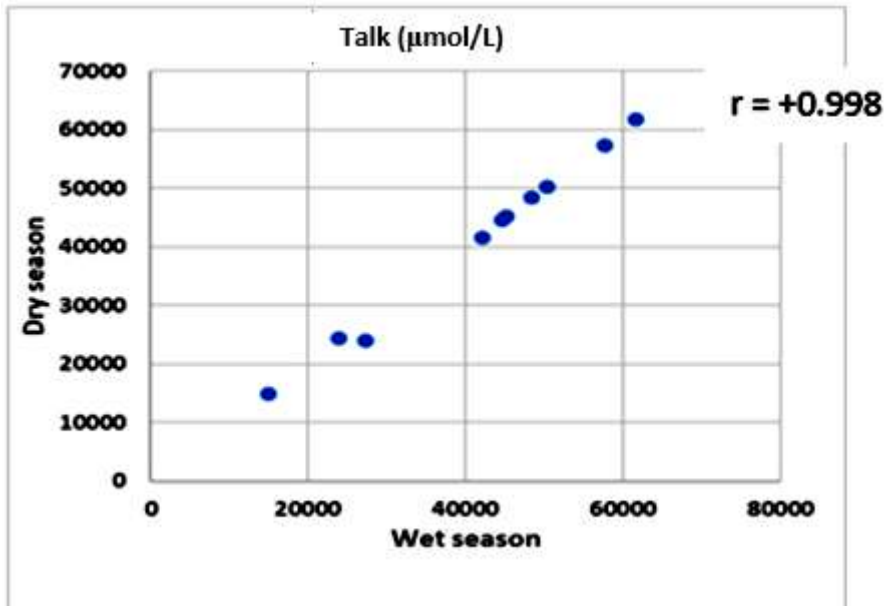
Figure 4.14: Pearson correlation of Talk between wet and dry seasons.
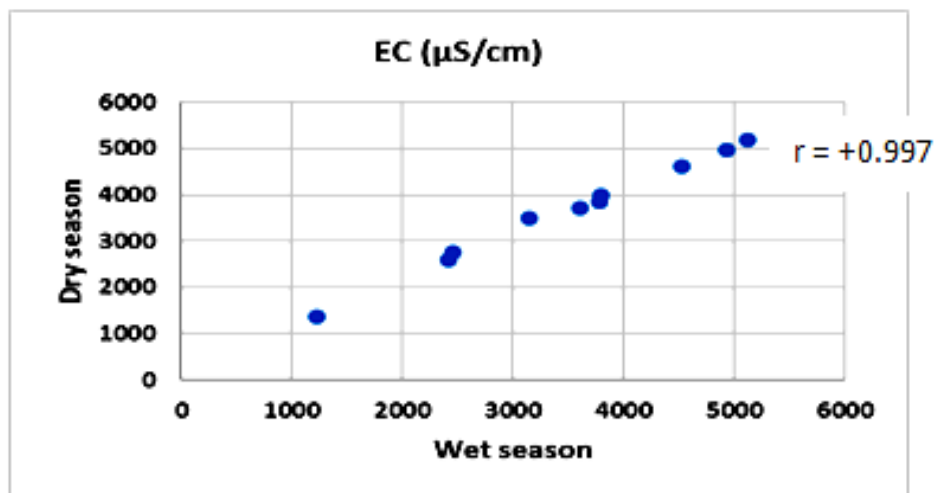
Figure 4.15: Pearson correlation of EC between wet and dry seasons.

The DIC-Talk difference indicated moderate positive correlation as shown in Figure 4.16. Environmental factors such as wind and land topography may affect ambient CO_2 as explained earlier in section 4.4 which in turn affect the dissolved CO_2 equilibrium in the system. This could lower the correlation cofficient. The seasonal comparison of pH measurements is given in Figure 4.17. The results indicated high degree of positive correlation between the wet and dry seasons.
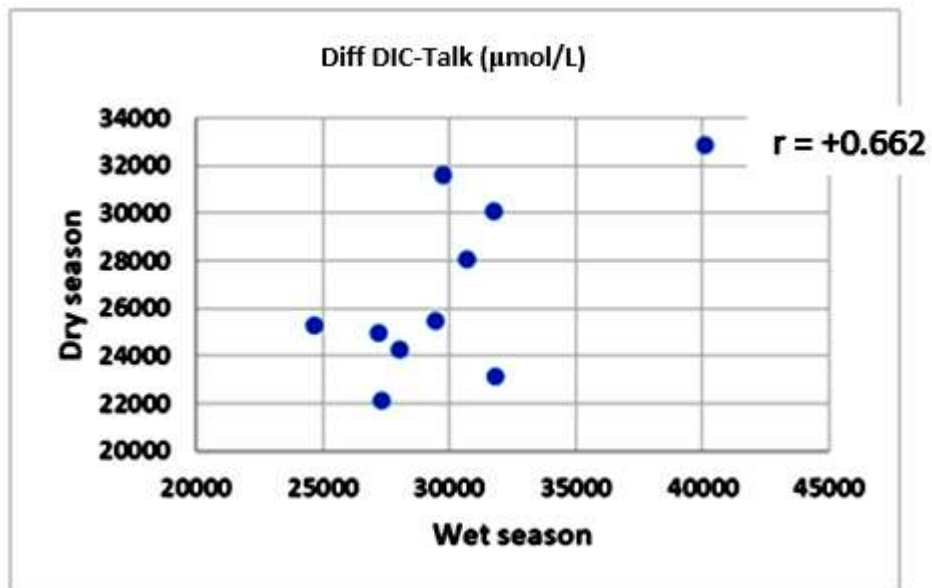
Figure 4.16: Pearson correlation of Difference DIC-Talk between wet and dry seasons.
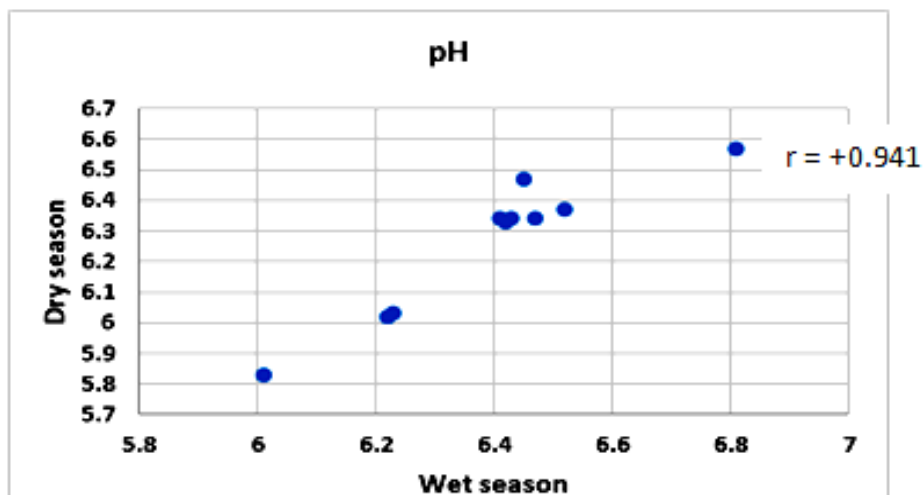
Figure 4.17: Pearson correlation of pH between wet and dry seasons.

A strong positive correlation was established for Na^+ ions between wet and dry seasons as seen in Figure 4.18, indicating consistent variation of the cation levels. Figure 4.19 illustrates the seasonal variation of Cl^-. The correlation between the two seasons was significantly high and hence the Cl^- measurements were comparable.
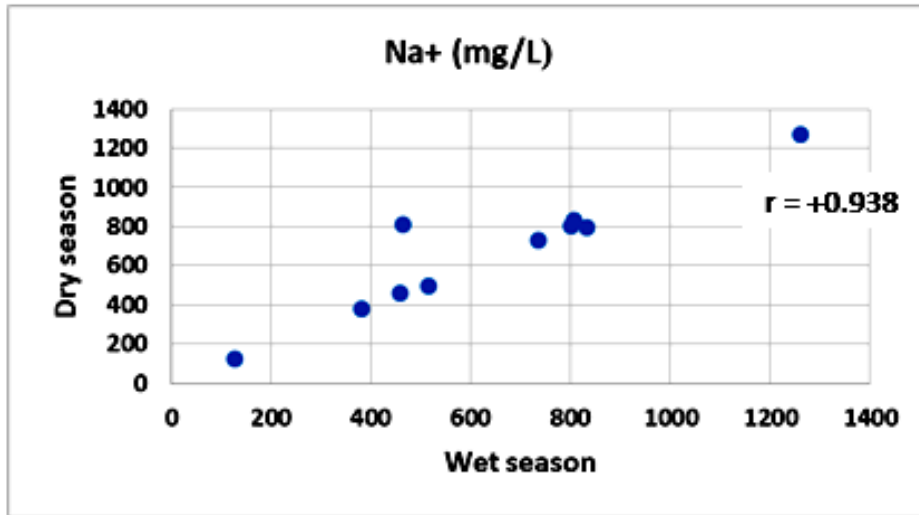
Figure 4.18: Pearson correlation of Na^+ between wet and dry season.
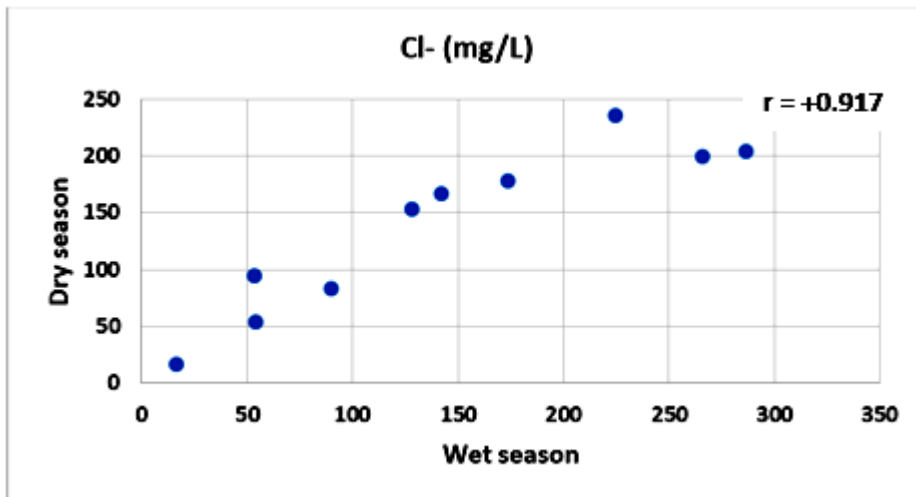
Figure 4.19: Pearson correlation of Cl^- between wet and dry seasons.

4.6.4 t-test values for major parameters

Table 4.9 summarises Pearson correlation coefficients and their respective *t*-test values for major parameters between the wet and dry season measurements. Most of the data showed very strong positive correlations (r > +0.9). The *t*-test values obtained were less than the $t_{1-\alpha/2}$ critical value of ±2.262, where $\alpha = 0.05$ and n -1 = 9, for two-tailed test and two-sample equal variance. This indicates that there were no significant statistical differences in the means between the wet and dry seasons at 97.5% confidence level (Rees, 2001; Roussas, 1997). This is possibly because the waters were saturated with dissolved CO_2 in both seasons. Thus acid controlled dissolution of minerals was fairly uniform.

Table 4.9: Wet and dry seasons Pearson correlation coefficients and *t*-test values.

Parameter	r value	*t-test value
δ ^{13}C	+0.986	+0.614
DIC	+0.984	+0.617
Talk	+0.998	+0.954
EC	+0.997	+0.768
Diff DIC-Talk	+0.662	+0.078
pH	+0.941	+0.194
Na$^+$	+0.938	+0.819
Cl$^-$	+0.917	+0.895

*Alpha (α) = 0.05, $t_{1-\alpha/2}$ = ±2.262 critical value, n-1 = 9

Figures 4.20 to 4.35 represents scatter plots and Pearson correlation coefficients (r) indicating the relationship between various water measurements taken during the wet and dry seasons. Figure 4.20 and 4.21 shows positive correlations of δ ^{13}C with DIC and Talk, in wet and dry seasons, respectively. This imply that the more the ^{13}C derived from the mantle and/or carbonate from rocks deep, the more the DIC and Talk (Stefansson *et al*., 2016).
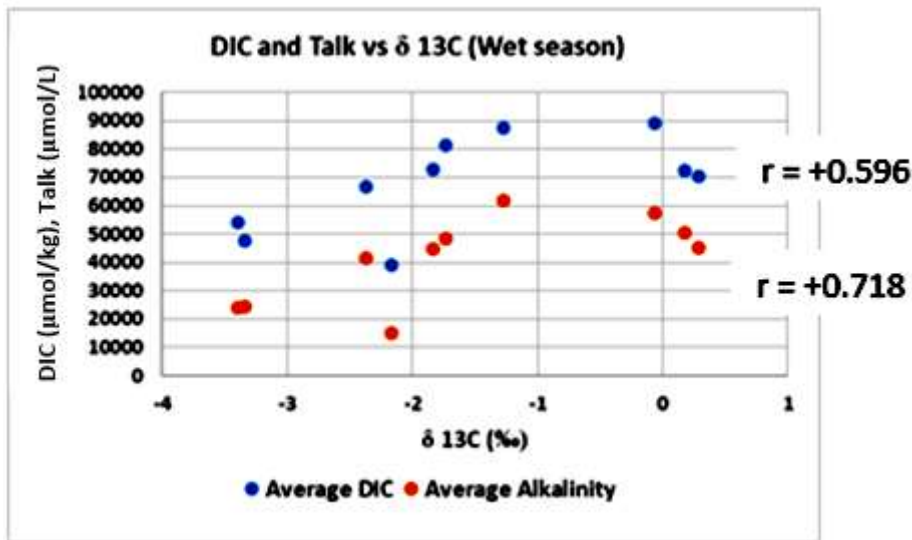
Figure 4.20: Pearson correlation of DIC and Talk versus δ ^{13}C in the wet season.
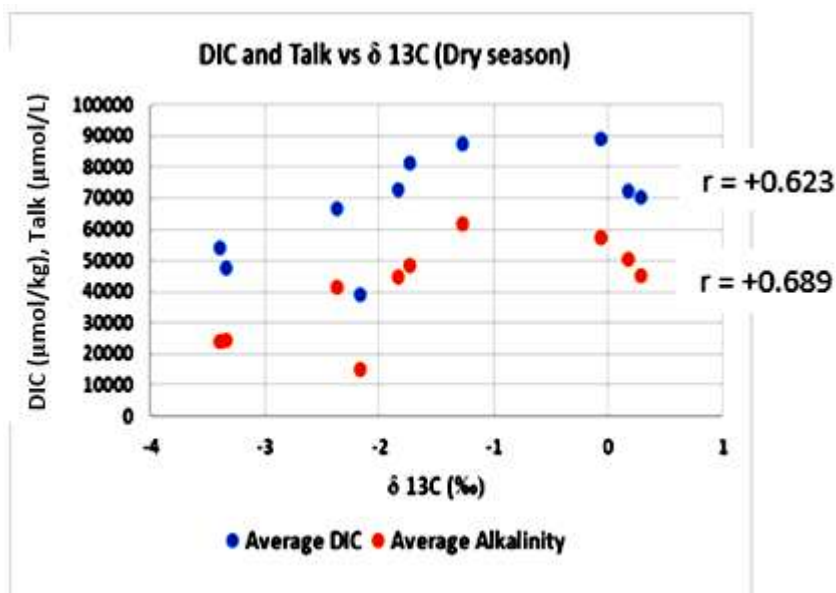
Figure 4.21: Pearson correlation of DIC and Talk versus δ ^{13}C in the dry season.

The amount of δ ^{13}C increased with EC during the wet and dry seasons as shown in Figures 4.22and 4.23, respectively. Therefore, the increase of CO_2 in the system is coupled with dissolution of carbonates and/or silicate minerals as a result of water-rock interactions (Mahar *et al*., 2014).
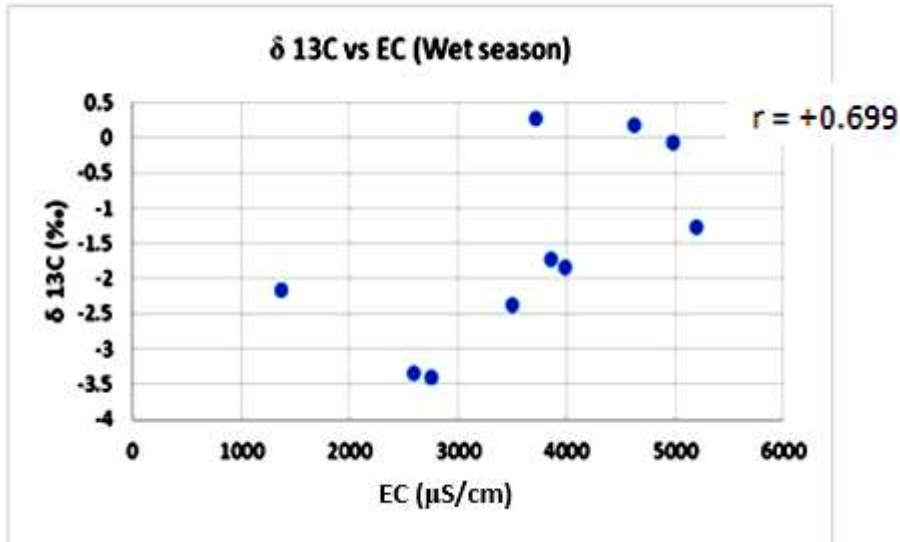
Figure 4.22: Pearson correlation of δ ^{13}C versus EC in the wet season.
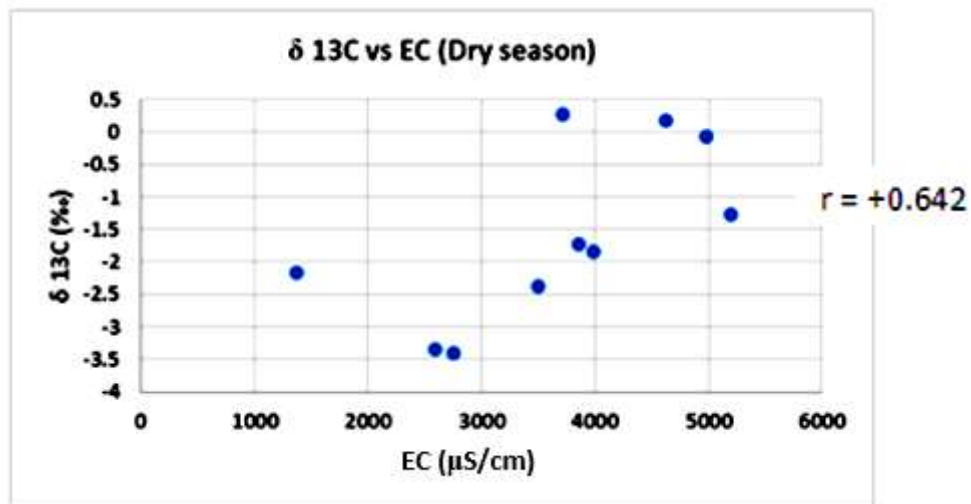
Figure 4.23: Pearson correlation of δ ^{13}C versus EC in the dry season.

According to Figures 4.24 and 4.25, EC showed very strong positive correlations (r > +0.9) with DIC and Talk, in both seasons. The high EC is due to the interaction between the CO_2-rich groundwaters and the underlying rocks leading to elevation of different types of minerals in the spring waters (Crundwell, 2014; Assayang *et al.*, 2009).
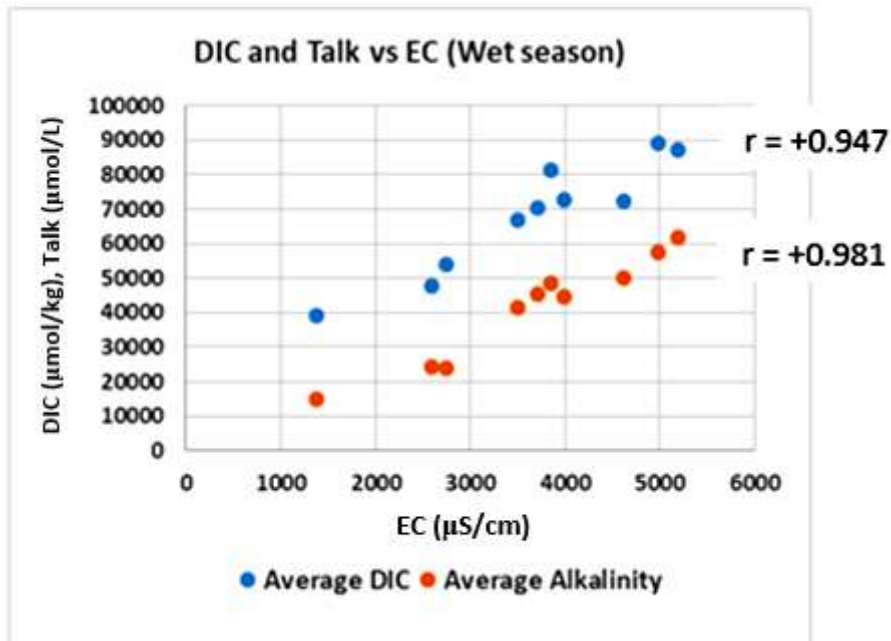
Figure 4.24: Pearson correlation of DIC and Talk versus EC in the wet season.
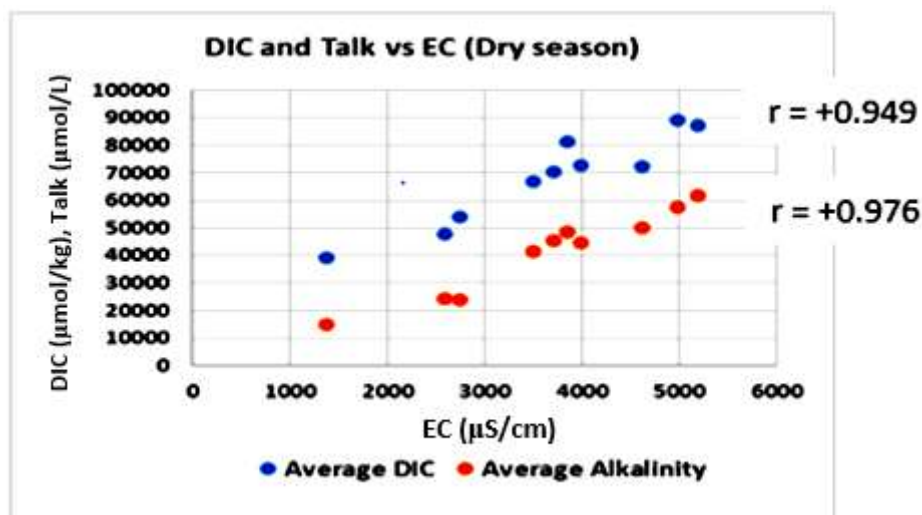
Figure 4.25: Pearson correlation of DIC and Talk versus EC in the dry season.

Figures 4.26 and 4.27 shows how pH correlates with DIC and Talk during the wet and dry seasons, respectively. It is apparent that the pH had a very strong positive correlation with DIC and Talk, in both seasons. This suggested that, the increase of dissociated H_2CO_3 is accompanied by dissolution of carbonates (Mahar *et al*., 2014; Andrews *et al*., 2004).
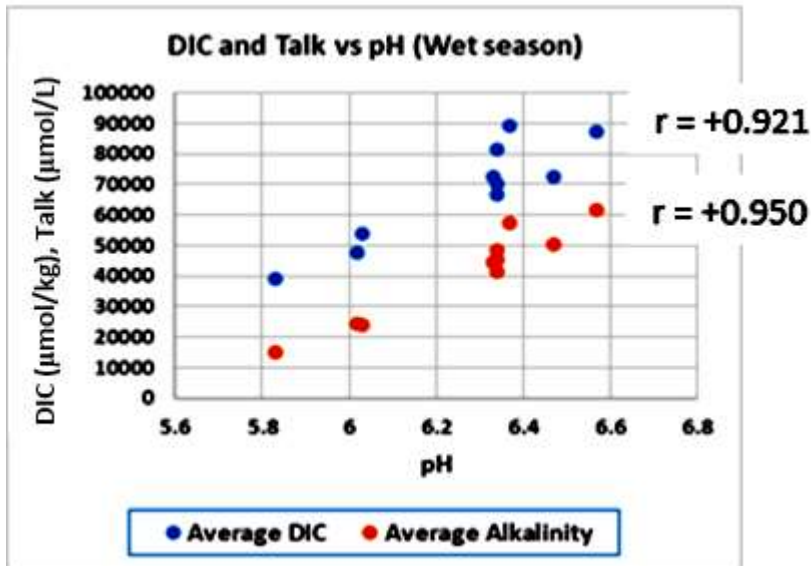
Figure 4.26: Pearson correlation of DIC and Talk versus pH in the wet season.
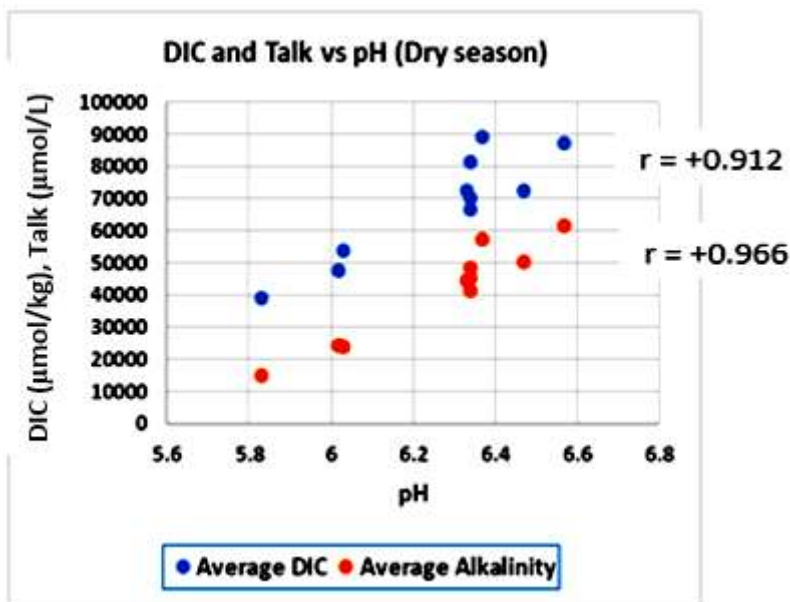
Figure 4.27: Pearson correlation of DIC and Talk versus pH in the dry season.

The relationship between pH and EC in Figures 4.28 and 4.29 showed a strong positive correlation This could be attributed to the acid hydrolysis of carbonate and silicate minerals from host rocks as described earlier in sections 4.6.1 and 4.6.2 (Andrews *et al.*, 2004).
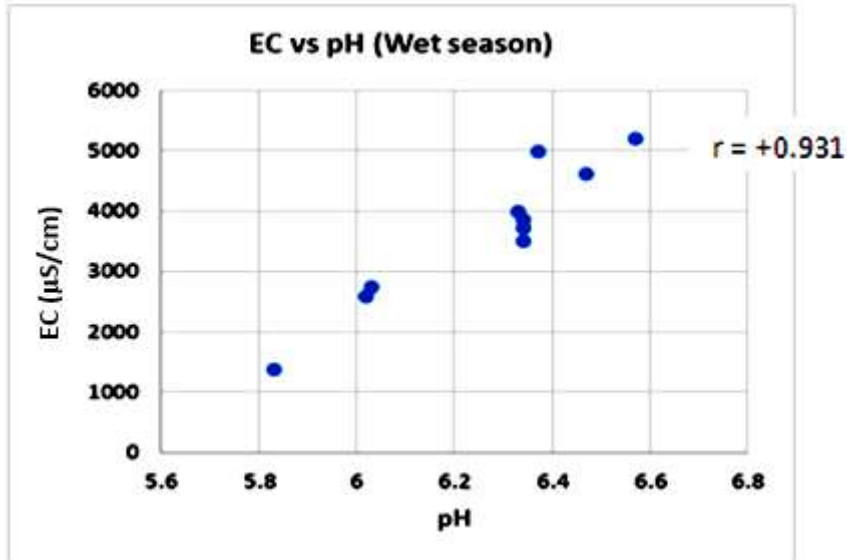
Figure 4.28: Pearson correlation of EC versus pH in the wet season.
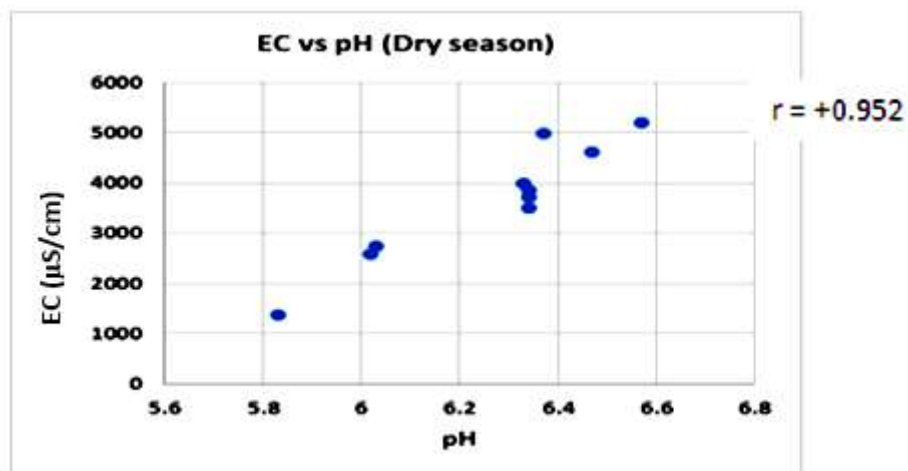
Figure 4.29: Pearson correlation of EC versus pH in the dry season.

There was only a slight increase especially in the dry season in DIC-Talk with increase in EC as shown in Figures 4.30 and 4.31 which suggested that the more CO_2 in the system, the more dissolution of carbonates and increase in alkalinity. According Koch *et al*. (2008), increase in DIC is accompanied by increase in alkalinity due to CO_2 buffering effect. This maintains DIC-Talk relatively constant thus giving near zero or no correlation.
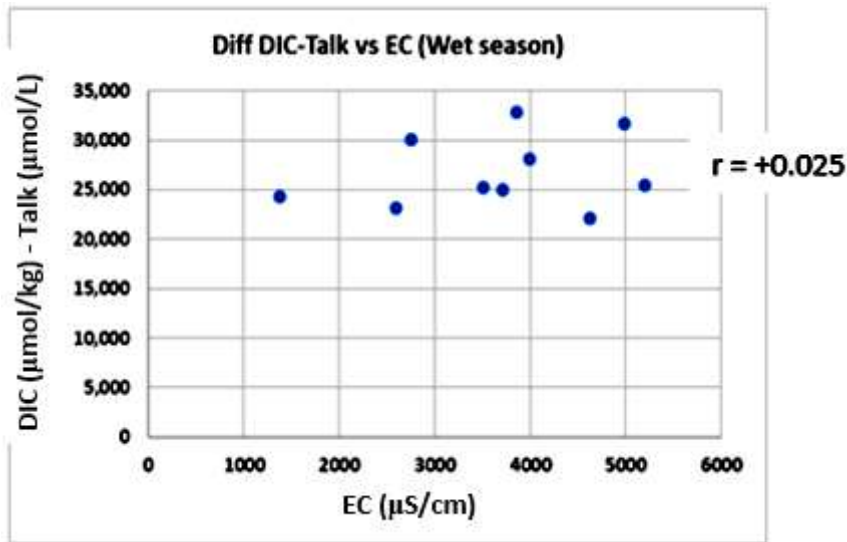
Figure 4.30: Pearson correlation of Difference DIC-Talk versus EC in the wet season.
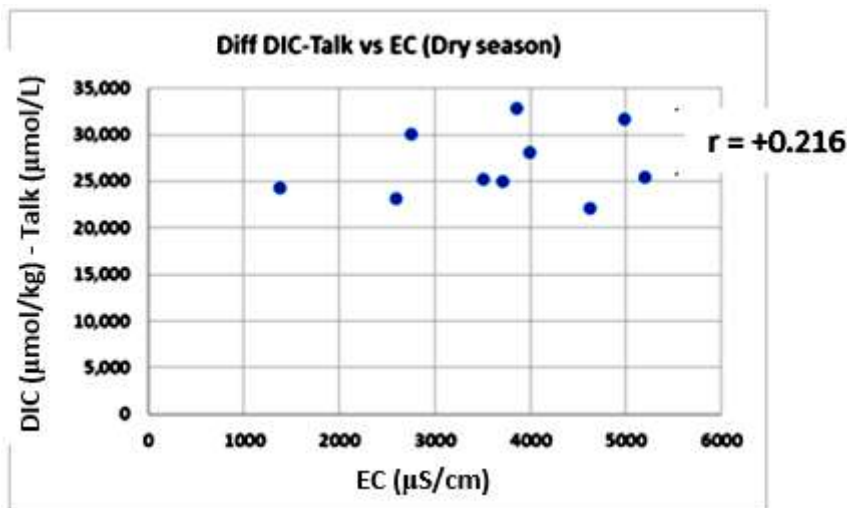
Figure 4.31: Pearson correlation of Difference DIC-Talk versus EC in the dry season.

There was a strong positive correlation between Na^+ ions with DIC and alkalinity as presented in Figure 4.32 and 4.33 which indicated that higher CO_2 in the system is matched with elevated mineral dissolution from the host rocks.
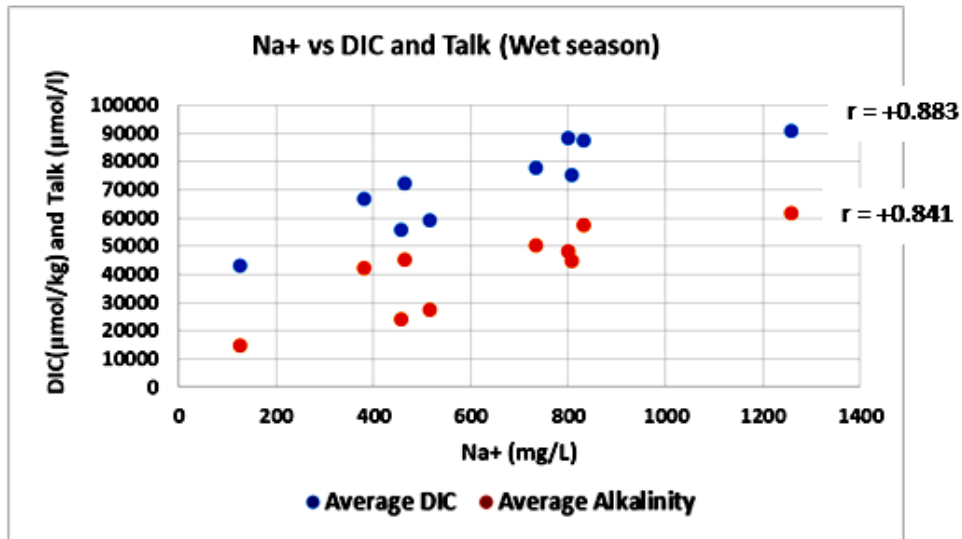
Figure 4.32: Pearson correlation of Na^+ versus DIC and Talk in the wet season.
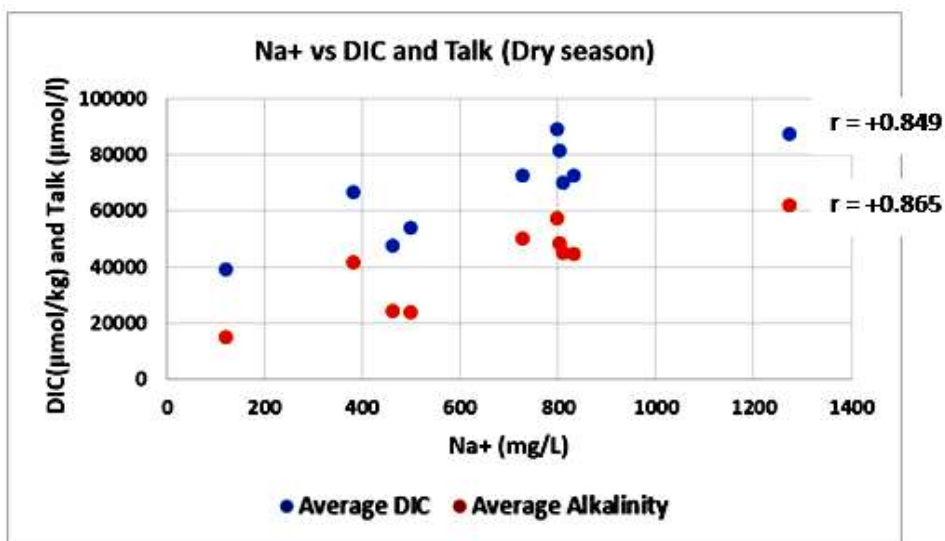
Figure 4.33: Pearson correlation of Na^+ versus DIC and Talk in the dry season.

Positive linear relationship existed between Na^+ ions and EC as shown in Figures 4.34 and 4.35. This implied that the resultant high EC is a manifestation of increasing Na^+ and mineralisation of the CO_2-rich waters (Crundwell, 2014; Assayang *et al.*, 2009).
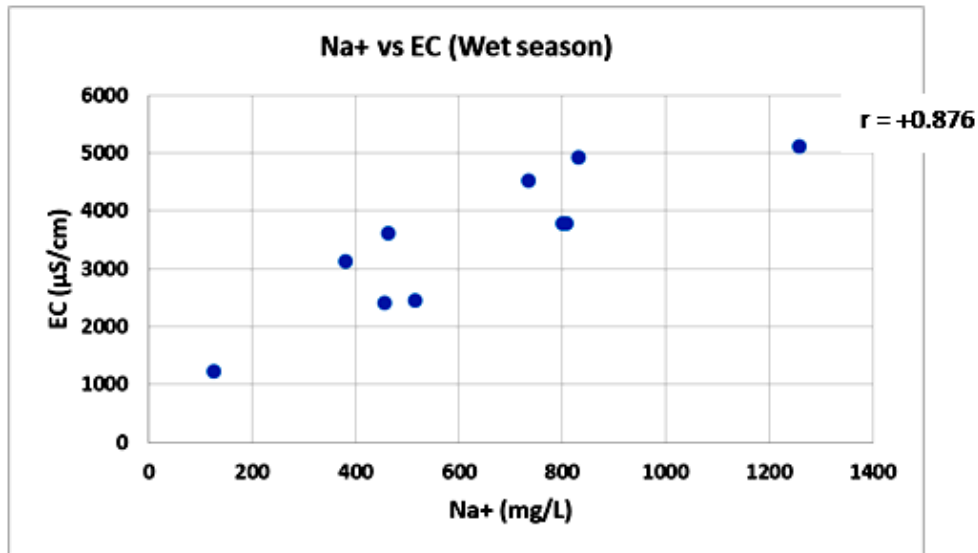
Figure 4.34: Pearson correlation of Na^+ versus EC in the wet season.
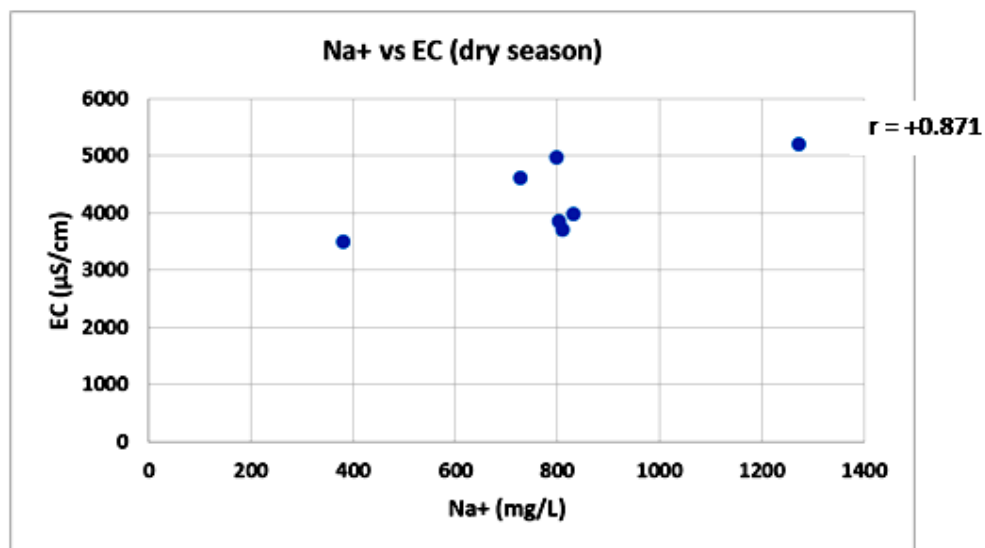
Figure 4.35: Pearson correlation of Na^+ versus EC in the dry season.

4.6.5 Classification of water-types

Piper diagrams for the classification of water-types are shown in Figures 4.36 and 4.37. GW_Chart Software was used to construct the Piper diagrams based on the major ions (Na^+, K^+, Ca^{2+}, Mg^{2+}, HCO_3^-, Cl^- and SO_4^{2-}). The species falls in same areas in these diagrams and this indicate similarity of the water-types or hydrochemical facies (Kumar, 2013).
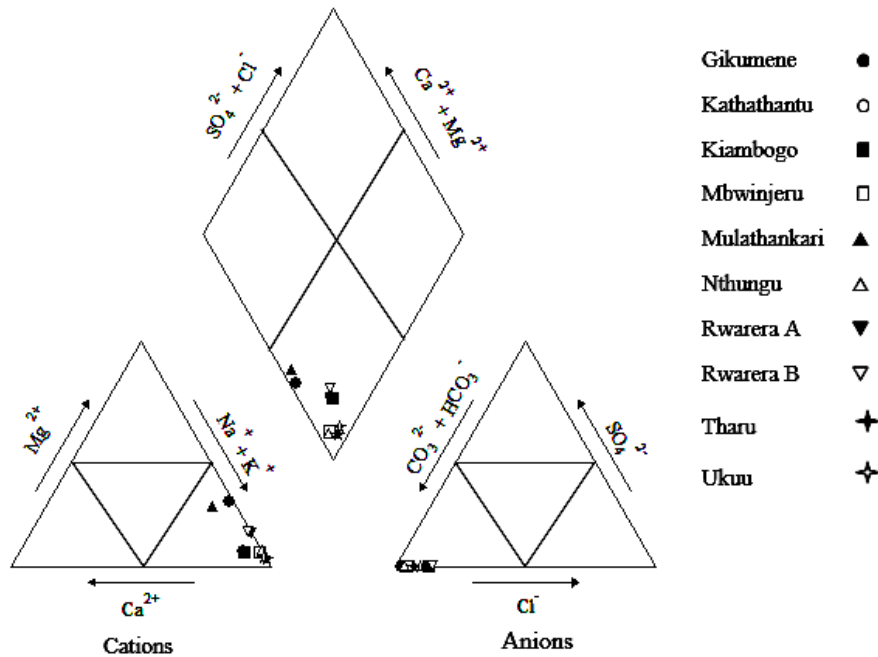
Figure 4.36: Piper plot for the classification of spring waters in the wet season.
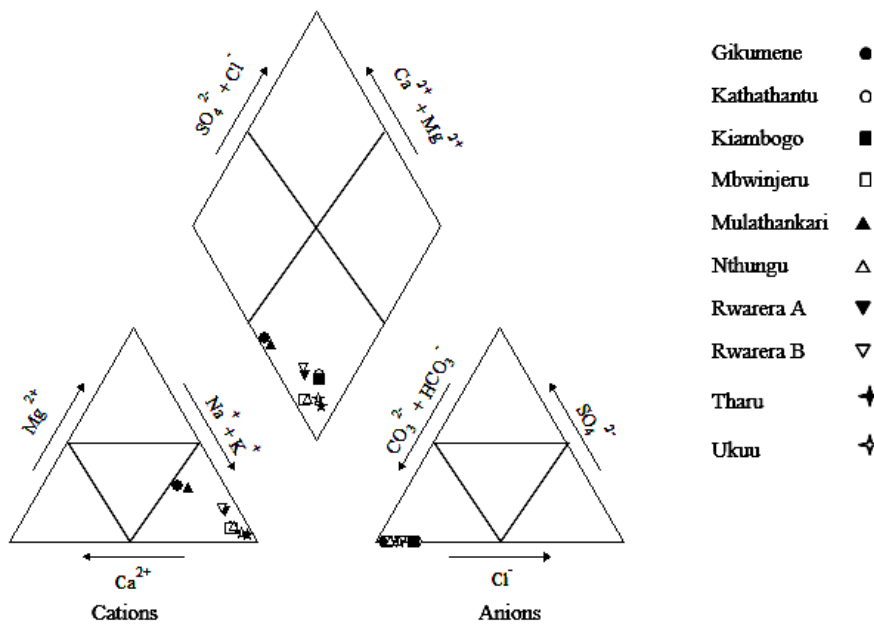
Figure 4.37: Piper plot for the classification of spring waters in the dry season.

The predominant ions were Na^+ and HCO_3^- in both seasons, constituting more than 50% of the major ions. The main water-type was therefore $Na-HCO_3$ (Bicarbonate-alkaline waters). The waters could also be classified into $Na-Ca-HO_3$ and $Na-Mg-HCO_3$ to some extent at Gikumene and Mulathankari springs. The dominance of Na^+ largely counterbalanced by HCO_3^- (weak acid anion) rather than of Cl^- and SO_4^{2-} (strong acid anions) is evidence for magmatic source of CO_2 as opposed to carbonate dissolution. Abundance of Na^+ in the cations also suggest that silicates are the dominant source of weathering products. Water-types evaluation helps in understanding the hydrogeochemical processes due to water-rock interaction in the subsurface which influences the groundwater chemistry (Kumar and James, 2016; Marques *et al*., 2001). According to a similar study in South Korea by Jeong *et al.* (2005), the water-types were classified as $Ca-HCO_3$, $Ca-Na-HCO_3$ and $Na-HCO_3$. Mofette springs in Swiss Alps Lower Engadine, in Switzerland showed $Na-HCO_3-Cl^-$, $Na-Mg-HCO_3-SO_4^{2-}$ and $Ca-HCO_3$ water-types (Wexsteen *et al*., 1988).

4.7 Essential trace elements and contaminants in the spring waters

Tables 4.10 and 4.11 show the average (n = 3) analytical data in µg/L (ppb) for 19 trace elements in wet and dry seasons, respectively. The analysis was performed by ICP-OES method. The levels of most trace minerals were generally high as would be expected of CO_2-rich waters. A few parameters were below the limits of quantitation (LOQ). A significant number of springs had arsenic (As), Boron (B) and Manganese (Mn) levels above the health guideline value for drinking-water, set by the Kenya Bureau of Standards (KEBS, 2018). A few springs had levels of Nickel (Ni) and Selenium (Se) exceeding the permissible limits. Due increase in volume of water in the wet season, the measured levels of these elements were relatively lower as compared to the dry season.

The action of acidic water on rocks enhances mineral dissolution (Jeong *et al*., 2005). A study on CO_2-rich waters in Iceland showed that water-rock interaction is responsible for elevated trace elements above WHO guidelines for drinking-water, especially As and Mn at < 0.01-1.08 µmol/kg and 0.1-184 µmol/kg, respectively (Thomas *et al*., 2016). Similarly, some CO_2-rich springs in Eastern Mt. Kenya region were found to be contaminated with toxic elements derived from rocks which include As, B, Mn, Ni and Se.

Table 4.10: Concentration (µg/L) of trace elements in the waters for wet season.

Element		GIK	KAT	KIA	MBW	MUL	NTH	RWA	RWB	THA	UKU	KEBS GDWQ
Ag	Mean	<1.2	<1.2	<1.2	<1.2	<1.2	<1.2	<1.2	<1.2	<1.2	<1.2	-
	RSD	-	-	-	-	-	-	-	-	-	-	
Al	Mean	30.1	148.1	113.8	187.6	24	17.5	15.3	24.9	8.5	21.2	-
	RSD	0.2	0.5	0.3	0.8	0.3	0.5	0.1	0.3	0.4	0.5	
As	Mean	<3.7	<3.7	<3.7	<3.7	<3.7	<3.7	**10.3***	**13.0***	<3.7	<3.7	10
	RSD	-	-	-	-	-	-	0.4	0.7	-	-	
B	Mean	15.2	130.5	102.1	236.9	16.4	151.6	154.3	181.7	**547.4***	292.6	300
	RSD	0.5	0.8	0.3	1.9	0.2	1.6	1.5	0.7	1.2	0.6	
Ba	Mean	73.5	126.9	117.4	184.1	12.8	16.7	95.5	66.3	78.2	2.4	700
	RSD	0.9	0.3	0.5	0.8	0.3	0.7	0.4	0.6	0.6	0.5	
Be	Mean	<0.4	2.2	1.5	0.8	<0.4	2.3	<0.4	<0.4	1.7	<0.4	-
	RSD	-	0.3	0.1	0.4	-	0.3	-	-	0.4	-	
Cd	Mean	<0.1	<0.1	<0.1	<0.1	<0.1	<0.1	<0.1	<0.1	<0.1	<0.1	3
	RSD	-	-	-	-	-	-	-	-	-	-	
Co	Mean	10.3	<1.6	<1.6	<1.6	3.8	<1.6	<1.6	<1.6	<1.6	<1.6	-
	RSD	0.4	-	-	-	0.2	-	-	-	-	-	
Cr	Mean	<0.2	<0.2	<0.2	<0.2	<0.2	<0.2	<0.2	<0.2	<0.2	<0.2	50
	RSD	-	-	-	-	-	-	-	-	-	-	
Cu	Mean	<0.1	<0.1	<0.1	3.1	<0.1	<0.1	5.0	4.7	5.3	5.8	1000
	RSD	-	-	-	0.2	-	-	0.2	0.4	0.3	0.2	
Fe	Mean	7,720	6,853	6,141	6,150	623	8,450	2,611	1,032	2,128	4,397	-
	RSD	3.3	2.1	2.4	2.5	1.9	3.7	1.3	1.5	1.8	2.0	
Hg	Mean	<0.8	<0.8	<0.8	<0.8	<0.8	<0.8	<0.8	<0.8	<0.8	<0.8	1
	RSD	-	-	-	-	-	-	-	-	-	-	
Mn	Mean	**1,143***	**796***	**903***	125	**1,150***	481	364	279	164	451	500
	RSD	1.6	0.8	0.9	0.5	1.8	0.4	0.4	0.5	0.3	0.6	
Mo	Mean	<1.0	<1.0	<1.0	<1.0	1.0	<1.0	1.4	<1.0	<1.0	1.8	-
	RSD	-	-	-	-	0.2	-	0.2	-	-	0.3	
Ni	Mean	8.0	<5.8	<5.8	<5.8	10.5	<5.8	<5.8	<5.8	<5.8	<5.8	20
	RSD	0.5	-	-	-	0.4	-	-	-	-	-	
Pb	Mean	<1.2	<1.2	<1.2	<1.2	<1.2	<1.2	<1.2	<1.2	<1.2	<1.2	10
	RSD	-	-	-	-	-	-	-	-	-	-	
Se	Mean	<4.9	<4.9	<4.9	<4.9	5.5	<4.9	4.9	8.3	**12.4***	<4.9	10
	RSD	-	-	0.3	-	0.2	-	0.5	0.4	0.7	-	
Si	Mean	876	778	835	877	651	1,051	1,086	905	913	749	-
	RSD	0.82	2.43	2.01	1.32	2.57	1.44	2.48	2.62	0.63	1.51	
Zn	Mean	9.2	<3.0	<8.0	9.9	<3.0	6.6	<3.0	<3.0	<3.0	<3.0	-
	RSD	0.5	-	-	0.4	-	0.5	-	-	-	-	

*Above KEBS guideline for drinking-water quality (GDWQ).

< Below the limit of quantitation (LOQ).

- Occurs in drinking water at concentrations well below those of health concern.

Table 4.11: Concentration (μg/L) of trace elements in the waters for dry season.

Element		GIK	KAT	KIA	MBW	MUL	NTH	RWA	RWB	THA	UKU	KEBS GDWQ
Ag	Mean	8.2	<1.2	<1.2	10.6	15.2	10.0	10.7	<1.2	<1.2	<1.2	-
	RSD	0.2	-	-	0.3	0.6	0.4	0.4	-	-	-	
Al	Mean	50.5	202.1	154.8	265.6	54.3	27.8	25.7	54.6	18.1	41.8	-
	RSD	0.7	0.9	1.2	1.5	0.6	0.4	0.6	0.5	0.3	0.5	
As	Mean	<3.7	8.8	6.5	**14.4***	5.1	**11.1***	**16.5***	**19.7***	**21.5***	**13.9***	10
	RSD	-	0.4	0.3	0.7	0.2	0.6	0.4	0.3	0.8	0.4	
B	Mean	34.6	210.2	192.8	**386.7***	44.1	241.1	**334.5***	**301.9***	**837.1***	**414.2***	300
	RSD	0.7	1.3	0.6	1.5	0.8	1.0	1.4	0.9	2.2	1.7	
Ba	Mean	133.1	188.2	166.5	247.5	34.4	45.1	143.7	91.0	213.7	8.6	700
	RSD	1.5	0.7	1.3	0.6	0.5	0.8	0.5	0.7	1.2	0.2	
Be	Mean	<0.4	3.5	2.4	1.6	<0.4	3.8	<0.4	<0.4	3.4	<0.4	-
	RSD	-	0.6	0.4	0.4	-	0.9	-	-	0.6	-	
Cd	Mean	0.5	0.3	<0.1	0.7	0.5	0.6	0.5	0.2	0.3	0.2	3
	RSD	0.6	0.6	-	0.5	0.8	0.4	0.6	0.5	0.7	0.4	
Co	Mean	15.1	<1.6	<1.6	<1.6	9.8	<1.6	2.4	2.6	<1.6	<1.6	-
	RSD	0.4	-	-	-	0.1	-	0.5	0.3	-	-	
Cr	Mean	0.6	0.6	0.8	2.5	1.2	1.3	1.3	0.8	0.6	0.7	50
	RSD	0.9	0.5	0.5	0.4	0.7	0.1	0.4	0.5	0.2	0.1	
Cu	Mean	4.2	6.1	6.4	10.8	7.8	8.4	11.1	10.9	11.5	11.9	1,000
	RSD	0.7	0.8	0.1	0.3	0.5	0.9	0.4	0.2	0.5	0.3	
Fe	Mean	7,077	8,757	8,077	7,070	1,972	6,678	4,207	2,538	2,602	6,079	-
	RSD	3.2	2.8	3.4	3.1	1.4	2.7	2.1	2.2	1.5	2.5	
Hg	Mean	<0.8	<0.8	<0.8	<0.8	<0.8	<0.8	<0.8	<0.8	<0.8	<0.8	1
	RSD	-	-	-	-	-	-	-	-	-	-	
Mn	Mean	**1,347***	**920***	**1,068***	135	**1,041***	**531***	444	329	224	**522***	500
	RSD	1.2	1.6	2.0	0.5	1.7	0.8	1.1	0.5	0.9	1.4	
Mo	Mean	1.5	1.4	1.8	1.8	2.4	1.9	2.2	<1.0	<1.0	2.6	-
	RSD	0.8	0.3	0.5	0.2	0.7	0.1	0.5	-	-	0.3	
Ni	Mean	**23.0***	<5.8	<5.8	<5.8	**25.5***	8.0	9.6	9.1	<5.8	<5.8	20
	RSD	0.5	-	-	-	0.2	0.2	0.1	0.5	-	-	
Pb	Mean	<1.2	<1.2	<1.2	4.3	<1.2	<1.2	3.2	4.1	3.1	2.6	10
	RSD	-	-	-	0.6	-	-	0.6	0.5	0.8	0.4	
Se	Mean	<4.9	<4.9	7.5	<4.9	9.2	6.0	**10.8***	**14.7***	**20.6***	6.0	10
	RSD	-	-	0.8	-	0.7	0.4	0.5	0.5	0.4	0.7	
Si	Mean	2,032	1,820	1,896	2,019	1,713	2,109	2,176	1,980	2,581	1,613	-
	RSD	1.2	1.6	0.9	2.6	1.9	2.1	2.4	1.5	1.2	0.7	
Zn	Mean	15.7	4.5	5.5	16.4	7.2	13.7	5.6	<3.0	4.0	6.2	-
	RSD	0.3	0.1	0.6	0.4	0.2	0.5	0.4	-	0.1	0.5	

*Above KEBS guideline for drinking-water quality (GDWQ).

< Below the limit of quantitation (LOQ).

- Occurs in drinking water at concentrations well below those of health concern.

4.7.1 Essential trace elements in the spring waters

Boron (B) levels of 15.2-547.4 µg/L in wet season and 34.6-837.1 µg/L in dry season were below the recommended WHO (2011) limit of 2,400 µg/L. However, during the dry season, MBW (386.7 µg/L), RWA (334.5 µg/L), RWB (301.9 µg/L), THA (837.1 µg/L) and UKU (414.2 µg/L) levels were above KEBS limit of 300 µg/L (KEBS, 2018). THA at 547.4 µg/L also exceeded the KEBS limit in the wet season. Cobalt (Co) ranged from <1.6 (below LOQ) to 10.3 and <1.6 to 15.1 µg/L, during the wet and dry seasons, respectively. WHO and KEBS have not indicated guideline value for Co in drinking water. Waters at GIK (15.1 µg/L), MUL (9.8 µg/L), RWA (2.4 µg/L) and RWB (2.6 µg/L) would possibly be an alternative natural source of cobalt. Chromium (Cr) values (wet season, <0.2 and dry season, 0.6-2.5 µg/L) were below the allowed maximum limit. WHO (2011) has given Cr a provisional guideline value of 50 µg/L because of uncertainties in its toxicological database while KEBS (2018) has set the safe limit at 50 µg/L.

Copper (Cu) levels (wet season, <0.1-5.8 and dry season, 4.2-11.9 µg/L) were safe because the WHO and KEBS guideline values in drinking water are 2,000 and 1,000 µg/L, respectively. Iron (Fe) was significant in the spring waters varying from 623 to 8,450 and 1,972 to 8,757 µg/L, during the wet and dry seasons, respectively. This accounts for the brown precipitates in the waters as indicated earlier in sections 4.2 and 4.3. There is no guideline value for Fe proposed by WHO and KEBS, since the level found in drinking water is not of any health concern (WHO, 2011; KEBS, 2018). The high Fe levels in the waters can be lowered by ion exchange using synthetic polymer or natural mineral ion exchangers such as zeolites. It can also be removed by filtration after oxidation with air, potassium permanganate, or chlorine (Khatri *et al*., 2017; Khadse *et al*., 2015; Korngold, 1994).

Manganese (Mn) concentration in the springs was 125-1,150 and 135-1,347 µg/L, in wet and dry seasons, respectively. According to WHO, Mn level found in drinking water is not of health concern and the previous guideline value of 400 µg/L was discontinued in 2011. However, KEBS has set the maximum limit at 500 µg/L. GIK (1143 µg/L), KAT (796 µg/L), KIA (903 µg/L) and MUL (1150 µg/L) exceed KEBS limit in wet season. While those below KEBS limits in the dry season were MBW (135 µg/L), RWA (444 µg/L), RWB (329 µg/L) and THA (224 µg/L). Like Fe, ion exchange method can be used to remove the excess Mn in the spring waters or by filtration after oxidation (Bastida *et al*., 2018; Tobiason *et al*, 2016; Taffarel *et al.,* 2009).

Molybdenum (Mo) values ranged from <1.0 (below LOQ) to 1.8 and <1.0 to 2.6 µg/L, during the wet and dry seasons, respectively. WHO and KEBS have not established a formal guideline value for Mo. Nickel (Ni) results were <5.8 (below LOQ)-10.5 and <5.8-25.5 µg/L, during the wet and dry seasons, respectively. These values were within the WHO guideline value of 70 µg/L. However, GIK (23.0 µg/L) and MUL (25.5 µg/L) were slightly above the KEBS limit of 20 µg/L, during the dry season. Selenium (Se) levels at <4.9 (below LOQ)-12.4 (wet season) and <4.9 to 20.6 µg/L (dry season) were below the WHO (2011) provisional guideline value of 40 µg/L. However, the levels at RWA (10.8 µg/L), RWB (14.7 µg/L) and THA (20.6 µg/L) were above the KEBS limit of 10 µg/L during dry season. THA with 12.4 µg/L was also above the KEBS limit in wet season.

Silicon (Si) levels ranged between 651-2,581 µg/L. WHO and KEBS have not established the limits for Si in drinking water because it is considered to have insignificant concern to human health. Zinc (Zn) levels at <3.0 (below LOQ)-9.9 and <3.0-16.4 µg/L were found in the springs during the wet and dry seasons, respectively. WHO and KEBS have not established guideline value considering that Zn is not of health concern at levels found in drinking water. However, drinking water containing Zn level above 3000 µg/L may be objectionable to consumers. Zinc levels in surface waters and groundwaters usually do not exceed 10 and 50 µg/L, respectively (WHO, 2011).

4.7.2 Inorganic contaminants in the spring waters

Silver (Ag) in the waters ranged from <1.2 (below LOQ) and <1.2 to 15.2 µg/L, during the wet and dry seasons, respectively. Due to inadequate supportive data, WHO (2011) and KEBS (2018) have not set a health-based guideline value for Ag in drinking water. Aluminium (Al) in the springs ranged from 8.5 to 187.6 and 18.1 to 256.6 µg/L, in wet and dry seasons, respectively. There is no established WHO and KEBS guideline values for Al because there is little evidence of ingested Al toxicity to humans (WHO, 2011; KEBS, 2018). The Al levels for KAT (202.1 µg/L), KIA (154.8 µg/L) and MBW (265.6 µg/L) are relatively higher than those of the other springs and therefore may be avoided.

Arsenic (As) varied from <3.7 (below LOQ)-13.0 and <3.7-21.5 µg/L, in wet and dry seasons, respectively, against WHO and KEBS guideline value of 10 µg/L. The levels for MBW (14.4 µg/L), NTH (11.1 µg/L), RWA (16.5 µg/L), RWB (19.7 µg/L), THA (21.5 µg/L) and UKU (13.9 µg/L) exceeded permissible limit during the dry season while RWA

(10.3 µg/L), RWB (13.0 µg/L) were also higher in the wet season. The source could be As-bearing sulphide and sedimentary mineral deposits such as arsenopyrite-FeAsS (Herath *et al.*, 2016). Carbonation of arsenic sulphide minerals helps in leaching of As into the groundwater under anaerobic conditions by forming stable arseno-cabonate complexes such as $As(CO_3)(OH)_2^-$, $As(CO_3)^{2-}$ and $AsCO_3^+$ (Kim *et al.*, 2000). Figure 4.38 shows a strong positive linear relationship (r = +0.8) between As levels and DIC. High amount of CO_2 in the waters enhances leaching of As from the underlying rocks posing health risk to users. The six springs above the As safe limits have higher DIC levels than the other four as shown earlier in Tables 4.5 and 4.6. The results ahead in section 4.8.3, Table 4.13, also indicate presence of As in host rocks throughout all the springs.
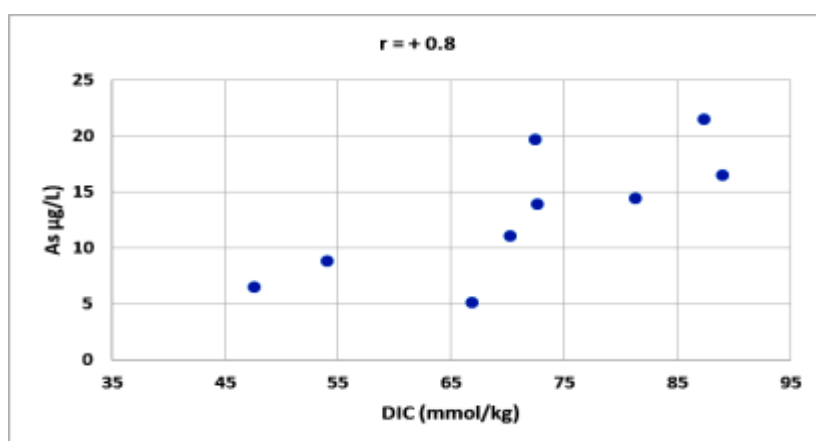
Figure 4.38: Correlation of As with DIC.

Arsenic can be removed from the waters prior to consumption using the available methods such as electrocoagulation (Ucar *et al.*, 2013; Ratna *et al.*, 2004), flocculation followed by microfiltration (Han *et al.*, 2002) and granular ferric hydroxide (Driehaus *et al.*, 1998). Barium (Ba) (wet season, 2.4-184.1 and dry season, 8.6-247.5 µg/L) was below the WHO and KEBS guideline value in drinking water which is 700 µg/L. Beryllium (Be) values were somewhat low at <0.4 (below LOQ) to 2.3 and <0.4 to 3.8 µg/L, during the wet and dry seasons, respectively. Beryllium is rarely found in drinking water at concentrations of health concern hence WHO and KEBS considers it not necessary to set a formal guideline value.

Cadmium (Cd) levels at <0.1 (below LOQ) to 0.7 µg/L were below the WHO and KEBS maximum approved limit of 3 µg/L and the waters could be considered safe as far as Cd toxicity is concerned. Mercury (Hg) measured in all the springs was <0.8 µg/L (below LOQ) during both seasons. WHO and KEBS guideline values for inorganic mercury are 6 µg/L and

1 µg/L, respectively. The waters were therefore not Hg contaminated. Lead (Pb) ranged from <1.2 (below LOQ) and <1.2-4.3 µg/L in wet and dry seasons, respectively. WHO and KEBS guideline value for Pb is 10 µg/L. All the springs were below the permissible level.

4.8 Geochemical composition of host rocks

For thorough scrutiny of structure and composition of parent rocks in the springs, AAS, XRF and XRD techniques were used. Chemical analysis of major oxides by AAS gave the percentage composition of major rock forming elements namely, Al_2O_3, CaO, Fe_2O_3, K_2O, MgO, MnO, Na_2O, SiO_2 and TiO_2. Loss on ignition (LOI) which represents the proportion of volatile matter in a mineral sample was expected to vary with the type of minerals in the rock. The XRF and XRD data provided further information on elemental composition and different types of minerals in the rocks, respectively. Unlike for the spring waters which were analysed in both wet and dry seasons, rocks were analysed once because seasonal variation in composition was not expected to be significant. The purpose of the host rock analysis was to determine the correlation between their geochemical compositions with the solutes content in the spring waters.

4.8.1 AAS analysis of major oxides in the rocks

The percentage composition of major oxides in the rocks and loss on ignition (LOI), obtained by AAS method are presented in Table 4.12. Three replicate samples were analysed for each spring. The SiO_2 content of 38.5-55.62 % found in eight sites suggests occurrence of basalt rocks. Based on the Total Alkali versus Silica (TAS) classification, basalt rocks contains 45-52 % SiO_2 (Le Maitre *et al*., 2002). These basalts may include alkali feldspars (albite-$NaAlSi_3O_8$, orthoclase-$KAlSi_3O_8$), plagioclase feldspars (Arnothite-$CaAl_2Si_2O_8$), olivine-$(Mg, Fe)_2SiO_4$ and pyroxenes such as augite-$(Ca,Na)(Mg,Fe,Al,Ti)(Si,Al)_2O_6$ (Mitchell, 1986; Rutley, 1988). The low SiO_2 at RWA (7.03 %) and RWB (5.11 %) and elevated CaO at 40.23 % and 38.83 %, respectively, could be attributed to the presence of sedimentary carbonate rocks such as calcite, $CaCO_3$ and dolomite, $CaMg(CO_3)_2$.

Table 4.12: AAS percentage composition and LOI of major oxides in the rocks.

SPRING		GIK	KAT	KIA	MBW	MUL	NTH	RWA	RWB	THA	UKU
Al_2O_3	Mean	14.86	21.43	15.43	16.07	16.3	21.40	1.02	0.66	14.48	14.58
	RSD	2.3	1.4	3.3	2.0	2.2	1.1	5.5	3.3	2.1	2.1
CaO	Mean	10.13	1.09	1.08	1.24	6.0	0.79	40.23	38.83	12.03	7.49
	RSD	2.8	1.5	5.5	3.5	0.8	1.4	3.9	1.4	1.5	5.8
Fe_2O_3	Mean	12.18	10.40	5.29	5.90	6.20	7.90	0.83	0.04	5.55	4.85
	RSD	5.2	2.5	3.6	1.0	1.3	2.2	4.2	4.2	1.7	3.6
K_2O	Mean	1.15	1.80	4.37	1.90	1.69	0.67	0.22	0.04	3.83	4.00
	RSD	5.6	0.9	5.8	0.9	0.6	0.9	2.7	2.7	0.9	2.6
MgO	Mean	6.07	2.60	0.12	2.8	2.70	1.60	4.71	9.90	1.03	0.51
	RSD	0.4	2.1	4.4	2.9	3.6	1.2	3.7	2.1	2.3	4.2
MnO	Mean	0.17	0.30	0.46	0.12	0.2	0.18	0.09	0.02	0.13	0.26
	RSD	4.3	6.8	5.8	1.1	1.2	1.1	2.6	3.3	1.4	2.9
Na_2O	Mean	2.90	3.92	5.45	3.84	3.89	3.78	0.25	0.20	4.21	4.81
	RSD	6.3	0.2	5.6	0.3	2.0	4.4	2.3	2.9	2.8	3.3
SiO_2	Mean	46.43	43.10	55.62	49.5	45.82	38.5	7.03	5.11	44.62	46.96
	RSD	0.8	5.6	1.7	1.3	1.5	1.7	2.0	2.9	2.1	1.3
TiO_2	Mean	2.08	1.78	1.11	3.35	1.99	3.49	1.07	0.96	1.46	1.05
	RSD	2.2	4.7	3.0	3.1	3.2	1.3	3.5	1.8	3.0	2.0
LOI	Mean	2.44	12.72	8.85	13.55	12.98	19.7	43.15	42.23	10.74	13.87
	RSD	4.6	1.3	2.4	3.3	1.8	1.5	1.8	1.4	1.3	1.8
Total (%)		**98.41**	**99.14**	**97.78**	**98.27**	**97.77**	**98.01**	**98.60**	**97.99**	**98.08**	**98.38**

This fact is supported by the high LOI values at RWA (43.15 %) and RWB (42.23 %) as the carbonates are decomposed by heat. Besides SiO_2, other oxides that dominate the samples are Al_2O_3 and Fe_2O_3. Oxygen (O) is usually the most abundant element in the Earth's crust followed by silicon (Si), aluminium (Al) and iron (Fe) in that order (Rutley, 1988). The same trend was observed in the reported data. The oxides of other minor and trace elements contribute the remaining percent to reach 100%.

4.8.2 Correlations between major elements in the rocks and spring waters

Figures 4.39 to 4.50 shows the scatter plots and correlation coefficients (r) of Na_2O, K_2O, CaO, MgO, Fe_2O_3 and MnO, oxides in the host rocks versus similar key metals found in the spring waters. Results in Figure 4.38 and 4.39 indicate very weak negative or no correlation between Na in the spring waters and Na_2O in the parent rocks, for both wet and dry seasons. Hence, there was very little contribution of Na from the rocks in the upper part of the Earth's crust into the spring waters. Sodium occurring in the waters most likely originated from the weathering of subsurface silicate rocks caused by H_2CO_3.
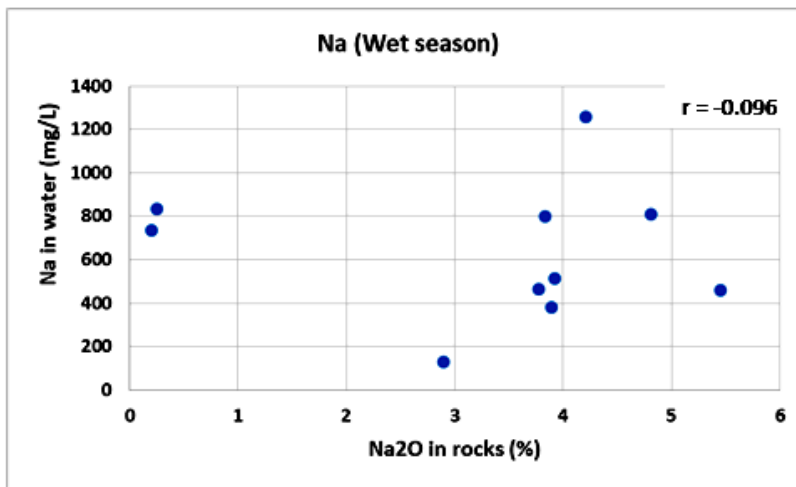
Figure 4.39: Pearson correlation of Na in waters versus Na₂O in rocks in the wet season.
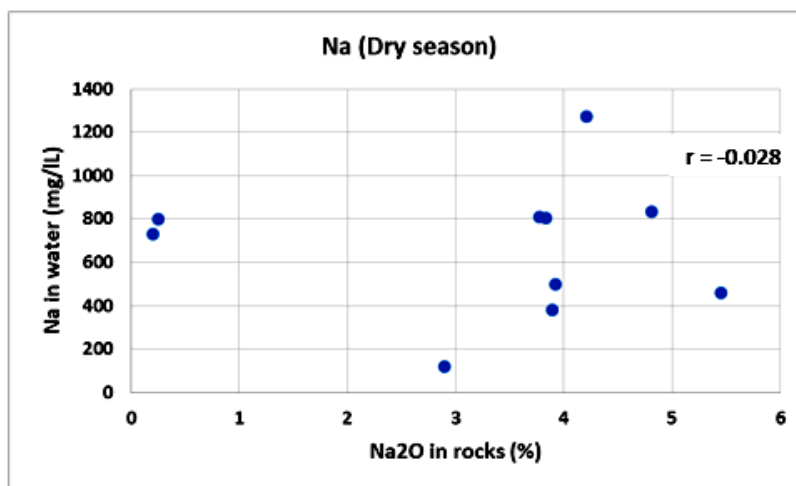
Figure 4.40: Pearson correlation of Na in waters versus Na₂O in rocks in the dry season.

The correlation of K in the spring waters and K_2O in the rocks is reported in Figure 4.41 and 4.42. There was very weak positive correlation meaning that the supply of K from the rocks near the surface into the spring waters was insignificant.
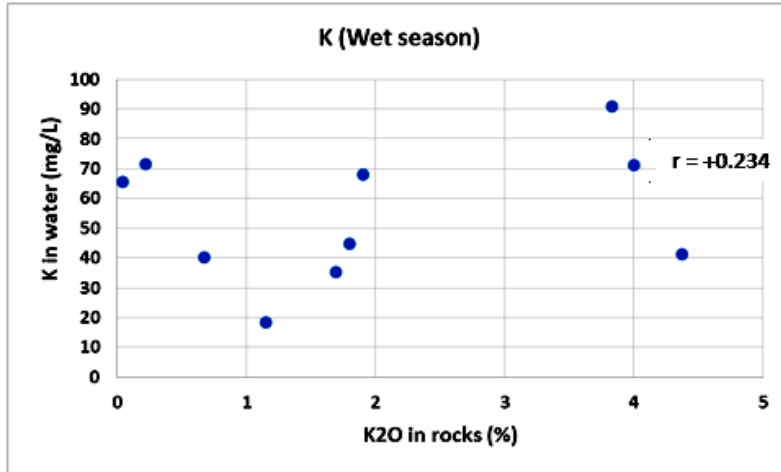
Figure 4.41: Pearson correlation of K in waters versus K_2O in rocks in the wet season.
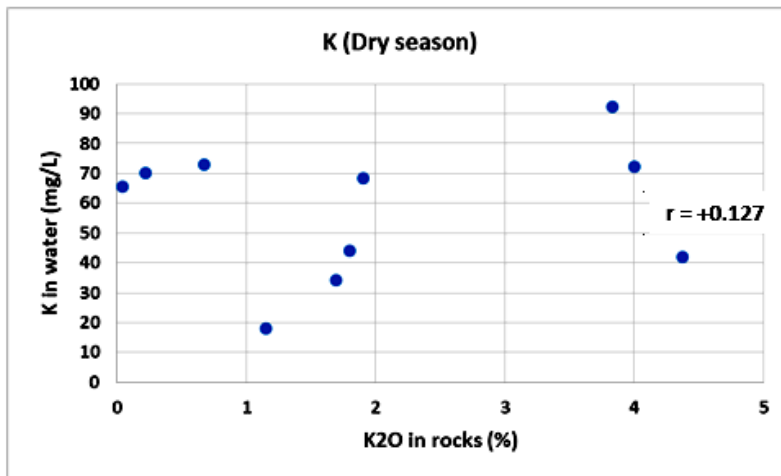
Figure 42: Pearson correlation of K in waters versus K_2O in rocks in the dry season.

Figure 4.43 shows slight negative correlation between Ca in the spring waters and CaO in the host rocks during the wet season. The negative correlation may be attributed to the dilution of the spring waters during the rainy season coupled with the ion-exchange of Ca with Na between the waters and rocks (Kumar and James, 2016). From Figure 4.44, there seems to be no correlation for the dry season samples. Therefore, the origin of Ca in the waters is likely to be deep carbonate rocks.
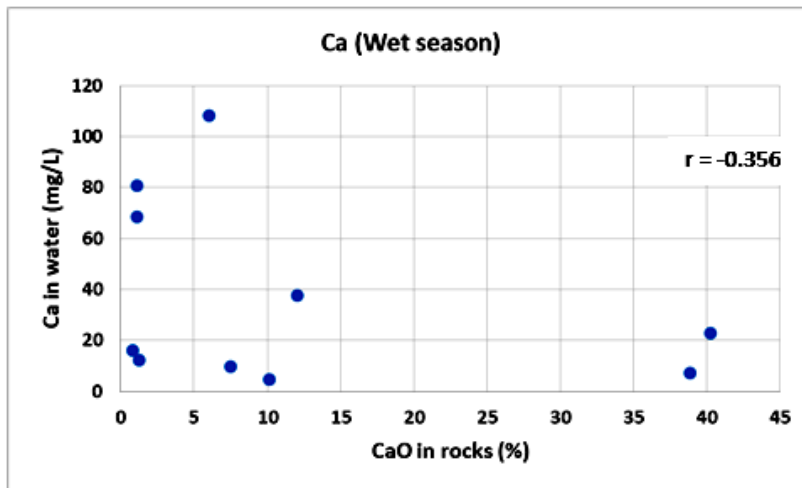
Figure 4.43: Pearson correlation of Ca in waters versus CaO in rocks in the wet season.
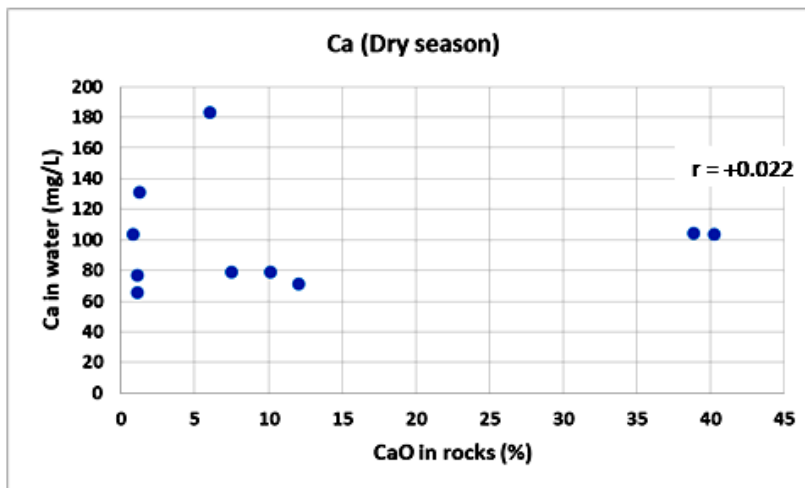
Figure 4.44: Pearson correlation of Ca in waters versus CaO in rocks in the dry season.

There was significant positive correlation of Mg in the spring waters and MgO in the rocks as illustrated in Figure 4.45 and 4.46. Thus, Mg in the waters could be associated with the rocks near the Earth's surface.
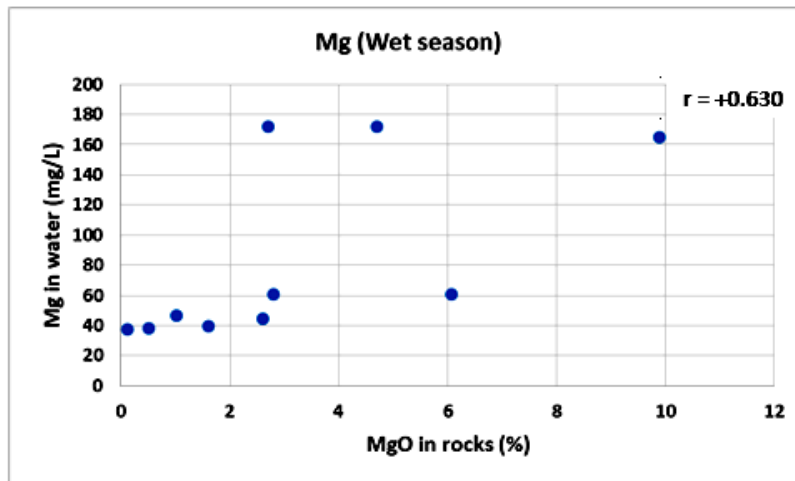
Figure 4.45: Pearson correlation of Mg in waters versus MgO in rocks in the wet season.
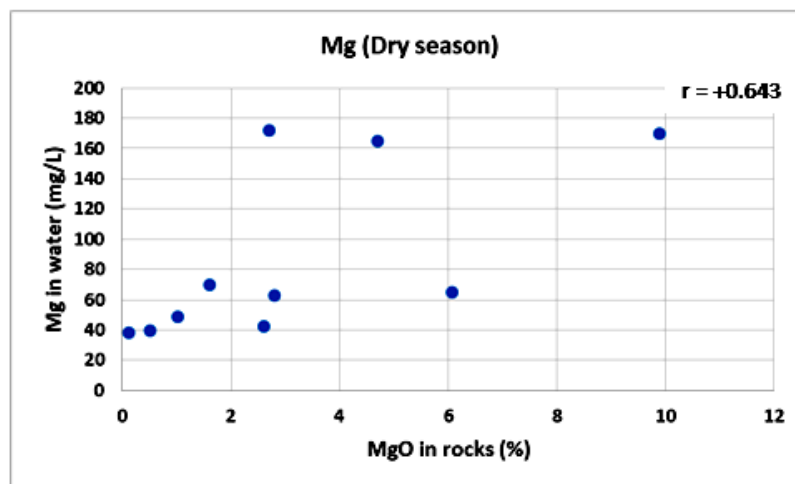
Figure 4.46: Pearson correlation of Mg in waters versus MgO in rocks in the dry season.

In both Figure 4.47 and 4.48, significant positive correlation was established between Fe and Fe_2O_3 in the spring waters and parent rocks. This suggests that the rocks near the surface contributed substantially to the Fe content in the waters.
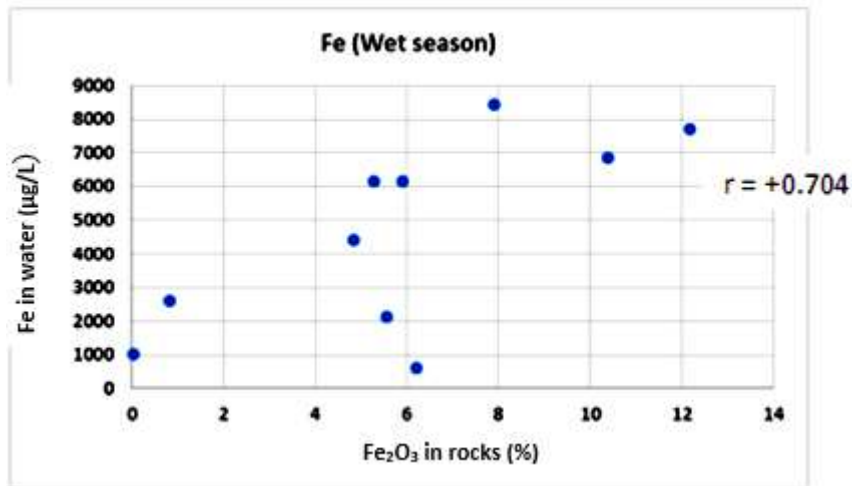
Figure 4.47: Pearson correlation of Fe in waters versus Fe_2O_3 in rocks in the wet season.
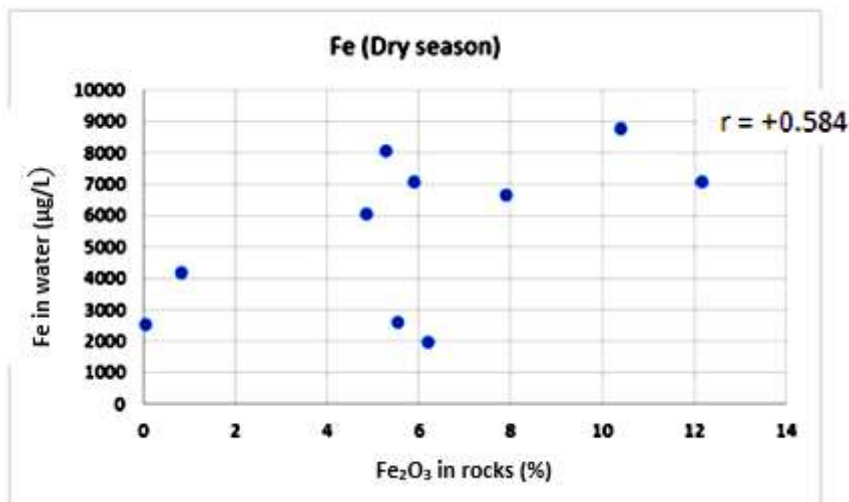
Figure 4.48: Pearson correlation of Fe in waters versus Fe_2O_3 in rocks in the dry season.

Figure 4.49 and 4.50 indicates moderate positive correlation between Mn in the spring waters and MnO in the host rocks. This implies that some of the Mn found in the waters originated from the sampled rocks.
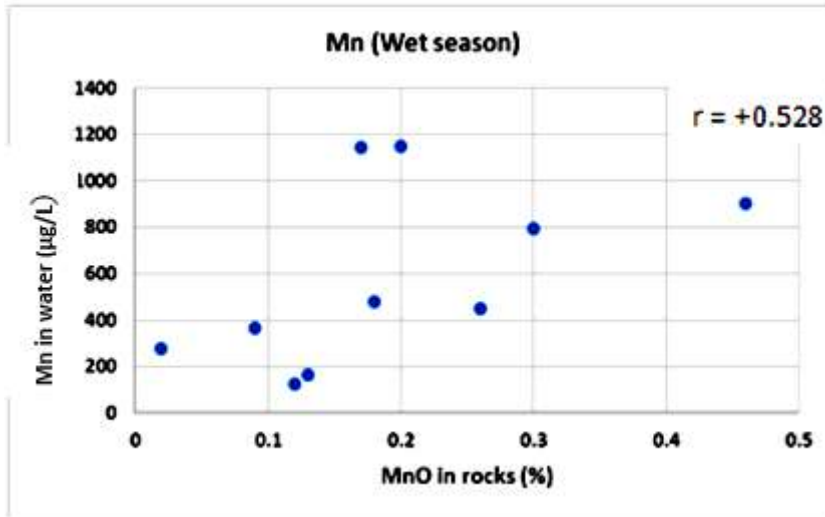

Figure 4.49: Pearson correlation of Mn in waters versus MnO in rocks in the wet season.
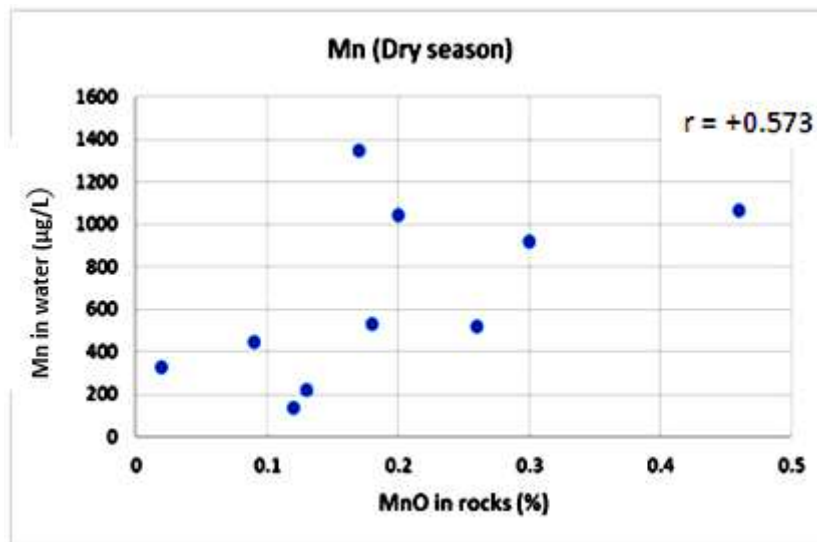
Figure 4.50: Pearson correlation of Mn in waters versus MnO in rocks in the dry season.

The results indicate near zero or no correlations for Na, K and Ca in the waters and their respective oxides in the rocks. Therefore, there is not much contribution of surface rocks to the huge presence of Na, K and Ca in the CO_2-rich waters. The waters could be sourcing these elements from the rocks deeper in the crust. However, Mg, Fe and Mn show significant positive correlations during the wet and dry seasons. Hence, substantial Mg, Fe and Mn in the spring waters may be directly originating from the rocks near the ground surface. This suggests occurrence of mafic rocks in the upper crust which are usually constituted by Mg and Fe. For example olivine, $(Mg, Fe)_2SiO_4$. Manganese is usually present together with iron minerals such as Manganocolumbite, $(Mn, Fe) (Nb, Tl)_2O_6$ (Sarah, 2014).

4.8.3 XRF elemental analysis of rocks

Three rock samples were analysed for every spring. Tables 4.13 shows the XRF mean compositions of the major and trace elements in the samples. The most abundant element is Si, followed by Al and Fe. However, Ca leads at RWA and RWB suggesting occurrence of carbonate sedimentary rocks and a similar pattern was noted with AAS analysis. Several essential trace elements such as Cu, Fe, Mn, Mo, Ni and Zn were confirmed to be present in the rocks. Among the toxic elements, As and Pb dominated in the rocks. This is consistent with the results obtained for the spring waters as discussed in Section 4.7, thus indicating that the trace elements are leached from the rocks.

The As concentration in the rocks was highest at KIA (170 ppm) but relatively low in the water compared to the other springs. This disparity could be due to the low amount of DIC at KIA hence low rate of As dissolution from rocks. Lead levels were high in the rock samples but not correspondingly high in the spring waters. Similarly, Cr and Cd were not detected in the rocks in most springs but it was found in the waters. This may indicate that besides water acidity and rock types, there are other factors that affect the transfer of trace elements from the rocks into the waters such as ion exchange and solubility of the minerals. The distribution and levels of the elements in the waters also depends on the types of aquifer supplying water to the springs (Sidibé *et al*., 2019; Kralik, 2015). In all the springs, Hg and Cd were below the instrument detection limit (<0.001 % or 10 ppm). The XRF method is limited to analysis of elements above atomic number 11 hence lighter elements such as Na and Mg are not easily analysed (Ryan *et al*., 2017; Lemiere *et al*., 2014).

Table 4.13: XRF percentage composition of elements in the rocks.

Element	GIK %	GIK RSD	KAT %	KAT RSD	KIA %	KIA RSD	MBW %	MBW RSD	MUL %	MUL RSD
*Al	10.269	0.918	15.23	1.01	9.78	0.078	16.615	1.03	14.375	1.03
As	0.003	0.002	0.017	0.002	0.005	0.002	0.005	0.001	0.003	0.002
*Ca	7.537	0.084	0.741	0.029	1.03	0.034	0.786	0.029	3.451	0.057
Ba	0.137	0.049	0.054	0.035	0.368	0.048	0.077	0.036	0.072	0.042
Cd	<0.001	-	<0.001	-	<0.001	-	<0.001	-	<0.001	-
Cl	<0.001	-	0.002	0.026	0.014	0.029	<0.001	-	<0.001	-
Co	0.007	0.007	<0.001	-	<0.001	-	<0.001	-	0.004	0.008
Cr	<0.001	-	<0.001	-	<0.001	-	<0.001	-	<0.001	-
Cu	0.016	0.003	0.014	0.003	0.004	0.002	0.004	0.002	0.01	0.003
*Fe	9.957	0.095	10.696	0.084	4.727	0.06	6.42	0.067	11.917	0.095
Hg	<0.001	-	<0.001	-	<0.001	-	<0.001	-	<0.001	-
*K	1.226	0.038	1.807	0.042	4.508	0.064	1.865	0.042	1.358	0.039
La	<0.001	-	<0.001	-	<0.001	-	0.051	0.058	<0.001	-
*Mg	1.351	3.089	<0.001	-	<0.001	-	<0.001	-	<0.001	-
*Mn	0.166	0.018	0.24	0.018	0.276	0.021	0.117	0.014	0.319	0.021
Mo	<0.001	-	0.002	0.002	0.002	0.002	<0.001	-	0.002	0.002
Nb	0.006	0.002	0.021	0.002	0.013	0.002	0.033	0.002	0.017	0.002
Ni	0.03	0.006	0.004	0.003	0.001	0.003	0.005	0.003	0.012	0.005
P	0.318	0.096	0.081	0.076	<0.001	-	0.158	0.076	0.119	0.088
Pb	0.031	0.005	<0.001	-	0.025	0.005	0.019	0.004	0.031	0.005
Pt	<0.001	-	<0.001	-	<0.001	-	0.001	0.003	0.001	0.003
Rb	0.004	0.001	0.007	0.001	0.02	0.002	0.008	0.002	0.006	0.002
S	0.128	0.037	0.227	0.04	0.242	0.035	0.158	0.034	0.173	0.042
Se	<0.001	-	<0.001	-	<0.001	-	<0.001	-	<0.001	-
*Si	25.014	0.887	26.035	0.847	31.989	0.979	26.463	0.852	24.246	0.846
Sn	<0.001	-	<0.001	-	<0.001	-	0.014	0.026	<0.001	-
Sr	0.099	0.004	0.015	0.002	0.006	0.002	0.048	0.002	0.033	0.002
Ta	<0.001	0.003	0.002	0.002	0.002	0.002	0.003	0.002	0.002	0.003
Th	<0.001	-	0.007	0.006	<0.001	-	<0.001	-	<0.001	-
*Ti	1.371	0.023	0.594	0.014	0.327	0.011	1.089	0.017	1.465	0.022
Tl	<0.001	-	0.003	0.002	<0.001	-	<0.001	-	<0.001	-
V	0.005	0.008	<0.001	-	0.003	0.005	0.002	0.007	<0.001	-
W	<0.001	-	<0.001	-	<0.001	-	0.001	0.002	<0.001	-
Y	0.003	0.002	0.004	0.002	0.006	0.002	0.009	0.002	0.007	0.002
Zn	0.01	0.002	0.016	0.002	0.013	0.002	0.013	0.002	0.019	0.003
Zr	0.023	0.002	0.068	0.002	0.048	0.002	0.124	0.003	0.056	0.002

*Major elements.

< Below the instrument detection limit (<0.001 % or 10 ppm).

Table 4.13: XRF percentage composition of elements in the rocks (continued).

Element	NTH %	NTH RSD	RWA %	RWA RSD	RWB %	RWB RSD	THA %	THA RSD	UKU %	UKU RSD
*Al	17.308	1.096	2.289	0.577	1.277	0.526	10.348	0.858	10.58	0.88
As	0.005	0.001	0.003	0.001	0.003	0.001	0.004	0.002	0.008	0.002
*Ca	0.382	0.023	49.363	0.198	47.091	0.19	4.994	0.065	2.699	0.05
Ba	0.064	0.039	<0.001	-	0.056	0.015	0.152	0.041	<0.001	-
Cd	<0.001	-	<0.001	-	<0.001	-	<0.001	-	<0.001	-
Cl	<0.001	-	0.035	0.019	<0.001	-	0.05	0.024	0.027	0.027
Co	<0.001	-	<0.001	-	<0.001	-	<0.001	-	0.001	0.003
Cr	<0.001	-	<0.001	-	0.008	0.005	0.004	0.004	0.01	0.004
Cu	0.009	0.002	0.007	0.003	0.018	0.003	0.012	0.002	0.016	0.003
*Fe	17.12	0.105	1.755	0.05	1.049	0.038	5.097	0.063	4.563	0.059
Hg	<0.001	-	<0.001	-	<0.001	-	<0.001	-	<0.001	-
*K	0.636	0.028	0.16	0.03	<0.001	-	4.58	0.062	5.139	0.066
La	<0.001	-	<0.001	-	<0.001	-	<0.001	-	0.052	0.06
*Mg	<0.001	-	7.767	3.964	14.917	4.744	1.267	2.806	<0.001	-
*Mn	0.297	0.019	0.076	0.015	0.045	0.012	0.245	0.019	0.262	0.019
Mo	0.003	0.002	<0.001	-	<0.001	-	<0.001	-	0.002	0.002
Nb	0.035	0.002	<0.001	-	<0.001	-	0.013	0.002	0.018	0.002
Ni	0.011	0.005	<0.001	-	<0.001	-	0.001	0.003	<0.001	-
P	0.039	0.08	0.418	0.133	0.22	0.123	0.108	0.07	0.036	0.063
Pb	0.027	0.005	0.037	0.006	0.028	0.005	0.031	0.005	0.024	0.004
Pt	0.002	0.003	<0.001	-	<0.001	-	0.001	0.003	<0.001	-
Rb	0.005	0.002	<0.001	0.001	<0.001	0.001	0.01	0.002	0.016	0.002
S	0.2	0.044	0.439	0.04	0.207	0.034	0.255	0.033	0.282	0.033
Se	<0.001	-	<0.001	-	<0.001	-	<0.001	-	<0.001	-
*Si	21.776	0.784	4.477	0.463	2.133	0.393	27.633	0.867	30.055	0.928
Sn	<0.001	-	0.038	0.04	0.018	0.046	<0.001	-	<0.001	-
Sr	0.013	0.002	0.268	0.005	0.198	0.004	0.067	0.003	0.026	0.002
Ta	0.004	0.003	<0.001	-	<0.001	-	<0.001	-	0.002	0.002
Th	<0.001	-	<0.001	-	<0.001	-	<0.001	-	<0.001	-
*Ti	1.336	0.02	0.189	0.016	0.122	0.015	0.354	0.012	0.097	0.008
Tl	<0.001	-	<0.001	-	<0.001	-	<0.001	-	<0.001	-
V	<0.001	-	0.001	0.009	0.003	0.009	0.007	0.005	0.002	0.004
W	<0.001	-	<0.001	-	<0.001	-	0.001	0.002	<0.001	-
Y	0.005	0.002	<0.001	-	<0.001	-	0.003	0.002	0.008	0.002
Zn	0.018	0.002	0.003	0.001	0.002	0.001	0.017	0.002	0.018	0.002
Zr	0.098	0.003	0.03	0.002	0.022	0.002	0.043	0.002	0.071	0.002

*Major elements.

< Below the instrument detection limit (<0.001 % or 10 ppm).

4.8.4 Correlation of AAS and XRF measurements in rocks

Comparisons of the relationship between the AAS and XRF results in rocks are represented in Figures 4.51 to 4.57. There are large positive correlations ranging from +0.668 to +0.986 which indicate that the measurements by the two methods were consistent and reliable. Figure 4.51 illustrates a strong positive correlation of Al analysis between AAS and XRF techniques. Hence, both analytical methods were consistent. A very strong positive correlation for Ca was also established between AAS and XRF methods as shown in Figure 4.52.
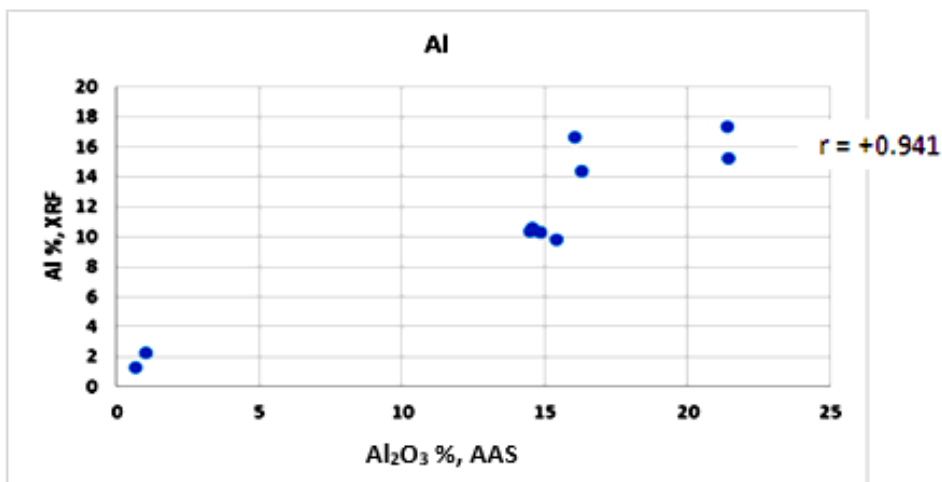
Figure 4.51: Pearson correlation of Al$_2$O$_3$ %, AAS versus Al %, XRF.
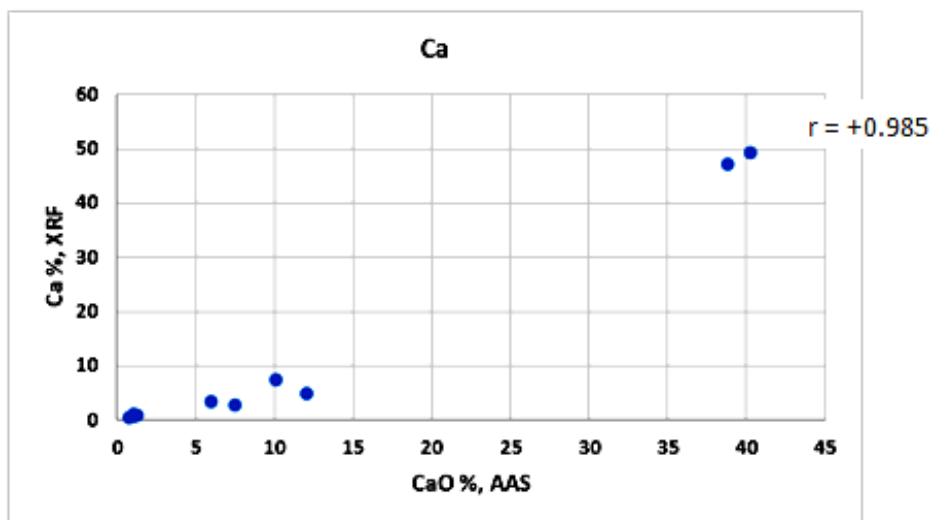
Figure 4.52: Pearson correlation of CaO %, AAS versus Ca %, XRF.

Figure 4.53 shows the correlation of Fe analysis using AAS and XRF methods. The correlation was significant and indicating reliability of both techniques. There was a good correlation between AAS and XRF analysis for Mn as shown in Figure 4.54.
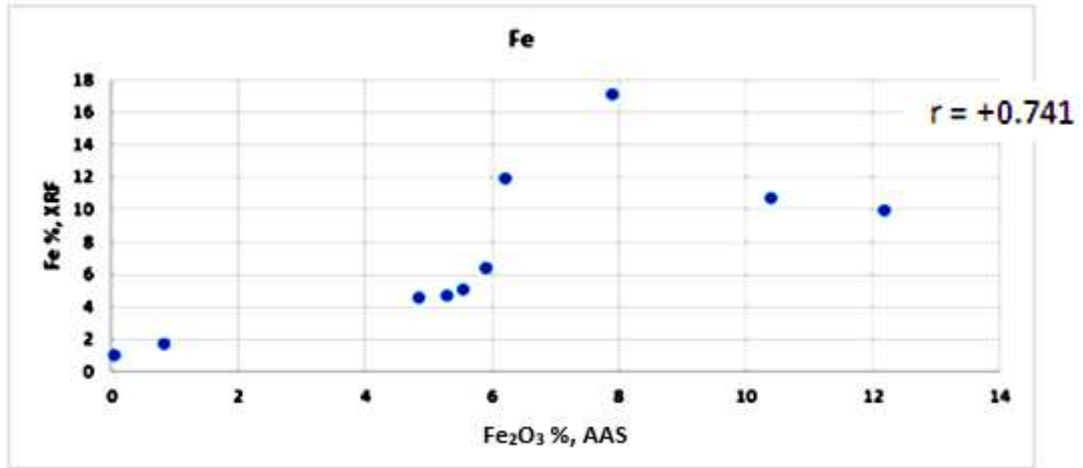
Figure 4.53: Pearson correlation of Fe$_2$O$_3$ %, AAS versus Fe %, XRF.
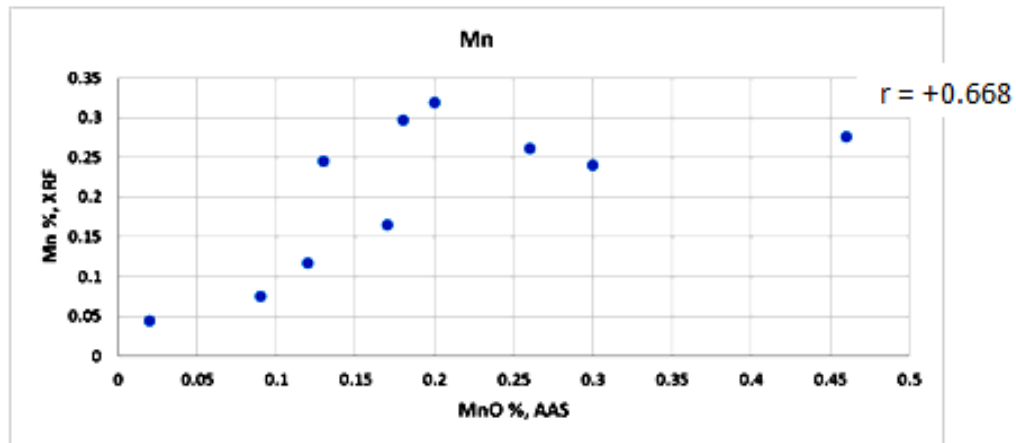
Figure 4.54: Pearson correlation of MnO %, AAS versus Mn %, XRF.

The AAS and XRF correlation for K analysis is shown in Figure 4.55. The results indicated very high positive correlation between the two methods. The AAS and XRF analysis for Si was reliable as confirmed by the strong positive correlation coefficient in Figure 4.56. Titanium also had significant correlation in both AAS and XRF analysis as seen in Figure 4.57.
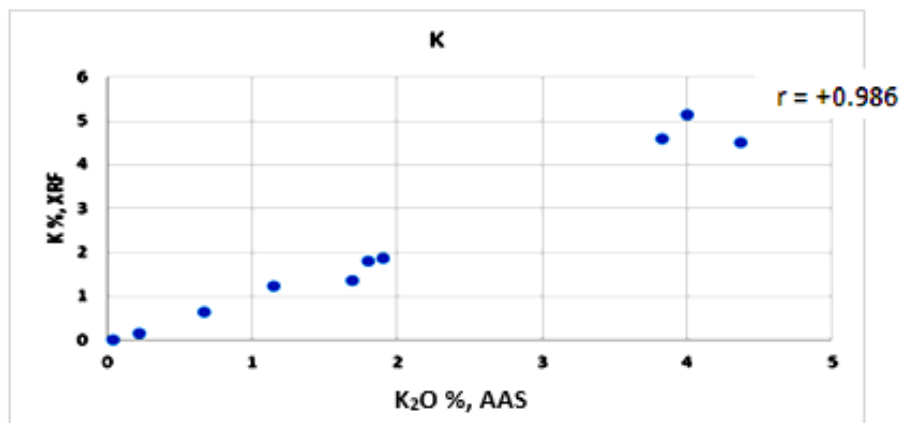
Figure 4.55: Pearson correlation of K_2O %, AAS versus K %, XRF.
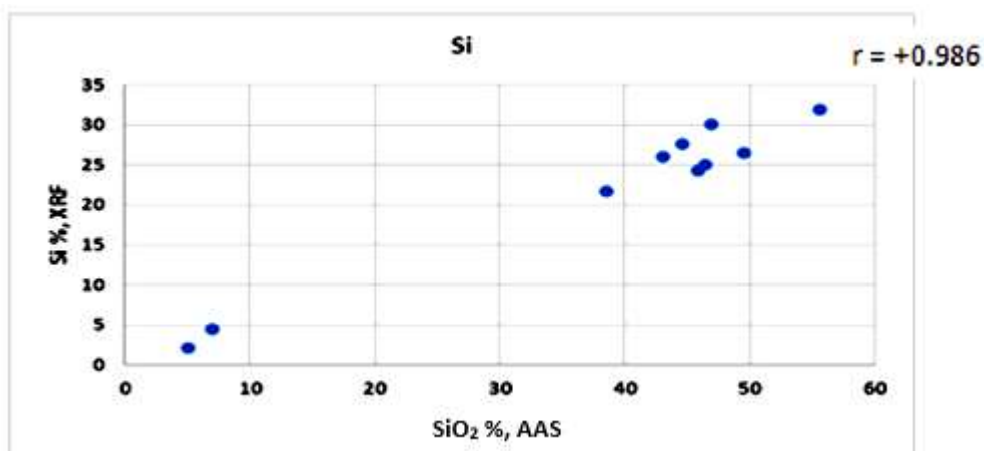
Figure 4.56: Pearson correlation of SiO_2 %, AAS versus Si %, XRF.
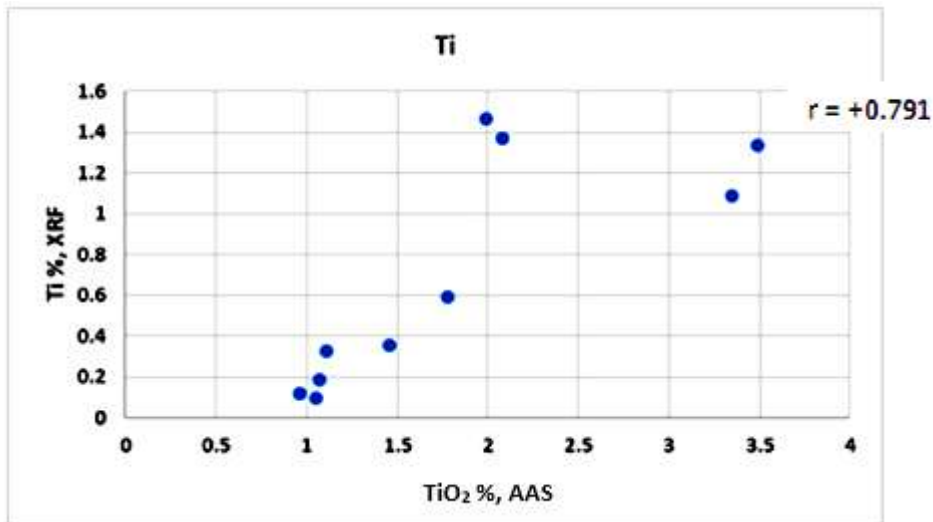
Figure 4.57: Pearson correlation of TiO$_2$ %, AAS versus Ti %, XRF.

Both AAS and XRF are reliable methods for elemental analysis as shown by the significant positive correlations above. However, there may be slight variations in the results because AAS involves preparation of samples prior to analysis. The samples may get contaminated by other reagents or apparatus and the accuracy of the AAS results could also be affected by dilution of samples during the preparation stages. On the other hand, XRF is a non-destructive technique which does not require sample preparation meaning that chances of contamination are reduced. This could explain why correlations of Fe, Mn and Ti are not as high compared with the rest which have r = >0.9.

4.8.5 XRD analysis of minerals in the rocks

Figures 4.58 to 4.67 show XRD search and match analysis of peaks for mineralogical composition of the surface rocks in each spring. Tables 4.14 to 4.23 show the mineral constituents and their relative abundancies. The XRD analysis of rocks at Gikumene spring is as shown in Figure 4.58 and Table 4.14. The leading minerals at Gikumene were anorthoclase (31.5 %), pyroxene-ideal (22.3%), djurleite (15.1%) and pigeonite (10.9%). Macphersonite (2.0%) was the only carbonate present. Arsenic (As) was present in durangite (3.6%) and simonite (0.9%) as NaAl(AsO$_4$)F and TlHgAs$_3$S$_6$, respectively. Mercury and lead were found in livingstonite HgS$_8$Sb$_4$ and macphersonite, Pb$_4$SO$_4$(CO$_3$)$_2$(OH)$_2$, respectively.
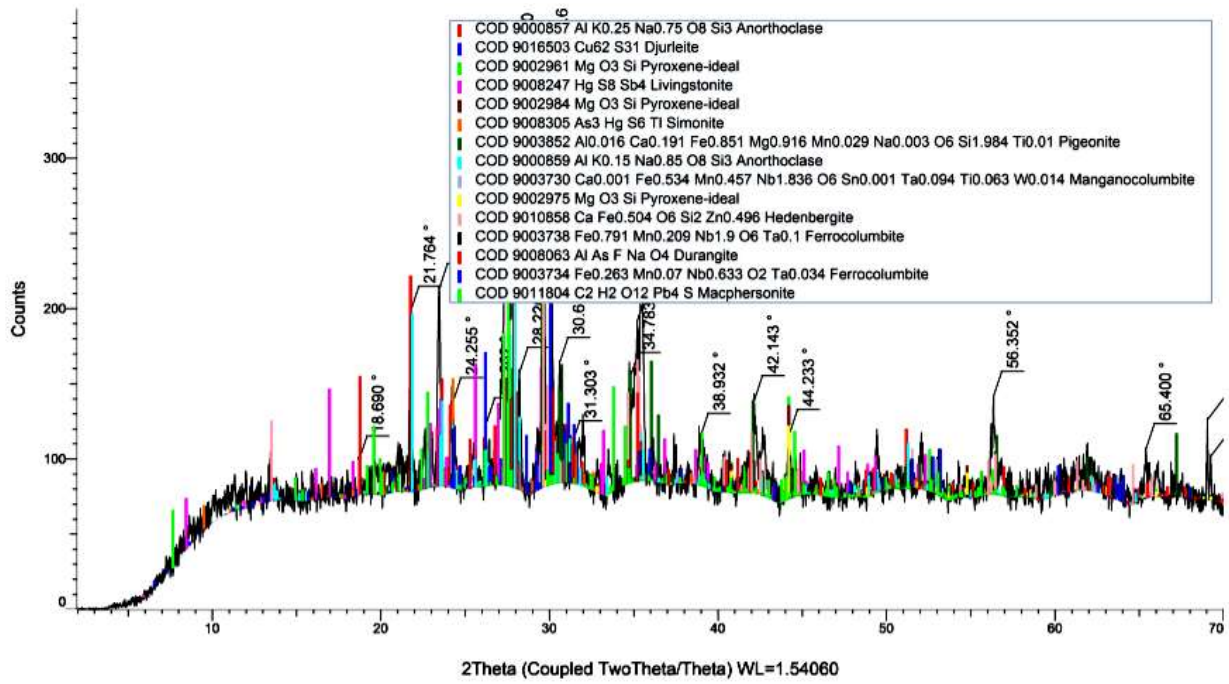
Figure 4.58: Gikumene XRD analysis peaks.

Table 4.14: XRD distribution of minerals in rocks at Gikumene.

Mineral	Formula	Percent
Anorthoclase	$(Na, K)AlSi_3O_8$	31.5
Pyroxene-ideal	$MgSiO_3$	22.3
Djurleite	$Cu_{31}S_{16}$	15.1
Pigeonite	$FeMgSi_2O_6$	10.9
Hedenbergite	$CaFeZnSi_2O_6$	6.8
Durangite	$NaAl(AsO_4)F$	3.6
Livingstonite	HgS_8Sb_4	3.0
Macphersonite	$Pb_4SO_4(CO_3)_2(OH)_2$	2.0
Ferrocolumbite	$FeNb_2O_6$	2.8
Manganocolumbite	$(Mn, Fe)(Nb, Tl)_2O_6$	1.1
Simonite	$TlHgAs_3S_6$	0.9
Total		100

In Figure 4.59 and Table 4.15 the XRD results at Kathathantu spring are presented. The bulk minerals at the site were alunogen (39.5%), alum-(K) (17.0%) and cristobalite II (15.7%). The carbonate minerals were zhonghuacerite (Ce) (8.5%) and macphersonite (6.0%). Lead occurred as macphersonite, $Pb_4SO_4(CO_3)_2(OH)_2$. Mercury was present in eglestonite, $(Hg_2)_3Cl_3O_2H$.
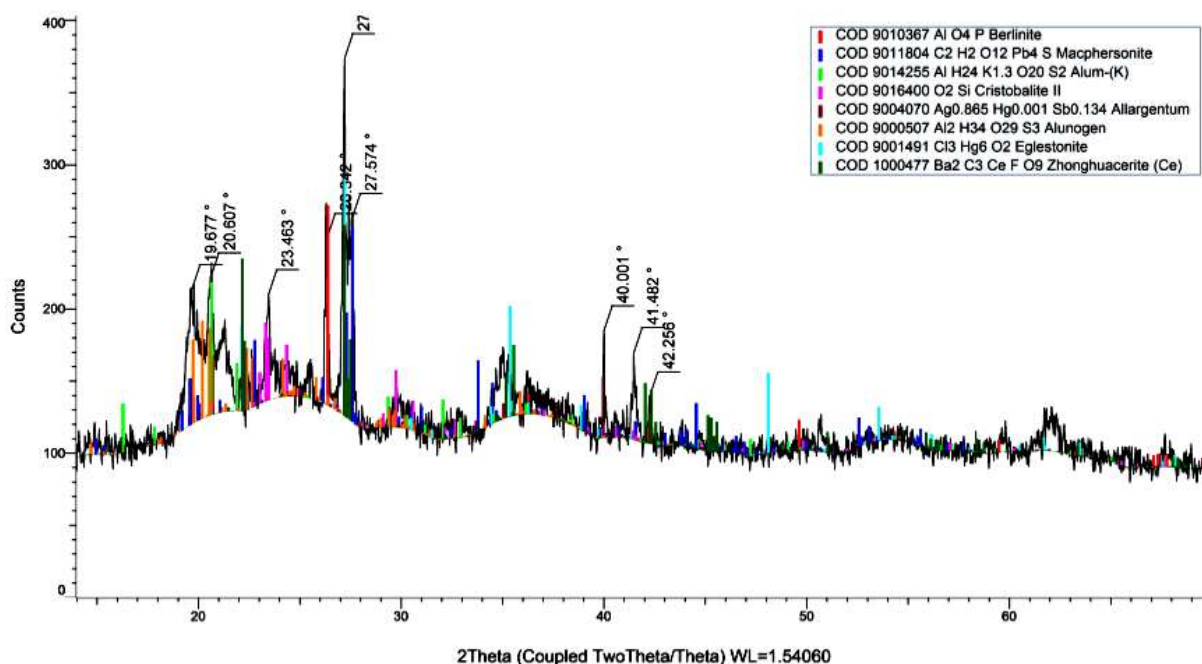
Figure 4.59: Kathathantu XRD analysis peaks.

Table 4.15: XRD distribution of minerals in rocks at Kathathantu.

Mineral	Formula	Percent
Alunogen	$Al_2(SO_4)_3.17H_2O$	39.5
Alum-(K)	$KAl(SO_4)_2.12H_2O$	17.0
Cristobalite II	SiO_2	15.7
Berlinite	$AlPO_4$	9.8
Zhonghuacerite (Ce)	$Ba_2Ce(CO_3)_3F$	8.5
Macphersonite	$Pb_4SO_4(CO_3)_2(OH)_2$	6.0
Eglestonite	$(Hg_2)_3Cl_3O_2H$	2.8
Allargentum	$Ag_{1-x}Sb_x$ (x = 0.134)	0.8
Total		100.1

112

The two major minerals found at Kiambogo spring were microcline (41.8%) and nepheline (13.4%) as shown in Figure 4.60 and Table 4.16. Other types of minerals were present in smaller amounts. Carbonate minerals were not found. Arsenic was found in kirkiite ($Pb_{10}Bi_3As_3S_{19}$). Lead was present in lead feldspar, $PbAl_2Si_2O_8$ and kirkiite, $Pb_{10}Bi_3As_3S_{19}$.
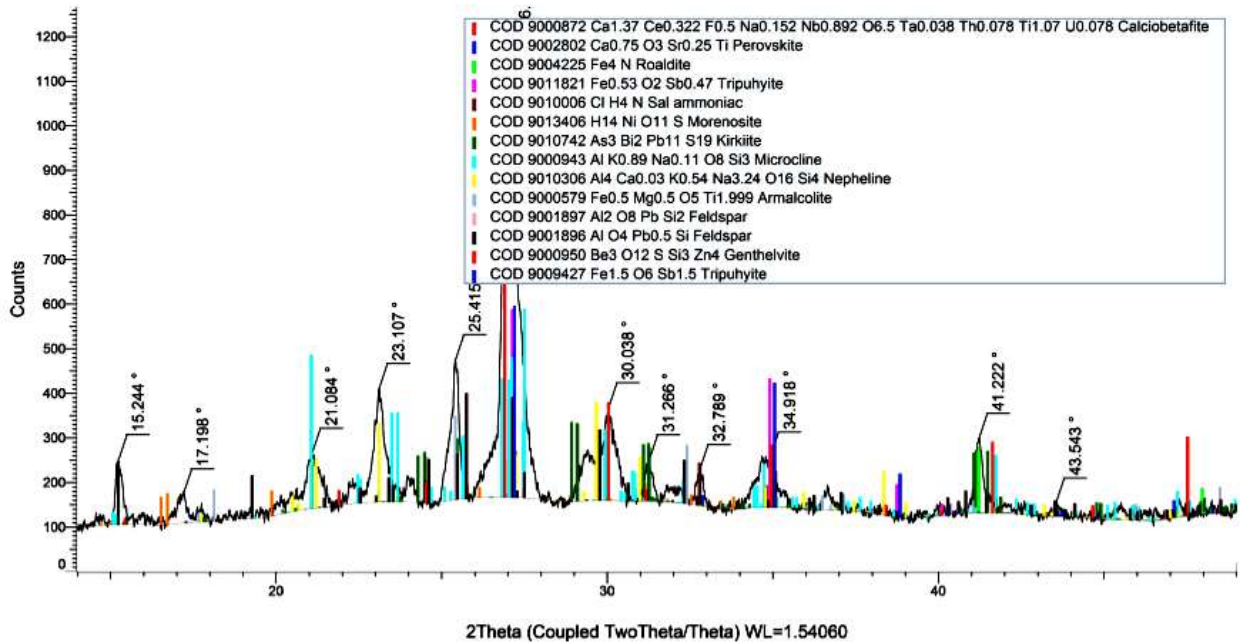
Figure 4.60: Kiambogo XRD analysis peaks.

Table 4.16: XRD distribution of minerals in rocks at Kiambogo.

Mineral	Formula	Percent
Microcline	$KAlSi_3O_8$	41.8
Nepheline	$Na_3KAl_4Si_4O_{16}$	13.4
Lead Feldspar	$PbAl_2Si_2O_8$	9.8
Genthelvite	$Zn_4Be_3(SiO_4)_3S$	8.3
Tripuhyite	$FeSbO_4$	6.1
Armalcolite	$MgFeTi_2O_5$	5.3
Morenosite	$NiSO_4.7H_2O$	5.2
Kirkiite	$Pb_{10}Bi_3As_3S_{19}$	5.0
Calciobetafite	$CaNbTiO_7F$	1.7
Perovskite	$CaTiO_3$	1.5
Sal ammoniac	NH_4Cl	1.0
Roaldite	Fe_4N	1.0
Total		100.1

The XRD data for Mbwinjeru is given in Figure 4.61 and Table 4.17. Ernstburkeite (49.9%), dolomite (20.8%) and quartz (17.2%) were the main minerals at the site. Carbonate rock was represented by dolomite. Ernstburkeite, $Mg(CH_3SO_3)_2.12H_2O$, contained organic carbon in form of methane sulphonate.
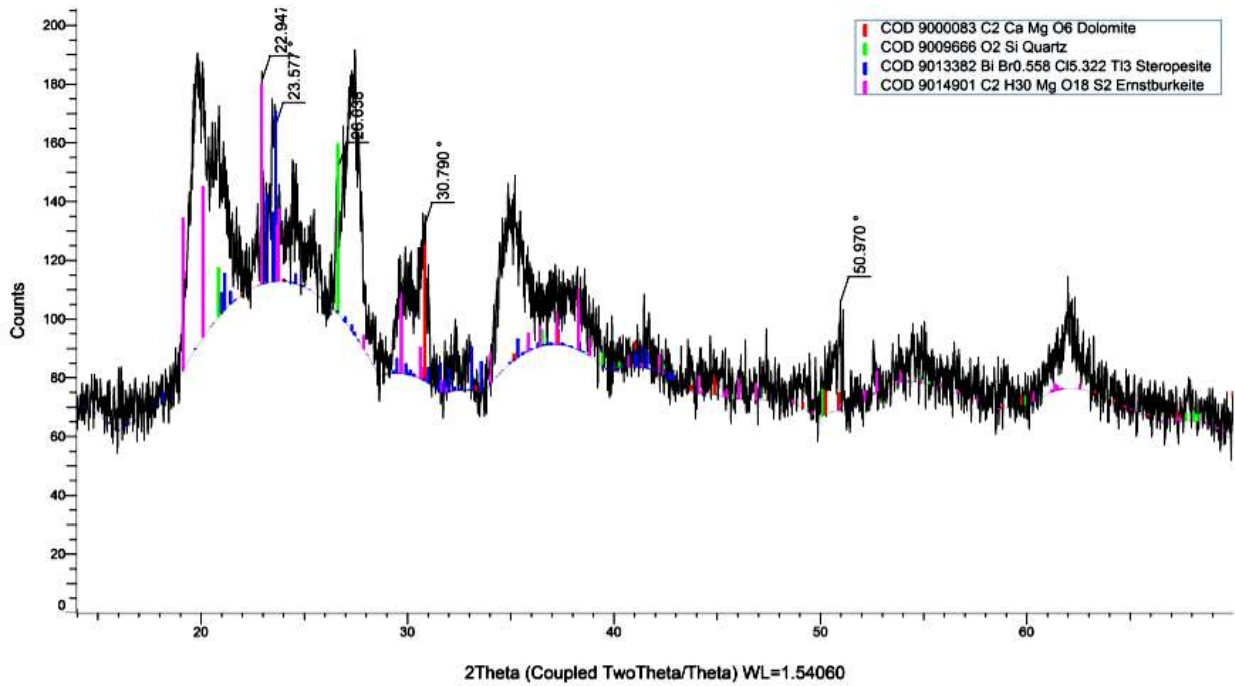
Figure 4.61: Mbwinjeru XRD analysis peaks.

Table 4.17: XRD distribution of minerals in rocks at Mbwinjeru.

Mineral	Formula	Percent
Ernstburkeite	$Mg(CH_3SO_3)_2.12H_2O$	49.9
Dolomite	$CaMg(CO_3)_2$	20.8
Quartz	SiO_2	17.2
Steropesite	$BiTl_3Cl_5Br$	12.2
Total		100.1

Figure 4.62 and Table 4.18 show the XRD results obtained at Mulathankari spring. Two main minerals in this site were tavorite (47.5%) and anorthoclase (27.9%). There was no carbonate found in these rocks. Lead was found in stolzite, $PbWO_4$.
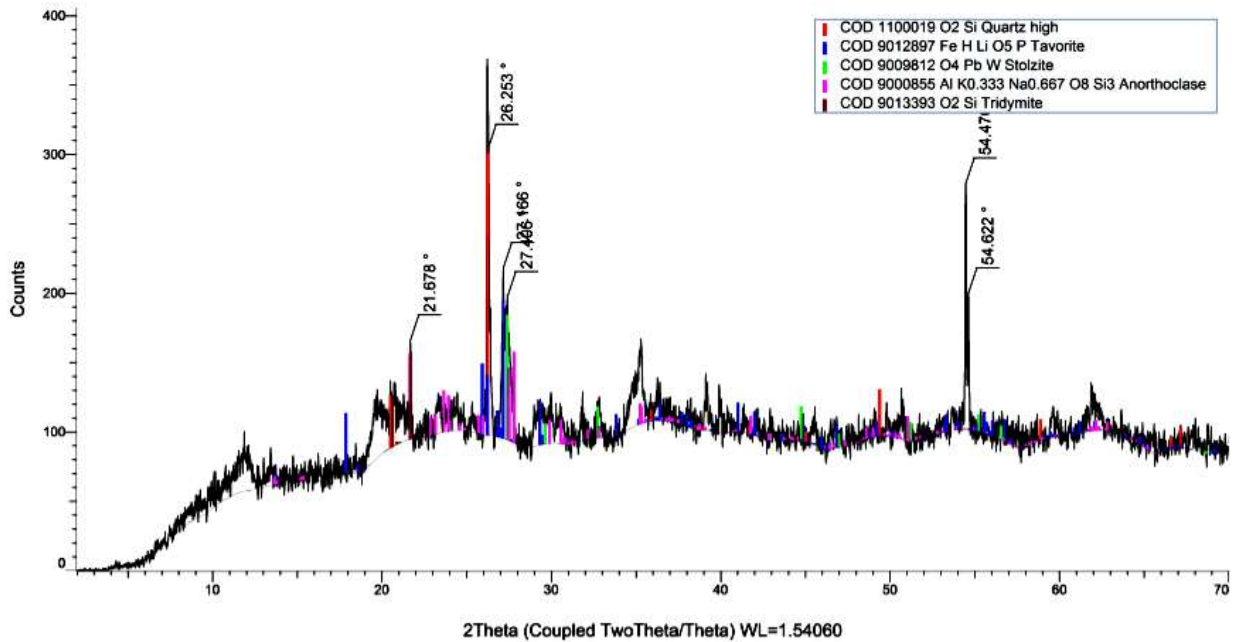
Figure 4.62: Mulathankari XRD analysis peaks.

Table 4.18: XRD distribution of minerals in rocks at Mulathankari.

Mineral	Formula	Percent
Tavorite	$LiFe(PO_4)OH$	47.5
Anorthoclase	$(Na, K)AlSi_3O_8$	27.9
Tridymite	SiO_2	11.9
Quartz high	SiO_2	11.3
Stolzite	$PbWO_4$	1.0
Total		99.6

The XRD data for Nthungu spring in Figure 4.63 and Table 4.19 showed that vaterite (45.3%), leucite (21.5%) and owyheeite (12.4%) were the leading minerals. Carbonate rocks included vaterite (45.3%) and mereheadite (2.6%). Silver and lead were present in owyheeite $Ag_2Pb_4Sb_6S_{14}$. Lead was also present in mereheadite, $Pb_{47}Cl_{25}(OH)_{13}O_{24} CO_3(BO_3)_2$.
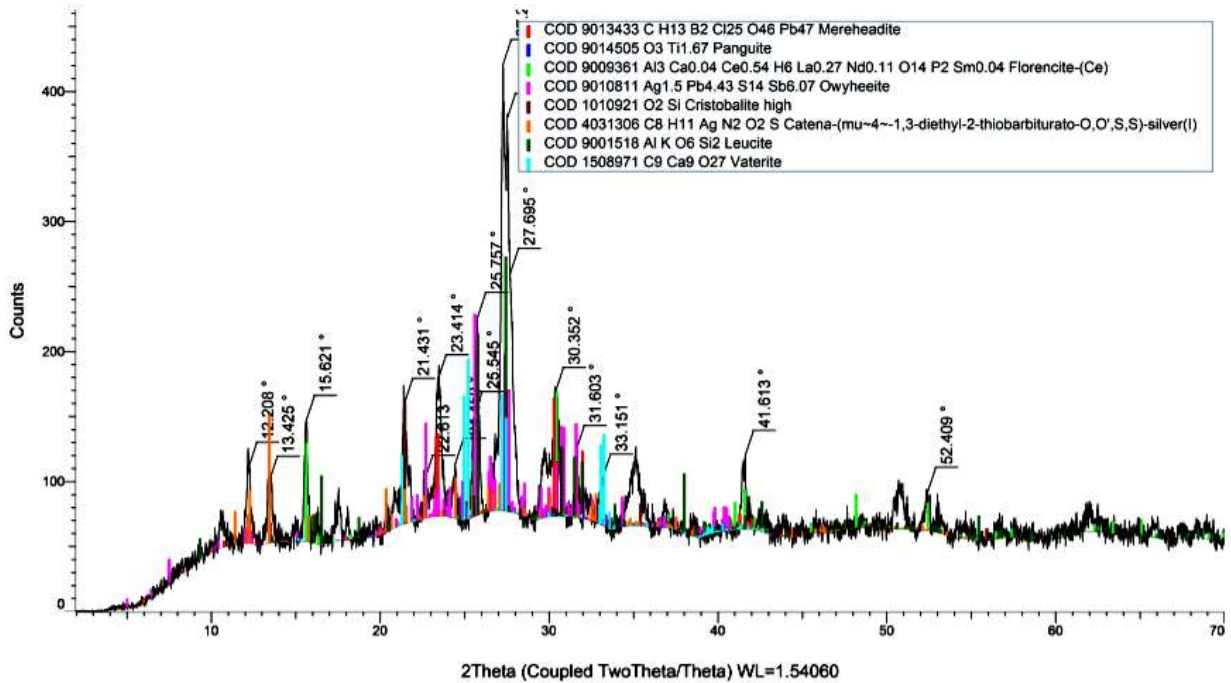
Figure 4.63: Nthungu XRD analysis peaks.

Table 4.19: XRD distribution of minerals in rocks at Nthungu.

Mineral	Formula	Percent
Vaterite	$CaCO_3$	45.3
Leucite	$KAlSi_2O_6$	21.5
Owyheeite	$Ag_2Pb_4Sb_6S_{14}$	12.4
Catena- (mu~4~-1,3-diethyl-2-thiobarbiturato-O,O',S,S)silver(I)	$AgN_2O_2C_8H_{11}S$	6.8
Florencite-(Ce)	$CeAl_3(PO_4)_2(OH)_6$	4.4
Panguite	Ti_2O_3	4.4
Mereheadite	$Pb_{47}Cl_{25}(OH)_{13}O_{24} CO_3(BO_3)_2$	2.6
Cristobalite high	SiO_2	2.5
Total		99.9

Figure 4.64 and Table 4.20 shows the XRD results for Rwarera-A spring. The rocks were dominated by carbonate minerals calcite (45.4%), aragonite (29.1%) and ankerite (17.5%) which constituted 92% of the whole rock. The presence of carbonate rocks was manifested by the high LOI value (43.15%) as earlier reported in section 4.8.1.
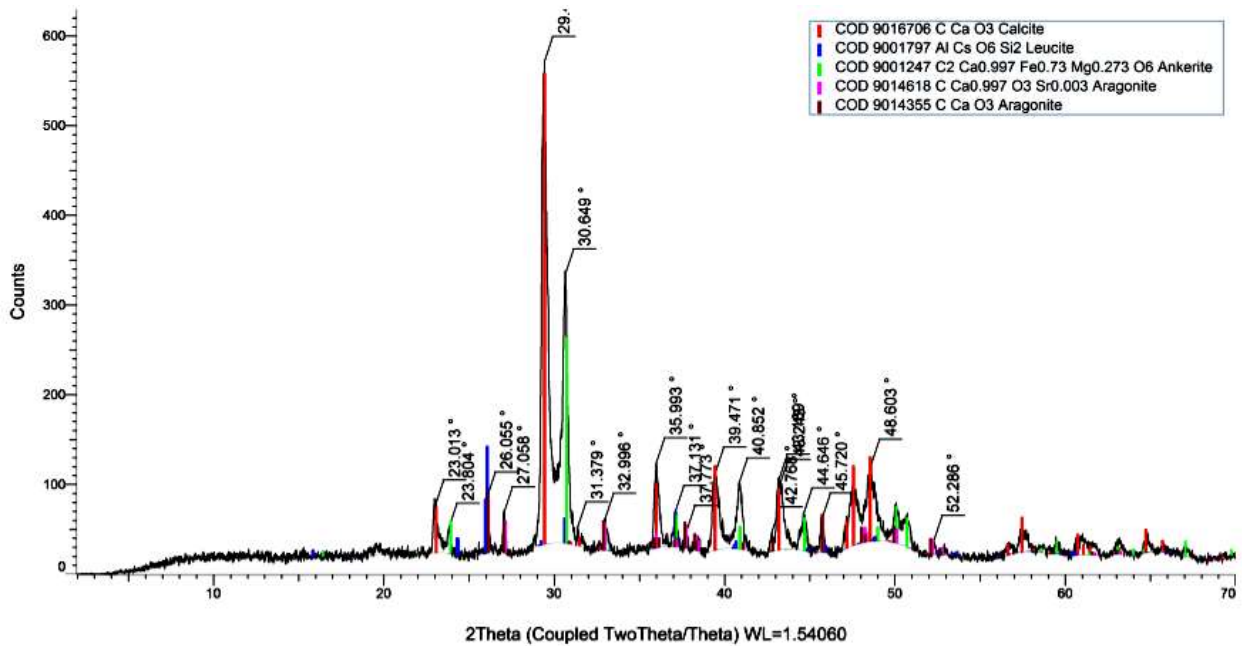
Figure 4.64: Rwarera-A XRD analysis peaks.

Table 4.20: XRD distribution of minerals in rocks at Rwarera-A.

Mineral	Formula	Percent
Calcite	$CaCO_3$	45.4
Aragonite	$CaCO_3$	29.1
Ankerite	$CaFe(CO_3)_2$	17.5
Leucite	$CsAlSi_2O_6$	8.0
Total		100.0

117

The XRD results for Rwarera-B spring are given in Figure 4.65 and Table 4.21. Djurleite (34.7%) and hiortdahlite (30.5%) were the major minerals. However, dolomite, calcite and otavite combined formed a significant portion (34.8%) of carbonate minerals. These carbonates and the sulphide in djurleite (34.7%) accounted for the high LOI (42.23%) reported in section 4.8.1. Cadmium was present in otavite, $CdCO_3$.
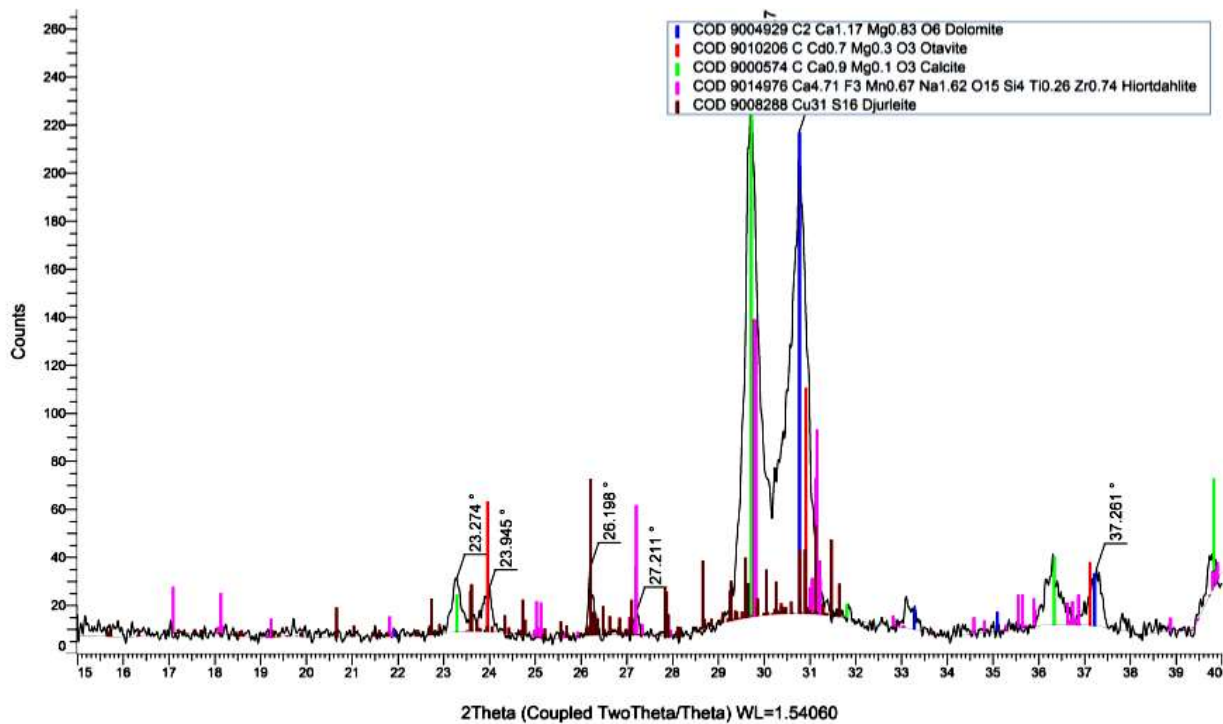
Figure 4.65: Rwarera-B XRD analysis peaks.

Table 4.21: XRD distribution of minerals in rocks at Rwarera-B.

Mineral	Formula	Percent
Djurleite	$Cu_{31}S_{16}$	34.7
Hiortdahlite	$Na_2Ca_4MnZr(Si_2O_7)_2OF_3$	30.5
Dolomite	$CaMg(CO_3)_2$	16.5
Calcite	$CaCO_3$	14.6
Otavite	$CdCO_3$	3.7
Total		100.0

Figure 4.66 and Table 4.22 shows the XRD results obtained from Tharu spring. The leading minerals were arrojadite (33.4%), wulfenite (15.1%), calzirtite (10.5%), and chloromagnesite (10.0%). Carbonate rocks were not found. Lead and mercury were present in wulfenite, $PbMoO_4$ and eglestonite, $Hg_6Cl_3O_2$, respectively.
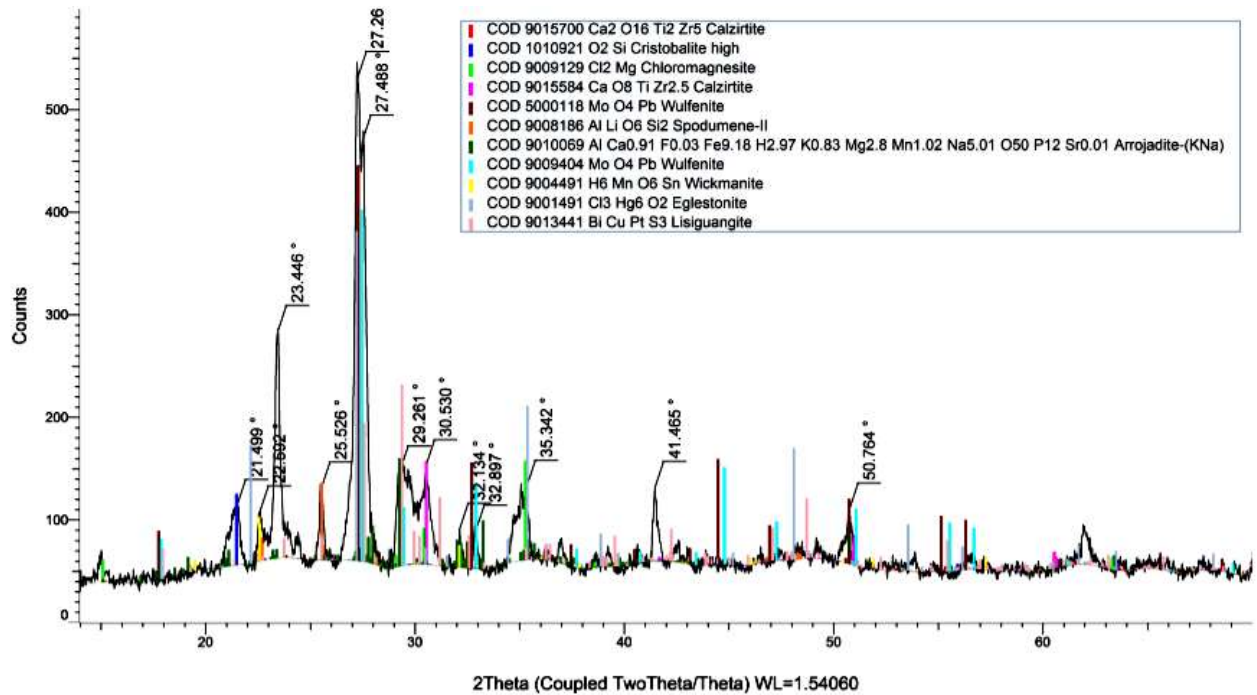
Figure 4.66: Tharu XRD analysis peaks.

Table 4.22: XRD distribution of minerals in rocks at Tharu.

Mineral	Formula	Percent
Arrojadite (KNa)	$KNa_5CaMg_3MnFe_9Al(PO_4)_{11}(HPO_4)(OH)_2$	33.4
Wulfenite	$PbMoO_4$	15.1
Calzirtite	$Ca_2Zr_5Ti_2O_{16}$	10.5
Chloromagnesite	$MgCl_2$	10.0
Spodumene-II	$LiAl(SiO_3)_2$	9.0
Lisiguangite	$CuPtBiS_3$	8.8
Eglestonite	$Hg_6Cl_3O_2$	6.8
Cristobalite high	SiO_2	4.4
Wickmanite	$MnSn(OH)_6$	2.1
Total		100.1

The XRD data for Ukuu spring is given in Figure 4.67 and Table 4.23. Anorthoclase (67.5%) was the main mineral component in the rocks. Carbonate minerals present were teschemacherite (7.7%) and roubaultite (1.3%). Arsenic was found in cobaltite, CoAsS and lead in rucklidgeite, $PbBi_2Te_4$.
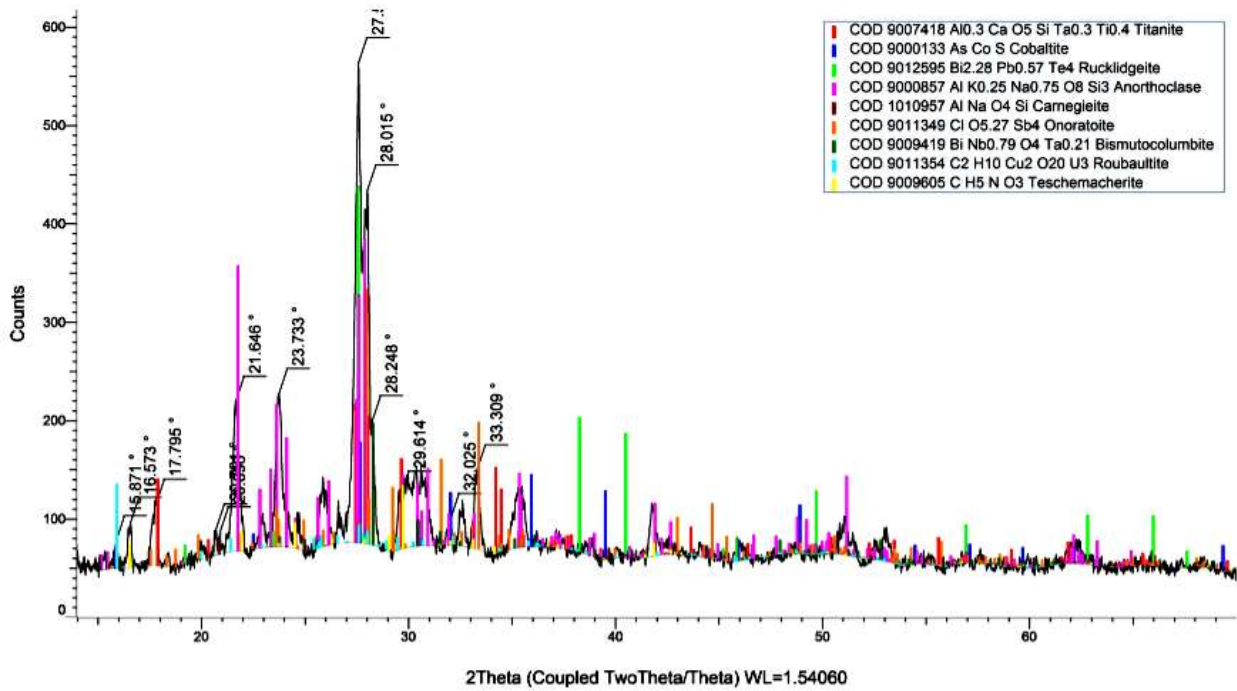
Figure 4.67: Ukuu XRD analysis peaks.

Table 4.23: XRD distribution of minerals in rocks at Ukuu.

Mineral	Formula	Percent
Anorthoclase	$(Na, K)AlSi_3O_8$	67.5
Titanite	$CaTiSiO_5$	7.9
Teschemacherite	$(NH_4)HCO_3$	7.7
Onoratoite	Sb_4ClO_5	7.1
Cobaltite	$CoAsS$	4.4
Rucklidgeite	$PbBi_2Te_4$	2.4
Roubaultite	$Cu_2(UO_2)_3(CO_3)_2O_2(OH)_2.4H_2O$	1.3
Bismutocolumbite	$BiNbO_4$	1.1
Carnegieite	$NaAlSiO_4$	0.7
Total		100.1

The XRD results revealed occurrence of a wide range of major and trace minerals in the rocks. These results are largely consistent with those obtained from XRF and AAS analysis. The XRD confirmed the presence of arsenic containing minerals at GIK, KIA and UKU. This explains the observed As in the spring waters which could be due to the sulphide and sedimentary mineral deposits derived from volcanic rocks (Herath *et al.*, 2016). Lead (Pb) minerals were present at GIK, KAT, KIA, MUL, NTH, THA and UKU springs. Some minerals with Hg were found at GIK, KAT and THA while Cd was found at RWB. Fluoride minerals were observed at GIK, KAT, KIA and THA which is consistent with the report given earlier in section 4.6.2. More than half of the springs contained chloride minerals confirming the source of Cl^- ions in the waters. The overall rock geochemistry correlated with elevated mineral content found in the CO_2-rich waters. While most of these elements are useful and harmless to the human body, the long-term ingestion of elements like As, Pb, Hg and fluoride may trigger serious health complications (Wani *et al.*, 2015; Jaishankar *et al.*, 2014; WHO, 2011).

Carbonates minerals such as calcite-$CaCO_3$, aragonite-$CaCO_3$, dolomite-$CaMg(CO_3)_2$, and ankerite-$CaFe(CO_3)_2$ were highly abundant at RWA and RWB. Further geochemical studies may be necessary at these two sites to ascertain the observed prominence of carbonate minerals with a view to exploit them. Other minerals which could have economic value include alum $KAl(SO_4)_2.12H_2O$, which is used for treating water. Djurleite $Cu_{31}S_{16}$ contains 79.36% Cu and can be used for extraction of Cu.

CHAPTER FIVE
CONCLUSIONS AND RECOMMENDATIONS

5.1 Conclusions

The views provided by the local community confirmed that mofette springs are widespread in the study area and they are popular for drinking, feeding the livestock, cooking and selling. They linked the CO_2-rich waters with therapeutic importance in humans such as reducing hyperacidity, indigestion and constipation. The respondents did not cite evidence of any harmful effects caused by drinking of the spring waters. However, potential dangers of consuming these highly mineralised natural waters cannot be completely ignored.

The springs had average ambient CO_2 levels between 3,417 and 4,804 ppm which were far above the reported global mean value (410.24 ppm) for August 2019. The CO_2-rich water releases the excess gas when the pressure is lowered at the Earth's surface leading to high ambient CO_2 levels at the spring sites. Therefore, there is significant CO_2 degassing taking place around the Mt. Kenya region which could have an adverse impact on climate change because of the greenhouse effect associated with it. The springs discharge high content CO_2 mineral waters throughout the year and hence they could be considered as permanent point sources of CO_2. This is a good sign for viable commercial exploitation of CO_2 gas deposits and mineral waters in the region.

The established δ ^{13}C isotope signature of the springs ranging from -3.597 to $+0.283$ ‰ VPDB is higher than the reported mantle range (-6 ± 2.5 ‰). This indicates that the CO_2 is from a deep-seated source or is mantle derived but could be partially mixed with CO_2 from deep carbonate minerals. Geologically, this suggests a passive magmatic CO_2 degassing through volcanic faults and fractures on the flanks of Mt. Kenya and could be partially enhanced by some carbonate rock formation in the region. The research findings contributes data which helps to understand the degassing behaviour of solid Earth in a volcano setting and closes some information gaps on the spatial distribution of ^{13}C isotopic signature.

The CO_2 gets dissolved in groundwater to form H_2CO_3 which is discharged naturally to the surface. The acid promotes dissolution of subsurface silicate and carbonate minerals through water-rock interaction. Hence, the springs were characterised by slightly acidic pH (5.83-6.81) with elevated DIC (39,184-89,013 µmol/kg), total alkalinity (14,925-61,810 µmol/L) and EC (1,221-5,195 µS/cm). The springs were characterised by relatively low discharge

temperatures (21.2-29.7 $^{\circ}$C) and were generally cold. The low discharge temperature allows large volume of CO_2 to remain dissolved in the waters. Sodium was the dominant cation (121-1,273 mg/L) which was largely counterbalanced by alkalinity to form $Na-HCO_3$ water-type. These findings supports mantle derived CO_2 as opposed to carbonate dissolution. Abundance of Na^+ in the cations also suggest that silicates are the dominant source of weathering products. Other ions found in lesser amounts included Mg^{2+}, Ca^{2+}, K^+, Fe^{2+}, Mn^{2+}, Si^{4+}, Cl^-, F^- and SO_4^{2-}. The levels of F^- ion (1.52-2.18 mg/L) at KAT, KIA and THA springs, were slightly above the WHO and KEBS recommended maximum limit of 1.5 mg/L. High F^- levels in water are usually associated with both dental and skeletal fluorosis.

The CO_2-rich waters contained substantial levels of essential trace elements (B, Co, Cu, Fe, Mn, Mo, Ni, Se and Zn) which have important biological functions in humans. However, some of these elements like B, Mn, Ni and Se were present in significant amounts of health concern in some springs. Concentration of Fe was high in all the spring waters ranging from 623 to 8,787 µg/L which resulted in the formation of yellow precipitates observed in the waters. Although WHO and KEBS have not set regulatory guideline values for Fe, excess intake of Fe is associated with the formation of harmful free radicals in the body. Some highly toxic trace elements were found in the waters such as As, Cd and Pb. The level of As (11.1-21.5 µg/L) exceeded WHO and KEBS guideline value of 10 µg/L in drinking water at MBW, NTH, RWA, RWB, THA and UKU. Use of the affected springs may be of health concern over time due to possible dangers of As toxicity with regard to the development of various types of cancers. Results for GIK, KAT and MUL were largely within the acceptable range and people can rely on the spring waters to acquire health benefits derived from the essential trace minerals. But the waters should be taken in moderation to avoid chronic overexposure to significant levels of Ag, Al, B, Ba, Cd, Cu, Fe, Hg, Mn, Pb, Ni and Se leached from the rocks.

The geochemistry of the parent rocks provided evidence for the elevated and wide range of minerals found in the spring waters. Arsenic containing minerals were found at GIK, KIA and UKU springs. Lead minerals were present at GIK, KAT, KIA, MUL, NTH, THA and UKU. Mercury was found at GIK, KAT and THA while Cd was present at RWB. Carbonates rocks (34.8-92%) containing calcite-$CaCO_3$, aragonite-$CaCO_3$, dolomite-$CaMg(CO_3)_2$ and ankerite-$CaFe(CO_3)_2$ were prominent at RWA and RWB.

The contributions of this study to the existing scientific knowledge may be summarised as follows: The findings could help in developing relevant climate change mitigation strategies that focuses on volcanic CO_2 emissions. The results gives a better understanding of the CO_2 origin, lithology, plate tectonics and other geochemical processes occurring in Mt. Kenya region. The data provides an opportunity for feasibility studies on socio-economic value of the mineral waters, CO_2 and carbonates deposits in this region. Moreover, the results indicate potential health risks posed to the local community by the regular intake of the contaminated spring waters.

5.2 Recommendations

1. The CO_2 flux within Mt Kenya region requires to be fully established and be included in the estimates of global CO_2 budget. This will help in mitigating and monitoring the long-term adverse climatic changes associated with global warming effects of CO_2.

2. Isotope systematics for more degassing subaerial volcanoes such as Mt. Kilimanjaro and Mt. Elgon needs to be investigated, for better comparison with the reported $\delta\ ^{13}C$ data and probably account for the different CO_2 sources.

3. It has been established that the springs are potential sources of both CO_2 and naturally carbonated mineral waters. Hence, feasibility studies on commercial exploitation of CO_2 gas and these mineral waters in Mt Kenya region may be carried out.

4. It is important to undertake thorough water quality analysis of the spring waters to ensure that it is free from microbial contamination and safe for the local human consumption or industrial processing.

5. Efforts should be made to lower toxic elements especially As levels in the affected springs to meet the WHO and KEBS requirements before using the waters.

6. Investigation of As levels in borehole waters in this region should also be done and compare them with the findings obtained from mofette springs.

7. Further biochemical and epidemiological studies should be carried out in the region to ascertain any health risks of such spring waters on human population, especially the clinical manifestation of As toxicity because it is carcinogenic.

8. Abundance of carbonate, iron, copper and aluminium containing minerals was reported in this region and therefore assessment of their economic value is important.

9. Speciation studies of the metal species found in the spring waters should be carried out in order to understand their mobility in the environment and toxicity better.

REFERENCES

Abbaspour, N., Hurell, R., and Kelishadi, R. (2014) Review on iron and its importance for human health. *J. Res. Med. Sci*. **19**: 164-174.

Abdul, K. S. M., Jayasinghe, S. S., Chandana, E, P, S., Jayasumana, C., and De Silva, P. M. C. S. (2015) Arsenic and human health effects: A review. *Environ. Toxicol. Pharmacol.* **40**: 828–846.

Aiuppa, A., Fischer, T. P., Plank, T., and Bani, P. (2019) CO_2 flux emissions from the Earth's most actively degassing volcanoes, 2005-2015. *Sci. Rep.* **9**: 5442.

Akech, N. O., Omuombo, C. A., and Masibo, M. (2013) General Geology of Kenya *Dev. Earth Surf. Process*. **16**: 3-10.

Alan, R. (2000) Volcanic eruptions and climate. *Rev. geophys.* **38**: 191-219.

Albertini, M. C., Dachà, M., Teodori L., and Conti, M. E. (2007) Drinking mineral waters: biochemical effects and health implication – the state-of-the-art. *Int. J. Environ. Health* **1**: 153–169.

Allibone, R., Cronin, S. J., Charley, D. T., Neall, V. E., Stewart, R. B., and Oppenheimer, C. (2012) Dental fluorosis linked to degassing of Ambrym Volcano, Vanuatu: a novel exposure pathway. *Environ. Geochem. Health* **34**: 155-170.

Alvin, B., and Ronald, B. (2008) *Basic Marketing Research (Second Ed.)*. Pearson Education, New Jersey: pp245.

Andrews, J. E., Brimblecombe, P., Jickells, T. D., Liss, P. S., and Reid, B. (2004) *An Introduction to Environmental Chemistry, Second edition*. Blackwell Publishing, Oxford UK: pp151-153, 179-180.

Assayang, N., Matter, J., Ader, M., Goldberg, D., and Agrinier, P. (2009) Water–rock interactions during a CO_2 injection field-test: Implications on host rock dissolution and alteration effects. *Chem. Geol.* **265**: 227-235.

ASTM. American Society for Testing and Materials. (1999) *Standard Test Method for Anions in Water by Chemically Suppressed Ion Chromatography. Method D4327-97 Vol. 11.01*. ASTM, West Conshohocken, Pennsylvania: pp420–427.

Bakirdere, S., Örenay, S., and Korkma, M. (2010) Effect of Boron on Human Health. *The Open Miner. Process. J*. **3**: 54-59.

Barbie, O., Jacquillet, G., Tauc, M., Cougnon, M., and Poujeol, P. (2005) Effect of heavy metals on and handling by the kidney. *Nephron Physiol*. **99**: 105-10.

Barry, P. H., Hilton, D. R., Fischer, T. P., de Moor, J. M., Mangasini, F., and Ramirez, C. (2013) Helium and carbon isotope systematics of cold 'mazuku' CO_2 vents and hydrothermal gases and fluids from Rungwe Volcanic Province, south Tanzania. *Chem. Geol.* **339**: 141-156.

Bastida, C. A., Miranda, V. M., Ríos, M. S., Hernández, I. L., Sequeira, A. T., and Mejía, G. V. (2018) Drinking water characterization and removal of manganese. Removal of manganese from water. *J. Environ. Chem. Eng.* **6**: 22119-2125.

Batayney, A., Ghrefat, H., Zaman, H., Mogren, S., Zumlot, T., Elawadi, E., Laboun, A., and Qaisy, S. (2012) Assessment of the physicochemical Parameters and Healthy Metal Toxicity: Application to Groundwater Quality in Unconsolidated Shallow Aquifer System. *Res. J. Environ. Toxicol.* **6**: 169-183.

Becker, M., Andersen, N., Fiedler, B., Fietzek, P., Körtzinger, A., Steinhoff, T. and Friedrichs, G. (2012) Using cavity ringdown spectroscopy for continuous monitoring of $\delta^{13}C(CO_2)$ and fCO_2 in the surface ocean. *Limnol. Oceanogr. Methods* **10**:752-766.

Bissig, P., Goldscheider, N., Mayoraz, J., Surbeck, H., and Vuataz, F. D. (2006) Carbogaseous spring waters, coldwater geysers and dry CO_2 exhalations in the tectonic window of the Lower Engadine Valley, Switzerland. *Eclogae geol. Helv.* **99**: 143–155.

Botto, R. I. (1984) Quality assurance in operating a multielement ICP emission spectrometer. *Spectrochim. Acta Part B: At. Spectrosc.* **39**: 95-113.

Brune, S., Williams, S. E., and Müller, R. D. (2017) Potential links between continental rifting, CO_2 degassing and climate change through time. *Nat. Geosci.* **10**: 941–946.

Bu bois, C. G., and Wash, J. (2007) *Geological Survey of Kenya, Minerals of Kenya, Bulletin No. 11*. Ministry of Petroleum and Mining, Republic of Kenya, Nairobi: pp10.

Bunaciu A. A., Udriştioiu, E. G., and Aboul-Enein, H. Y. (2015) *Crit. Rev. Anal. Chem.* **45**: 289-299.

Cangemi, M., Madonia, P., Albano, L., Bonfardeci, A., Di Figlia, M. G., Di Martino, R. M. R., Nicolosi, M., and Favara, R. (2019) Heavy Metal Concentrations in the Groundwater of the Barcellona-Milazzo Plain (Italy): Contributions from Geogenic and Anthropogenic Sources. *Int. J. Environ. Res. Public Health* **16**: 285.

Cartwright, I., Weaver, T., Tweed, S., Ahearne, D., Cooper, M., Czapnik, K., and Tranter, J. (2002) Stable isotope geochemistry of cold CO_2-bearing mineral spring waters, Daylesford, Victoria, Australia: sources of gas and water and links with waning volcanism. *Chem. Geol.* **185**: 71–91.

Cefalu, W. T., and Hu, F. B. (2004) Role of chromium in human health and in diabetes. *Diabetes Care* **27**: 2741-51.

Cempel, M., and Nikel, G. (2006) Nickel: A Review of Its Sources and Environmental Toxicology. *Pol. J. Environ. Stud.* **15**: 375-382.

Céron, J. C., Pulido-Bosch, A., and Galdeano, C. S. (1998) Isotope identification of CO_2 from a deep origin in thermomineral waters Southeastern Spain. *Chem. Geol.* **149**: 251–258.

Chen, P., Bornhorst, J., and Aschner, M. (2018) Manganese metabolism in humans. *Biosci. (Landmark Ed.)* **23**: 1655-1679.

Chen, Y. C., Su, H. J. J., Guo, Y. L. L., Hsueh, Y. M., Smith, T. J., Ryan, L. M., Lee, M. S., and Christiani, D. C. (2003). Arsenic methylation and bladder cancer risk in Taiwan. *Cancer Causes Control* **14**: 303–310.

Chiodini, G., Caliro, S., Cardellini, C., and Avino, R. (2008) Carbon isotopic composition of soil CO_2 efflux, a powerful method to discriminate different sources feeding soil CO_2 degassing in volcanic-hydrothermal areas. *Earth Planet. Sci. Lett.* **274**: 372–379.

Christian, G. D. (2004) *Analytical Chemistry, 6th edition*. John Willey & Sons, Inc., USA: pp52- 53.

Cooper, R. G., and Harrison, A. P. (2009) The uses and adverse effects of beryllium on health. *Indian J. Occup. Environ. Med.* **13**: 56-76.

Crundwell, F. K. (2014) The mechanism of dissolution of minerals in acidic and alkaline solutions: Part II Application of a new theory to silicates, aluminosilicates. *Hydrometall.* **149**: 265–275.

Czarnek, K., Terpilowska, S., and Siwicki, A. K. (2015) Selected aspects of the action of cobalt ions in the human body. *Cent. Eur. J. Immunol.* **40**:236-242.

Darling, W. G., Griesshaber, E., Andrews, J. N., Armannsson, H., and O'nions, R. K. (1995) The origin of hydrothermal and other gases in the Kenyan Rift Valley. *Geochem. et Cosmochim. Acta* **59**: 2501-2512.

Dasgupta, R., and Hirschmann, M. M. (2010) The deep carbon cycle and melting in Earth's interior. *Earth Planet. Sci. Lett.* **298**: 1–13.

Davidson, P. W., Myers, G. J., and Weiss, B. (2004) Mercury exposure and child development outcomes. *Pediatrics*. **113**: 1023–9.

De Oliveira, S. M. B., Pessenda L. R., Gouveia, S. M., and Deborahi.T., and Favaro, D. T. (2011) Heavy metal concentrations in soils from a remote oceanic island, Fernandode Noronha, Brazil. *Anaisda Academia Brasileirade Ciências* **83**:1193-1206.

Department of Geography and Environmental Studies. (2018) University of Nairobi.

Department of Geology. (2018) University of Nairobi.

Dickinson, D., Bode, S., and Boeck, X. P. (2017) Measuring ^{13}C enriched CO_2 in air with a cavity ring-down spectroscopy gas analyser: Evaluation and calibration. *Rapid Comm. Mass Spectro.* **31**: 1892-1902.

Diliberto, I. S., Gurrieri, S., and Valenza, M. (2002) Relationships between diffuse CO_2 emissions and volcanic activity on the island of Vulcano (Aeolian Islands, Italy) during the period 1984-1994. *Bull. Volcanol.* **64**: 219-228.

Driehaus, W., Jekel, M., and Hildebrandt, U. (1998) Granular ferric hydroxide-a new adsorbent for the removal of arsenic from natural water. *J. Water SRT-Aqua* **47**: 30-35.

Eaton, A, D. (2005) *Standard Methods for Examination of Water and Waste Water, 21st Edition*. America Public Health Association, American Water Works Association, Water Environment Federation. Washington D.C: Chapter 3, pp1-99.

Exley, C. (2016). The toxicity of aluminium in humans. *Morphol.* **100**: 51-5.

Faber, J., and Fawcett, T. (2002) The Powder Diffraction File: present and future. *Acta Cryst.* **B58**: 325-332.

Fantarella, D., and Kotlow, L. (2014) The 9.3μm CO_2 Dental Laser. *Sci. Rev. J Laser Dent.* **1**: 10–27.

Fassel, V. A. (1986) Analytical Inductively Coupled Plasma Spectroscopies – Past, Present, and Future', *Fresenius Z. Anal. Chem.* **324**: 511–518.

Freeze, R. A., and Cherry, J. A. (1979) *Groundwater.* Prentice-Hall International Inc., London: pp96-97.

Friedlingstein, P., Andrew, R. M., Rogelj, J., Peters, G. P., Canadell, J. G., Knutti, R., Luderer, G., Raupach, M. R., Schaeffer, M., Van Vuuren, D. P., and Le Quéré, C. (2014) Persistent growth of CO_2 emissions and implications for reaching climate targets. *Nat. Geosci.* **7**: 709–715.

Fritz, B. (2014) Skin Resurfacing. In Charles Thorne (ed.). *Grabb and Smith's Plastic Surgery (7 Ed.)*. Lippincott Williams & Wilkins, Philadelphia: pp455.

Frodl, R., and Tille, T. A. (2006) High-precision NDIR CO_2 gas sensor for automotive applications. *IEEE Sens. J.* **6**: 1697–1705.

Garbarino, J. R., Jones, B. E., Stein, G. P., Belser, W. T., and Taylor, H. E. (1985) Statistical Evaluation of an Inductively Coupled Plasma Atomic Emission Spectrometric Method for Routine Water Quality Testing. *Appl. Spectrosc.* 39: 535-541.

Garman, E. F., and Schneider, T. R. (1997) Macromolecular Crystallography. *J. Appl. Cryst*. **30**: 211.

Gasbarrini, G., Candelli, M., Graziosetto, R. G., Coccheri, S., and Di Iorio, F. (2006) 'Evaluation of thermal water in patients with functional dyspepsia and irritable bowel syndrome accompanying constipation', *World J. Gastroenterol.* **12**: 2556–2562.

Giggenbach W. F. (1990) Water and gas chemistry of Lake Nyos and its bearing on the eruptive process. *J. Volcanol. Geotherm. Res.* **42**: 337-362.

Golekar, R. B., Patil, S. N., and Baride, M. V. (2013) Human health risk due to trace element contamination in groundwater from the Anjani and Jhiri river catchment area in northern Maharashtra, India. *Earth Sci. Res. J*. **17**: 17 – 23.

Grassi, M., Lucchetta, M. C., Grossi, F., and Raffa, S. (2002) Possibilities of thermal medicine in gastrointestinal functional disorders. *ClinicaTerapeutica* **153**: 195–206.

Gregory, J. W. (1900). Contributions to the Geology of British East Africa. -Part II. The Geology of Mount Kenya. *Quart. J. Geol. Societ.* **56**: 205-222.

Gros, N., and Gorenc, B. (1997) Performance of ion chromatography in the determination of anions and cations in various natural waters with elevated mineralization. *J. Chromatogr. A*. **770**:119–124.

Guyonnet, S. G., Andrieu, S., and Vellas, B. (2017) The potential influence of silica present in drinking water on Alzheimer's disease and associated disorders. *J. Nutr. Health Aging* **11**: 119-24.

Haddad, P. R. (2004) Ion Chromatograpy. *Anal. Bioanal. Chem.* **379**: 341-3.

Han, B., Runnellsb, T., Zimbron, J., and Wickramasinghea R. (2002) Arsenic removal from drinking water by flocculation and microfiltration. *Desalination* **145**: 293–298.

Hansell, A., and Oppenheimer, C., (2004) Health hazards from volcanic gases: a systematic literature review. *Arch. Environ. Health* **59**: 628-639.

Harris, C., Stock, W. D., and Lanham, J. (1997) Stable isotope constraints on the origin of CO_2 gas exhalations at Bongwan, Natal. *S. Afr. J. of Geol.* **100**: 261–266.

Hartmann, J., West, A. J., Renforth, P., Köhler, P., De La Rocha, C. L., Wolf-Gladrow, D. A., Dürr, H. H., and Scheffran, J. (2013) Enhanced chemical weathering as a geoengineering strategy to reduce atmospheric carbon dioxide, supply nutrients, and mitigate ocean acidification. *Rev. Geophys.* **51:** 113-149.

He, Z. L., Yang, X. E., and Stoffella, P. J. (2005) Trace elements in agroecosystems and impacts on the environment. *J. Trace Elem. Med. Biol*. **19**:125–140.

Herath, I., Vithanage, M., Bundschuh, J., Maity, J. P., and Bhattacharya, P. (2016) Natural Arsenic in Global Groundwaters: Distribution and Geochemical Triggers for Mobilization. *Curr. Pollut. Rep.* **2**: 68-89.

Higson, S. P. J. (2006) *Analytical Chemistry*. Oxford University Press Inc., New York: pp193-203.

Hoeffs, J. (1997) *Stable Isotope Geochemistry 4th Ed*. Springer-Verlag, Berlin: pp201.

Homma, A., and Tsukahara, H. (2008) Chemical Characteristics of Hot Spring Water and Geological Environment in the Northernmost Area of the Itoigawa Shizuoka Tectonic Line. *Bull. Earthq. Res. Inst. Univ. Tokyo* **83**: 217-225.

Hou, X., and Jones, B. T. (2000) *Inductively Coupled Plasma/Optical Emission Spectrometry in Encyclopedia of Analytical Chemistry. R.A. Meyers (Ed.)*. John Wiley & Sons Ltd, Chichester: pp9468–9485.

Huck, S. W. (2004) *Reading statistics and Research, 4th Ed. International Edition*. Pearson Education Inc., New York: pp486-512.

Hunt, J. A., Zafu, A., Mather, T. A., Pyle, D. M., and Barry, P. H. (2017) Spartially variable CO_2 degassing in the Main Ethiopian Rift: Implications for magma storage, volatile transport and rift related emissions. *Geochem. Geophys. Geosyst.* **18**: 3714-3737.

Hutchison, W., Mather, T. A., Pyle, D. M., Biggs, J., and Yirgu, G. (2015) Structural controls on fluid pathways in an active rift system: A case study of the Aluto volcanic complex. *Geosph.* **11**: 542-562

Hyeon-Su C., Yong-Kwon, K., Dae-Seok, B., Seong-SooK, P., Ian, H., and Seong-Taek, Y. (2005) Estimation of Deep-Reservoir Temperature of CO_2-Rich Springs in Kangwon District, South Korea. *J. Volcanol. Geotherm. Res.* **141**: 77- 89.

Irwin, W. P., and Barnes, I. (2012) Tectonic relations of carbon dioxide discharges and earth-quakes. *J. Geophys. Res: Solid Earth* **85**: 315-3121.

Jaishankar, M., Tseten, T., Anbalagan, N., Blessy B., Mathew, B. B., Krishnamurthy N., and Beeregowda, K. N. (2014) Toxicity, mechanism and health effects of some heavy metals. *Interdiscip. Toxicol.* **7**: 60–72.

Jeong, C. H., Kim, H. J., and Lee, S. Y. (2005) Hydrochemistry and genesis of CO_2-Rich Springs from Mesozoic granitoids and their adjacent rocks in South Korea. *Geochem. J.* **39**: 517-530.

Jolie, E., Klinkmueller, M., Moeck, I. and Bruhn, D., (2016) Linking gas fluxes at Earth's surface with fracture zones in an active geothermal field. *Geol.* **44**: 187–190.

Kalia, L.V., Lee. L., Kalia, S.K., Pirouzmand, F., Rapoport, M. J., Aviv, R. I, Mozeg, D., and Symons, S. P., (2010). Thoracic myelopathy from coincident fluorosis and epidural lipomatosis. *Can. J. Neuro. Sci*. **37**: 276-278.

Kämpf, H., Bräuer, K., Schumann, J., Hahne, K., and Strauch, G. (2013) CO_2 discharge in an active, non-volcanic continental rift area (Czech Republic): Characterisation (delta C-13, He-3/He-4) and quantification of diffuse and vent CO_2 emissions. *Chem. Geol*. **339**: 71–83.

Kaur, J., Adamchuk, V. I., Whalen, J. K. and Ismail, A. A. (2015) Development of an NDIR CO_2 Sensor-Based System for Assessing Soil Toxicity Using Substrate-Induced Respiration. *Sensors* **15**: 4734-4748.

Kawahara, M., Konoha, K., Nagata, T., and Sadakane, Y. (2007) Aluminum and Human Health: Its Intake, Bioavailability and Neurotoxicity. *Biomed. Res. Trace Elem.* **18**: 211-220.

KEBS. Kenya Bureau of Standards. (2018) *Limits for inorganic contaminants in drinking water and containerised drinking water*. KEBS, Nairobi.

Kelvin, R. G., and Huan, V. L. (2016) Improved method for measuring total dissolved solids. *Analytical letters*. **49**: 1772-1882.

Kenneth, A. M., Michael, P. D., Richard, K., and Terrence, M. G. (1997) *Impacts of Volcanic Gases on Climate, the Environment, and People. U.S. Geological Survey Open-File Report*. U.S. Geological Survey, Washington: pp97-262.

Kenya Meteorological Department (2019). *Rainfall observation at Meru Meteorological Station. Registration No. 8937065*. Kenya Meteorological Department, Meru.

Khadse, G. K., Patni, P. M., and Labhasetwar, P. K. (2015) Removal of iron and manganese from drinking water supply. *Sustain. Water Resour. Manag.* **1:** 157–165.

Khatri, N., Tyagi, S., and Rawtani, D. (2017) Recent strategies for the removal of iron from water: A review. *J. Water Process Eng.* **19**: 291-304.

Kim, M. J., Nriagu, J., and Haack, S. (2000) Carbonate Ions and Arsenic Dissolution by Groundwater. *Environ. Sci. Technol*. **34**: 3094– 3100.

Koch, U., Brauer, K., Heinicke, J., and Kampf, H. (2008) The gas flow at mineral springs and mofettes in the Vogtland∕NW Bohemia: an enduring long-term increase. *Geofluids* **8**: 274–285.

Koh, Y., Kim, C., Bae, D., and Han, K. (2002) The isotopic and chemical compositions of the CO_2-rich waters in Korea. *Geofísica Internacional* **41**: 491-498.

Korngold, E. (1994) Iron removal from tap water by a cation exchanger. *Desalin.* **94**: 243-249.

Kralik, M. (2015) How to Estimate Mean Residence Times of Groundwater. *Procedia Earth Planet. Sci.* **13**: 301-306.

Kravchenko, J., Darrah, T. H., Miller, R. K., Lyerly, H. K., and Vengosh, A. (2014) A review of the health impacts of barium from natural and anthropogenic exposure. *J. Environ. Geochem. Health* **36**: 797-814.

Kucharič, L., Bodiš, D., Panák, D., Liščák, P., and Božíková, J. (2015) A contribution of CO_2 released from mineral springs into overall volume of annual CO_2 emissions in the Slovak Republic. *Environ. Earth Sci.* **73**: 231-238.

Kumar, P. J. S. (2013) Interpretation of groundwater chemistry using piper and Chadha's diagrams: a comparative study from perambalur taluk. *Elixir Geosci.* **54**: 12208-12211.

Kumar, P. J. S., and James, E. J. (2016) Identification of hydrogeochemical processes in the Coimbatore district, Tamil Nadu, India. *Hydrol. Sci. J.* **61**: 719-731.

Lansdown, A, B. (2006) Silver in health care: antimicrobial effects and safety in use. *Curr. Probl. Dermatol.* **33**: 17-34.

Laughrey, C. D., and Baldassare, F. (2003) Some applications of isotope geochemistry for determining sources of stray carbon dioxide gas. *Environ. Geosci.* **10**: 107-122.

Lee, H., Muirhead, J. D., Fischer, T. P., Ebinger, C. J., Kattenhorn, S. A., Sharpand, Z. D., and Kianji, G. (2016) Massive and prolonged deep carbon emissions associated with continental rifting. *Nature Geosci.* **9**: 145–149.

Le Maitre, R. W., Streckeisen, A., Zanettin, B., Le Bas, M. J., Bonin, B., Bateman, P., Bellieni, G., Dudek, A., Efremova, S., Keller, J., Lamere, J., Sabine, P. A., Schmid, R., Sorensen, H., and Woolley, A. R. (2002) *Igneous Rocks: A Classification and Glossary of Terms, Recommendations of the International Union of Geological Sciences, Subcommission of the Systematics of Igneous Rocks 2nd Ed.* Cambridge University Press, London: pp33-38.

Lemiere, B., Laperche, V., Haouche, L., and Auger, P. (2014) Portable XRF and wet materials: Application to dredged contaminated sediments from waterways. *Geochem. Explor. Environ. Anal.* **14**: 257-264.

Liu, Y., Xiao, T., Baveye, P. C., Zhu, J., Ning, Z., and Li, H. (2015) Potential health risk in areas with high naturally-occurring cadmium background in southwestern China. *Ecotoxicol. Environ. Saf.* **112**: 122–131.

L'vov, B. (1988) Graphite furnace atomic absorption spectrometry-On the way to absolute analysis. *J. Anal. At. Spectrom.* **3**: 9-12.

Maas, B. J. and Wicks, C. M. (2017) CO_2 Outgassing from Spring Waters. *Aquat. Geochem.* **23**: 53-60.

Mahar, D. T., Santos, I. R., and Tait, D. R. (2014) Mapping methane and carbon dioxide concentrations and $\delta\ ^{13}C$ values in the atmosphere of two Australian coal gas fields. *Water, Air and Soil Pollut. J.* **225**: 2216.

Mao, X., Wang, Y., Chudaev, O.V., and Wang, X. (2009) Geochemical Evidence of Gas Sources of CO_2-Rich Cold Springs from Wudalianchi, North East China. *J. Earth Sci.* **20**: 959-970.

Marques, J. M., Carreira. P. M. M., Aires-Barros, L., and Graça, R. C. (2000) Nature and role of CO_2 in some hot and cold HCO_3/Na/CO_2-rich Portuguese mineral waters: A review and reinterpretation. *Environ. Geol.* **40:** 53-63.

Marques, J. M., Monteiro, S. F. A., Graca, R. C., Castro, R., Aires-Barros, L., and Mendes Victor, L. A. (2001) A geochemical and geophysical approach to derive a conceptual circulation model of CO_2-rich minerals waters: A case study of Vilarelho da Raia, northern Portugal. *Hydrogeol. J.* **9**: 584–596.

Mason, E., Edmonds, M., and Turchyn, A. V. (2017) Remobilization of crustal carbon may dominate volcanic arc emissions. *Sci.* **357**: 290-294.

Mason, P. (2007) *Geology of the Meru - Isiolo Area Report No.31*. Ministry of Petroleum and Mining, Kenya, Nairobi: pp3-5, 24.

Mathew, J. E., Louis A. D., and Christian, F. L. (2008) Degassing of metamorphic carbon dioxide from the Nepal Himalaya. *Geochem. Geophys. Geosys. Electron. J. Earth Sci.* **9**: 1-18.

Matthews, H. D., Gillett, N. P., Stott, P. A., Zickfeld, K. (2009) The proportionality of global warming to cumulative carbon emissions. *Nature* **459**: 829–832.

Mathu, E. M., and Davies, T. C. (1996) Geology and the environment in Kenya. *J. Afri. Earth Sci.* **23**: 511-539.

Maxwell, N. I. (2014) *Understanding Environmental Health*. Jones and Barlette, Burlington: pp226.

Mermet, J. M. (2008) Limit of quantitation in atomic spectrometry: An unambiguous concept? *Spectrochim. Acta Part B At. Spectrosc.* **63**: 166-182.

Michalski, R. (2006) Chromatography as a Reference Method for Determination of Inorganic Ions in Water and Wastewater. *Crit. Rev. Anal. Chem.* **36**: 107-127.

Ministry of Petroleum and Mining in Kenya. (2018) Geological Survey Department. Nairobi.

Mitchell, R. H. (1986) *Kimberlites: Mineralogy, Geochemistry and Petrology*. Plenum Press, New York: pp442.

Mungai, G. N., Njenga, L. W., Mathu, E. M., and Kamau, G. N. (2014) Study of minerals in the water and source rocks of Rurii spring in Meru County, Kenya. *Int. J. Biochemiphys.* **22**: 11-19.

Nielsen, F. H. (2014) Update on human health effects of boron. *J. Trace Elem. Med. Biol.* **28**: 383-387.

Onyango, M. S., and Matsuda, H. (2006) Chapter 1 Fluoride Removal from Water Using Adsorption Technique. *Adv. Fluor. Sci.* **2**: 1-48.

Pamela, L., Drake, K. J., and Wood, H. (2005) Exposure-related Health Effects of Silver and Silver Compounds: A Review. *The Ann. Occup. Hyg.* **49**: 575-585.

Park, J., Cho, H., and Yi, S. (2010) NDIR CO_2 gas sensor with improved temperature compensation. *Procedia Eng.* **5**: 303–306.

Pham-Huy, L. A., He, H., and Chuong P. H. (2008) Free Radicals, Antioxidants in Disease and Health. *Int. J. Biomed Sci.* **4**: 89–96.

Piper, A. M. (1944) A graphic procedure in the geochemical interpretation of water-analyses. *Eos, Transactions Am. Geophys. Union*, **25**: 914–928.

Prashanth, L., Kattapagari, K. K., Chitturi, R. T., Baddam, V. R., and Prasad, L. K. (2015) A review on role of essential trace elements in health and disease. *J. NTR. Univ. Health Sci.* **4**: 75-85.

Ratna, K. P., Chaudhari, S., Kartic, C. K., and Mahajan, S. P. (2004) Removal of arsenic from water by electrocoagulation. *Chemosphere* **55**: 1245-1252.

Rayman, M. P. (2012) Selenium and human health. *Lancet* **379**: 1256-68.

Rees, D. G. (2001) *Essential Statistics, 4th Ed*. Chapman and Hall/CRC, London, UK: pp161-178.

Robertson, E., Biggs, J., Edmonds, M., Clor, L., Fischer, T. P., Vye-Brown, C., Kianji, G., Koros, W., and Kandie, R. (2016) Diffuse degassing at Longonot volcano, Kenya: Implications for CO_2 flux in continental rifts. *J. Volcanol. Geotherm. Res.* **327**: 208-222.

Rondeau, V., Gadda, H. J., Commenges, D., Helmer, C., and Dartigues, J. F. (2009) Aluminum and Silica in Drinking Water and the Risk of Alzheimer's Disease or Cognitive Decline: Findings From 15-Year Follow-up of the PAQUID Cohort. *Am. J. Epidemiol.* **169**: 489–496.

Roohani, N., Hurrell, R., Kelishadi, R., and Schuler, R. (2013) Zinc and its importance for human health: An integrative review. *J. Res. Med. Sci.* **18**: 144-157.

Rouessac, F., and Rouessac, A. (2007) *Chemical Analysis. Modern Instrumentation Methods and Techniques. Second Ed.* John Wiley & Sons, Ltd, Wet Sussex: pp93-108, 263-281.

Roussas, G. G. (1997) *A Course in Mathematical Statistics, 2nd Ed.* Academic Press, New York: pp397.

Rusydi, A. F. (2018) Correlation between conductivity and total dissolved solid in various type of water: A review. *IOP Conf. Ser. Earth Environ. Sci.* **118**: 012019.

Rutley, F. (1988) *Rutley's Elements of Mineralogy 27th Ed.* CBS publisher and Distributors, New Delhi: pp151-170.

Ryan, J. G., Shervais, J. W., Li, Y., Reagan, M. K., Li, H. Y., Heaton, M., Godard, M., Kirchenbaur S.A., Whattam, J. A., Pearce, T., Chapman, W., Nelson, J., Prytulak, K., and Shimizu, K. (2017) Application of a handheld x-ray fluorescence spectrometer for real-time, high-density quantitative analysis of drilled igneous rocks and sediments during IODP Expedition 352. *Chem. Geol.* **451**: 55-66.

Sadashivaiah, C., Ramakrishnaiah, C. R., and Ranganna, G. (2008) Hydrochemical Analysis and Evaluation of Groundwater Quality in Tumkur Taluk, Karnataka State, India. *Int. J. Environ. Res. Public Health* **5**: 158-164.

Sarah, G. (2014) *Pocket Guide to the Rocks & Minerals of North America*. National Geographic, pp.23.

Schoppen, S., Pérez-Granados, A. M., Carbajal, A., Oubina, P., Sanchez-Muniz, F. J., GomezGerique, J., and Vaquero, M. P. (2004) A sodium-rich carbonated mineral water reduces cardiovascular risk in postmenopausal women, *J. Nutr.* **134**: pp.1058–1063.

Shestakova, A., Guseva, N., Kopylova, Y., Khvaschevskaya, A., David A., Polya, D. A., and Tokarev, I. (2018) Geothermometry and Isotope Geochemistry of CO_2-Rich Thermal Waters in Choygan, East Tuva, Russia. *Water* **10**: 729-59.

Shinohara, H. (2008) Excess degassing from volcanoes and its role on eruptive and intrusive activity. *Rev. Geophys.* **46**: 2.

Sidibé, A. M., Lin X., and Koné, S. (2019) Assessing Groundwater Mineralization Process, Quality, and Isotopic Recharge Origin in the Sahel Region in Africa. *Water*, **11**: 1-19.

Siebe, C., Goff, F., Armienta, M. A., Pounce, D., Poreda, R., and Chipera, S. (2007) Geology and Hydrogeo-chemistry of the Jungapeo CO_2-rich thermal springs, State of Michoacán, Mexico. *J. Volcanol. Geotherm. Res.* **163**: 1-33.

Siegel, D. I., Lesniak, K. A., Stute, M., and Shaun, F. (2004) The isotopic geochemistry of Saratoga Springs: Implications for the origin of solutes and source of carbon dioxide gas. *Geol.* **32**: 257-260.

Skoog, D. A., Holler, F.J., and Crouch, S. R. (2007) *Instrumental Analysis.* Thomson Brooks / Cole, New Delhi: pp28-29, 200, 343-354, 918-921, 936, 1055-1076.

Skoog, D. A., West D. M., Holler, F. J., and Crouch, S. R. (2004) *Fundamentals of Analytical Chemistry, 8th Ed*. Thomson Brooks/ Cole, USA: pp771-772.

Srivastava, A., and Vekouteren, R. M. (2018) Metrology for stable isotope reference materials: $^{13}C/^{12}C$ and $^{18}O/^{16}O$ isotope ratio value assignment of pure carbon dioxide gas samples on Vienna Pee Dee Belemnite-CO_2 scale using dual-inlet mass spectrometry. *Anal. Bioanal. Chem*. **410**: 4153-4163.

Stanjek, H., and Häusler, W. (2004) Basics of X-ray Diffraction. *Hyperfine Interact.* **154**: 107–119.

Stefansson, A., Sveinbjornsdottir, A. E., Heinemeier, J., Arnorsson, S., Kjartansdottir, R., and Kristmannsdottir, H. (2016) Mantle CO_2 degassing through the Iceland crust: Evidence from carbon isotopes in groundwater. *Geochem. et Cosmochim. Acta* **191**: 300-319.

Sunitha, V., and Reddy, B. M. (2004) Determination of Fluoride Concentration in Ground Water by Ion Selective Electrode. *Int. J. Curr. Res. Aca. Rev*. **2**: 159-166.

Swanner, G. M. (1988) Saratoga – *Queen of spas North County Books*. INC. Utica, New York: pp8-14.

Symonds, R. B., Rose, W. I., Bluth, G., and Grenache, T. M. (1994) Volcanic gas studies: methods, results and applications. Volatiles in magmas. *Mineral. Soc. America Rev. Mineral.* **30**: 1-66.

Taffarel, S. R., and Rubio, J. (2009) On the removal of Mn^{2+} ions by adsorption onto natural and activated Chilean zeolites. *Miner. Eng*. **22**: 336–43.

Thomas, D. L., Bird, D. K., Arnorsson, S., and Maher, K. (2016) Geochemistry of CO_2-rich waters in Iceland. *Chem. Geol.* **444**: 158-179.

Tjaša, K., Fausto, G., Jennifer, M., Vekoslava, S., Marija, U. S., Ivan, S., and Sergej, J. (2014) A geochemical and stable isotope investigation of groundwater/surface-water interactions in the Velenje Basin, Slovenia. *Hydrogeol. J.* **10040**: 1103-7.

Tobiason, J. E., Bazilio, A., Goodwill, J., Mai, X., and Nguyen, C. (2016) Manganese Removal from Drinking Water Sources. *Curr. Pollut. Rep.* **2:** 168–177.

Tsuji, K., Nakano, K., Takahashi, Y., Hayashi, K., and Ro, C. U. (2012) X-ray spectrometry. *Anal. Chem.* **84**: 636–668.

Uauy, R., Maass, A., and Araya, M. (2008) Estimating risk from copper excess in human population. *American J. Clin. Nutr.* **88**: 867S-871S.

Ucar, C., Baskan, M. B., and Pala, A. (2013) Arsenic removal from drinking water by electrocoagulation using iron electrodes. *Korean J. Chem*. Eng. **30**: 1889–1895.

Ulrich, H. S. (2003). *Volcanism*. Springer, Berlin: pp71.

Van der Aa, N. G. F. M. (2003) Classification of mineral water types and comparison with drinking water standards. *Environ. Geol.* **44**: 554–563.

Vincent, M., Wei, E. T., Malagoli, C., Bergomi, M., and Vivoli, G. (2001). Adverse health effects of selenium in humans. *Rev. Environ. Health* **16**: 233-51.

Wada, O. (2004) What are trace elements? Their deficiency and excess states. *J. Japan Med. Assoc*. **47**: 351-8.

Waghmare, S. S., and Arfin, T. (2015) Fluoride Removal from Water by various techniques: Review. *Int. J. Innov. Sci. Eng*. Technol. **2**: 560-571.

Wahl, E. D., Fidric, B., Rella, C., Koulikov, S., Kharlamov, B., Tan, S., Kachanov, A., Richman, B., Crosson, E. R., Paldus, B., Kalaskar, S., and Bowling, D. R. (2006). Applications of cavity ring-down spectroscopy to high precision isotope ratio measurement of $^{13}C/^{12}C$ in carbon dioxide. *Isot. Environ. Health Stud.* **42**: 21-35.

Wang, Y., Nakayama, M., Yagi, M., Nishikawa, M., Fukunaga, M., and Watanabe, K. (2005) The NDIR CO_2 monitor with smart interface for global networking. *IEEE Trans. Instrum. Meas*. **54**: 1634–1639.

Wani, A. L., Ara, A., Usmani, J. A. (2015). Lead toxicity: a review. *Interdiscip. Toxicol.* **8**: 55-64.

Wexsteen, P., Jaffé, F. C., and Mazor, E. (1988) Geochemistry of cold CO_2-rich springs of Scoul-Tarasp region, Lower Engadine, Swiss Alps. *J. Hydrol.* **104**: 77-92.

Zaid M. A. (2015) *Correlation and Regression Analysis Textbook*. Oran, Ankara –The Statistical, Economic and Social Research and Training Centre for Islamic Countries (SESRIC), Turkey: pp4-26.

Zdrojewicz, Z., Popowicz, E., and Winiarski, J. (2016) Nickel-role in human organism. *Pol. Merkur Lek.* **41**: 115-8.

Zhang, H., Walker, T. R., Davis, E., and Ma, G. (2019) Ecological risk assessment of metals in small craft harbour sediments in Nova Scotia, Canada. *Mar. Pollut. Bull.* **146**: 466–475.

Zink, S. (1993) *New York office of parks, recreation and Historic preservation, Saratoga – capital District region, Saratoga Springs*. Person Communication, New York: pp11-14.

Internet References

Baker, B, H. (1967). Geology of the Mount Kenya Area. Geological Survey of Kenya. Ministry of Natural Resources, Kenya. https://library.wur.nl › fulltext › isricu_i2754_001 [Valid 10th December 2019].

Cauduro, J., and Ryan, A. (2017) Ultra-fast ICP-OES determination of trace elements in water, as per US EPA 200.7. Agilent Technologies Melbourne, Australia: 5991-4821EN. https://www.agilent.com/cs/library/applications/5991-4821EN.pdf [Valid 21st August 2019].

IARC. (2019) International Agency for Research on Cancer. Agents classified by IARC Monographs.
https://monographs.iarc.fr › uploads › 2018/09 › ClassificationsAlphaOrder. [Valid 28th August 2019].

Kapadnis, G., Jain, V., and Vyas, S. (2016). environmental analysis determination of elements in drinking water as per bureau of Indian standards 10500, 14543 & 13428 using the Agilent 5110 ICP-OES. Agilent Technologies Manesar India: 5991-6631EN. https://www.agilent.com/cs/library/applications/5991-6631EN.pdf [Valid 21st   August 2019].

Kenya Vision 2030. (2008) Transform Kenya into a newly industrialising, middle-income country providing a high quality of life to all its citizens by 2030 in a clean and secure environment. http://vision2030.go.ke/ [Valid 9th October 2020].

KNBS. Kenya National Bureau of Statistics. (2018) Statistical Abstract 2018. p156. https://www.knbs.or.ke [Valid 28th October 2019].

NOAA. National Oceanic and Atmospheric Administration. (2019) Trends in atmospheric carbon dioxide. Earth System Research Laboratory. NOAA. https://www.esrl.noaa.gov › gmd › ccgg › trends › weekly [Valid 23rd August 2019].

UN. United Nations. (2015) Resolution adopted by the General Assembly on 25 September 2015. Transforming our world: the 2030 Agenda for Sustainable Development. United Nations General Assembly. https://www.un.org/ga/search/view_doc.asp?symbol=A/RES/70/1&Lang=E [Valid 9th August 2020].

US EPA. "Method 300.1 (1997) Determination of Inorganic Anions in Drinking Water by Ion Chromatography," Revision 1.0. Cincinnati, OH. https://www.epa.gov/esam/epa-method-3001-revision-10-determination-inorganic-anions-drinking-water-ion-chromatography [Valid 21st August 2019].

US EPA. Method 200.7 Revision 5.0 (2001) Trace elements in water, solids, and biosolids by inductively coupled plasma-atomic emission spectrometry. U.S. Environmental Protection Agency. Washington, D.C. 20460. https://nepis.epa.gov/Exe/ZyPURL.cgi?Dockey=P1002CW0.TXT [Valid 21st August 2019].

US EPA. (1993) The Determination of Inorganic Anions in Water by Ion Chromatography. Method 300.0: Cincinnati, Ohio. https://www.epa.gov › files › documents › method_300-0_rev_2-1_1993 [Valid 21st August 2019].

WHO. (2017) Guidelines for drinking-water quality. Fourth Edition incorporating 1st addendum. Geneva. https://www.who.int/water_sanitation_health/publications/drinking-water-quality-guidelines-4-including-1st-addendum/en/ [Valid 21st August 2019].

WHO. (2011) Guidelines for drinking-water quality 4th Ed. Geneva, World Health Organization, Geneva. ISBN 978 92 4 154815 1. apps.who.int/iris/bitstream/10665/44584/1/9789241548151_eng.pdf [Valid 21st August 2019].

WHO/FAO/IAEA. (1996) World Health Organization. Switzerland: Geneva. Trace Elements in Human Nutrition and Health. https://www.who.int/nutrition/publications/micronutrients/9241561734/en/ [Valid 21st August 2019].

Calibration of instruments and evaluation of analytical procedures was performed using certified reference materials. During the validation process, calibration curves, percentage recoveries of check standards and spiked samples, LOQ and RSD were established to maintain the methods in control.

Appendix A.1: Calibration for DIC measurements

The Picarro CRDS instrument was calibrated for accuracy using $CaCO_3$ standards ranging between 0.3 and 2.0 mg (3-20 μmol) as shown in Table A-1.1. Calibration curve in Figure A-1.1 with acceptable linear regression line ($R^2 = 0.999$) was obtained.

Table A.1.1: DIC calibration standards.

$CaCO_3$ standard (μmol)	CO_2 (ppm)
0	0
3	270
7	566
10	775
13	1012
16	1254
20	1598
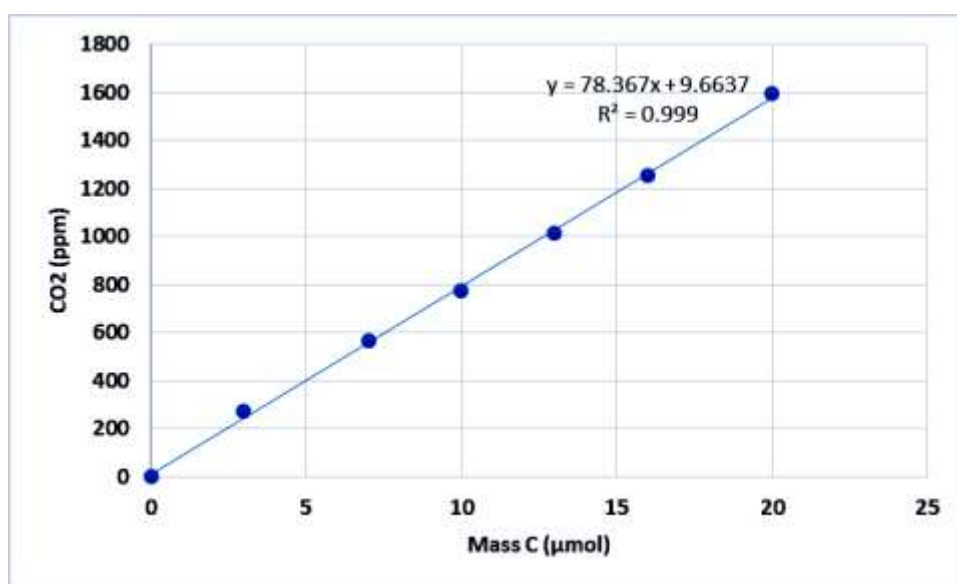
Figure A.1.1: Calibration curve for DIC analysis.

Appendix A.2: Calibration and performance evaluation for IC method

The calibration standards and the curve for Na^+ are given in Table A-2.1 and Figure A-2.1, respectively. Calibration curves for the other ions were obtained in the same way using the standards prepared as outlined earlier in Table 3.3, section 3.7.3.

Table A.2.1: Na^+ IC standards response.

Na^+ standard (mg/L)	Peak area
0	0
0.849	0.1514
1.061	0.1676
1.212	0.1915
1.414	0.2408
1.697	0.2855
2.122	0.3525
2.425	0.4004
2.829	0.4642
3.394	0.5536
4.243	0.6877
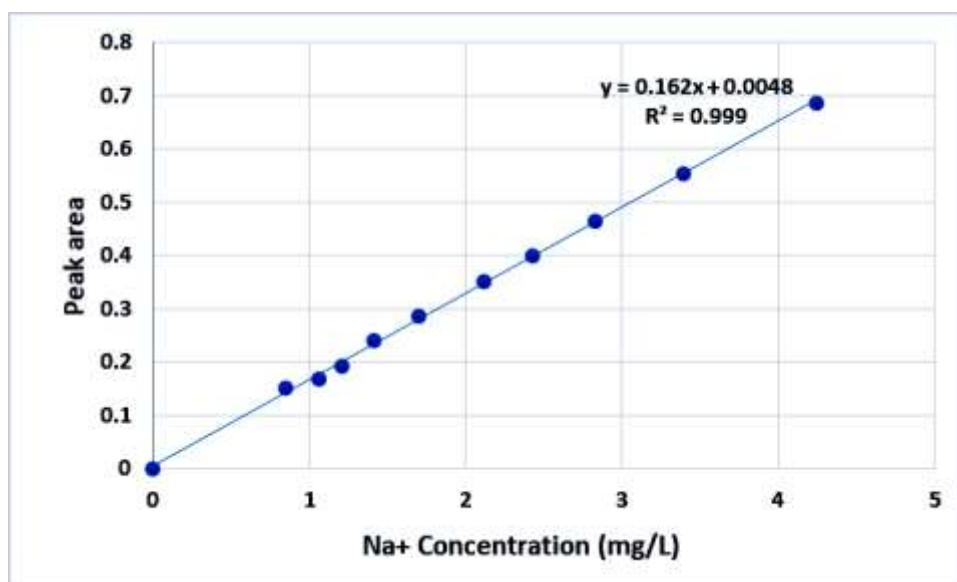
Figure A.2.1: Na^+ IC calibration curve.

Percent recoveries of NIST traceable high purity check standards IC-CAT-1 6 component multi-cation standard 1 and IC-1 7 component multi-anion standard are summarised in Table A-2.2. The recoveries ranging from 92.74 to 99.28 % and RSD $<\pm5\%$ (n = 3) were considered acceptable (Eaton, 2005). The LOQs were ten times the standard deviations of the calibration blank (Mermet, 2008).

Table A.2.2: Percent recoveries of IC check standards and LOQ.

Ion	Certified value (mg/L)	Measured value (mg/L)	RSD	% Recovery	LOQ (mg/L)
F^-	100	99.28	4.68	99.28	0.168
Cl^-	200	190.64	1.48	95.32	0.081
NO_2^-	1000	987.5	2.80	98.75	0.131
Br^-	400	370.96	2.40	92.74	0.004
NO_3^-	400	377.92	1.66	94.48	0.064
PO_4^{3-}	600	565.92	3.75	94.32	3.17
SO_4^{2-}	400	384.64	1.27	96.16	0.326
Li^+	50	48.545	0.42	97.09	0.098
Na^+	200	193.58	0.66	96.79	0.088
NH_4^+	250	239.45	1.30	95.78	0.347
K^+	500	484.1	0.69	96.82	0.248
Ca^{2+}	500	487.05	0.69	97.41	0.168
Mg^{2+}	250	243.375	0.66	97.35	0.406

Appendix A.3: Calibration and performance evaluation for ICP-OES method

Table A-3.1 and Figure A-3.1 shows the calibration data and the resultant curve for Fe, respectively. High regression value (R^2 >0.99) was achieved meaning that over 99% of changes in signal intensity were directly proportional to changes in concentration. Similar calibration curves were obtained for the other parameters using the same concentration range of the standards.

Table A.3.1: Fe ICP-OES standards response.

Fe standard (µg/L)	Intensity
0	0
100	3268
250	8236
500	15472
750	23355
1000	30873
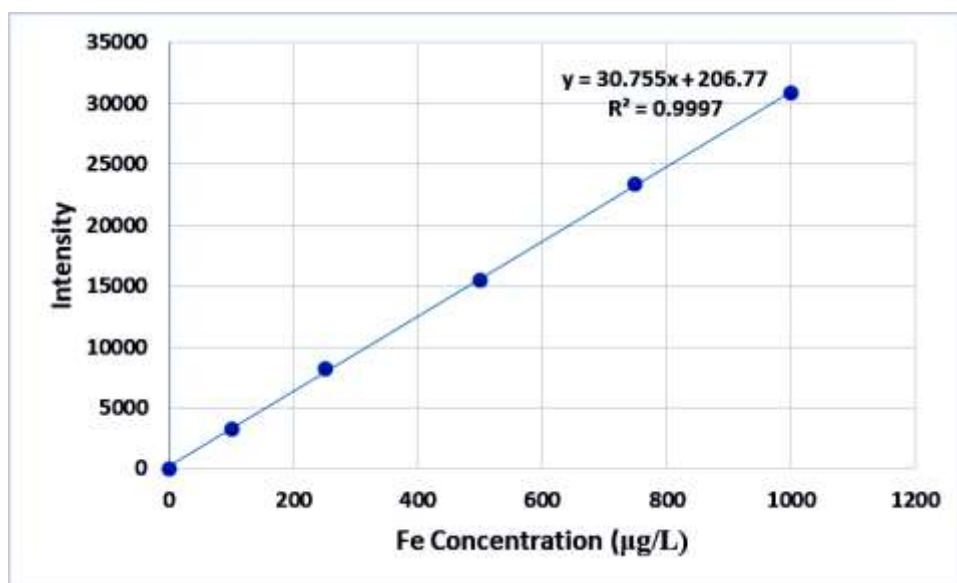
Figure A.3.1: Fe ICP calibration curve.

The limits of quantitation (LOQs) given in Table A-3.2 were established by analysing ten replicates of calibration blanks and multiplying the obtained standard deviations by ten. This ensured that the measured values in the samples were reliably detected and quantified (Mermet, 2008).

Table A.3.2: Limits of quantitation for ICP-OES.

Element	Wavelength (nm)	LOQ (µg/L)
Ag	328.068	1.2
Al	396.152	2.8
As	188.980	3.7
B	249.772	6.8
Ba	455.403	0.4
Be	313.042	0.4
Cd	214.439	0.1
Co	238.892	1.6
Cr	267.716	0.2
Cu	327.395	0.1
Fe	238.204	1.5
Hg	184.887	0.8
Mn	257.610	0.2
Mo	202.032	1.0
Ni	231.604	5.8
Pb	220.353	1.2
Se	196.026	4.9
Zn	213.857	3.0

The recoveries of analytes (n = 3) in water standard reference material (SRM 1643d) traceable to NIST are contained in Table A-3.3. The SRM 1643d simulated the elemental constituents of fresh water. Good recoveries within ±5% of the certified value were obtained thus qualifying the accuracy of the ICP-OES method used. The established precision of $<\pm5\%$ RSD indicates acceptable repeatability of the method.

Table A.3.3: ICP-OES recoveries (%) for elements in SRM 1643d.

Element	Certified value (µg/L)	Measured value (µg/L)	RSD	% Recovery
Ag	1.27 ± 0.057	1.28	3.3	100.79
Al	127.6 ± 3.5	130.60	0.21	102.35
As	56.02 ± 0.73	55.08	1.7	98.32
B	144.8 ± 5.2	145.54	1.8	100.51
Ba	506.5 ± 8.9	519.06	0.27	102.48
Be	12.53 ± 0.28	12.50	0.32	99.76
Cd	6.47 ± 0.37	6.38	0.16	98.61
Co	25.0 ± 0.59	25.16	1.1	100.64
Cr	18.53 ± 0.20	18.40	0.76	99.3
Cu	20.5 ± 3.8	20.67	0.36	100.83
Fe	91.2 ± 3.9	92.54	0.61	101.47
Mn	37.66 ± 0.83	38.47	0.57	102.15
Mo	112.9 ± 1.7	112.32	0.83	99.49
Ni	58.1 ± 2.7	58.32	2.7	100.38
Pb	18.15 ± 0.64	18.0	1.2	99.17
Se	11.43 ± 0.17	11.26	1.7	98.51
Zn	72.48 ± 0.65	73.16	0.82	100.94

Appendix A.4: XRF instrument performance check

The XRF instrument performance was checked by taking ten measurements of soil check sample CS-M2. The average measured values in percent weights are reported in Table A-4.1. They were all found within the acceptance limits.

Table A.4.1: XRF instrument performance check.

Parameter	Average measured value (%)	RSD	Acceptance limit MIN (%)	Acceptance limit MAX (%)
Al_2O_3	12.9945	3.49	10.7271	15.2619
SiO_2	72.1349	1.93	65.1570	79.1128
K_2O	5.0151	1.83	4.5559	5.4743
Mn	0.1051	3.52	0.0680	0.1423
Fe	1.6947	1.22	1.5915	1.7979
Ni	0.0023	4.35	0.0000	0.0046
Cu	0.0203	3.45	0.0130	0.0277
Pb	0.0868	1.96	0.0698	0.1037

Appendix A.5: Evaluation of AAS method

The instrument was calibrated with respective SY-4 and MRG-1 rock standards before analysis of the samples. The calibration results for Al_2O_3 are given in Table A-5.1 and Figure A-5.1. Calibration curves for the other oxides were obtained in the same way using the standards prepared as earlier indicated in Table 3.4, section 3.9.3.

Table A.5.1: SY-4 Al_2O_3 calibration data.

| Al_2O_3 standard (%)	Intensity
0	0
2.07	0.024
10.35	0.108
20.69	0.216
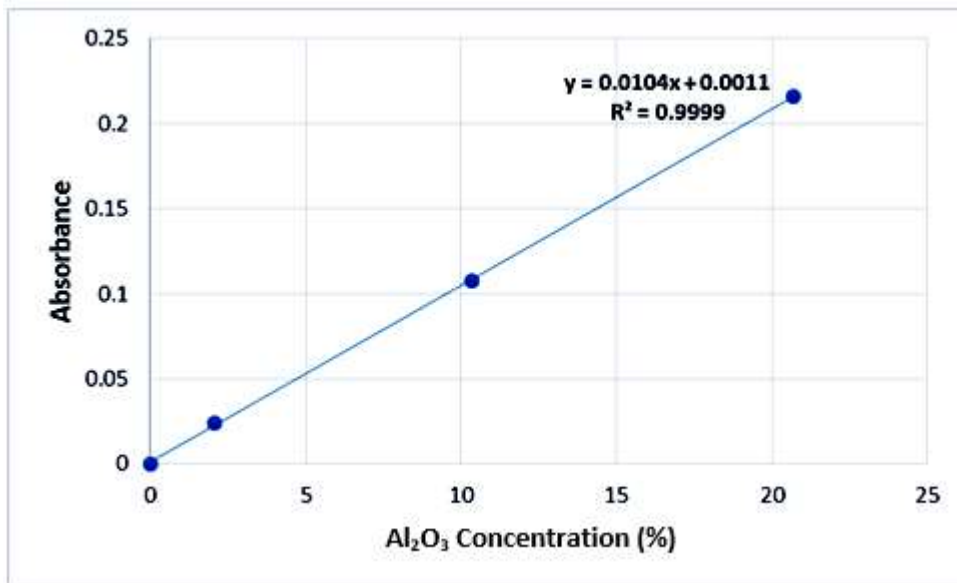
Figure A.5.1: Al$_2$O$_3$ calibration curve.

Rock samples were spiked with known amounts of respective standards (SY-4 and MRG-1) to check the extent of matrix interference. Good recoveries ranging from 95.65 to 101.44% were obtained as indicated in Table A-5.2 which fell within the standard range of 85-115% (Eaton, 2005).

Table A.5.2: AAS spike recoveries (%) in rock samples.

Metal oxide	Present (%±RSD)	Added (%)	Total (%)	Found (%±RSD)	Recovery (%)
Al$_2$O$_3$	14.86 ± 2.3	2.07	16.93	16.85 ± 3.5	99.53
CaO	10.13 ± 2.8	0.54	10.67	10.60 ± 2.2	99.34
Fe$_2$O$_3$	12.18 ± 5.2	3.11	15.29	15.13 ± 3.7	98.95
K$_2$O	1.15 ± 5.6	0.48	1.63	1.61 ± 4.4	98.77
MgO	6.07 ± 0.4	0.27	6.34	6.28 ± 1.6	99.05
MnO	0.17 ± 4.3	0.06	0.23	0.22 ± 2.8	95.65
Na$_2$O	2.90 ± 6.3	0.71	3.61	3.57 ± 3.3	98.89
SiO$_2$	46.43 ± 0.8	4.99	51.42	52.16 ± 2.0	101.44
TiO$_2$	2.08 ± 2.2	0.74	2.82	2.79 ± 1.8	98.94

<u>**Title**</u>

Genesis of carbon dioxide and associated characteristics of selected mofette springs in the Eastern Mt. Kenya region.

<u>**Introduction**</u>

The purpose of this survey is to gather information relating to the general characteristics, uses and effects of mofette springs (*Muonyo*) from residents in the study area. The data is intended for learning and scientific use only. The information provided by respondents will be treated as private and confidential. The respondents may give their names and contact information in case follow up is needed in future but it is not a must to do so.

This research has been approved by the National Commission for Science, Technology and Innovation (NACOSTI) and Meru County Government through the University of Nairobi, Kenya.

<u>**Instructions: Please tick in the box and fill the gaps as appropriate.**</u>

1. Gender

   Male ☐   Female ☐

2. Age bracket

   18-35 years ☐   over 35 years ☐

3. County_____Village_____

4. Are there mofette springs (*Muonyo*) in your area?

   Yes ☐   No ☐

   If yes, give their name(s)

   a._____

   b._____

   c._____

   d._____

   e._____

   f._____

5. How does the water seem to emerge from the source of the springs named above?

Spring	Emerge vigorously	Emerge quietly
a._____	☐	☐
b._____	☐	☐
c._____	☐	☐
d._____	☐	☐
e._____	☐	☐
f._____	☐	☐

6. How often do you use this water?

Most regularly ☐   Regularly ☐   Not regularly ☐   Rarely ☐   Not at all ☐

7. For what purpose is the water mainly used?

_____

_____

_____

_____

_____

_____

8. Does the spring water have a special taste?

Yes ☐   No ☐

If yes, describe the taste.

Normal ☐   Sour ☐   Bitter ☐   Others (specify) _____

9. After fetching the water, does the special taste remain the same with time?

Yes ☐   No ☐

If no, for how long does the taste last?

Less than a day ☐   1-2 days ☐   2-3 days ☐   Over 3 days ☐

10. When you observe the water, is it colourless?

Yes [ ]   No [ ]

If no, describe the colour.

_____

11. Does the water have any smell?

Yes [ ]   No [ ]

If yes, describe the smell_____

12. Does any precipitate or solid form in the fetched water after sometime?

Yes [ ]   No [ ]

If yes, describe the colour of precipitate.

_____

13. Does the water show any reaction with common substances? E.g. when preparing food.

Yes [ ]   No [ ]

If yes, what is the nature of the reaction?

_____

_____

_____

14. Which are the main positive effects of the water to the users including animals, if any?

_____

_____

_____

_____

_____

15. Which are the main negative effects of the water to the users including animals, if any?

_____

_____

_____

_____

_____

16. Do the springs affect the nearby environment (soil, air, plants, animals or buildings)?

Yes [ ]   No [ ]

If yes, describe the adverse effects.

_____

_____

_____

_____

_____

_____

17. Provide any other relevant information about these kind of springs.

_____

_____

_____

_____

_____

_____

18. Contact information **(optional)**

Name _____

Phone number_____E-mail_____

APPENDIX C: MAPS

## Appendix C.1: Geological Map of Embu-Meru Area

Courtesy of Ministry of Petroleum and Mining, Kenya (2018).

Appendix C.2: Geological Map of Meru-Isiolo Area

Courtesy of Ministry of Petroleum and Mining, Kenya (2018).

Appendix C.3: Lithology Map of Meru County

Courtesy of Department of Geography and Environmental Studies, University of Nairobi (2018).